Fujita, et.al

NASA-CR-182,914

Temp. Dependent Tensile & Shear Response of Gr/Al. (Va Tech Es

CCMS-87-08
VPI-E-87-8

VIRGINIA TECH

CENTER FOR COMPOSITE MATERIALS AND STRUCTURES

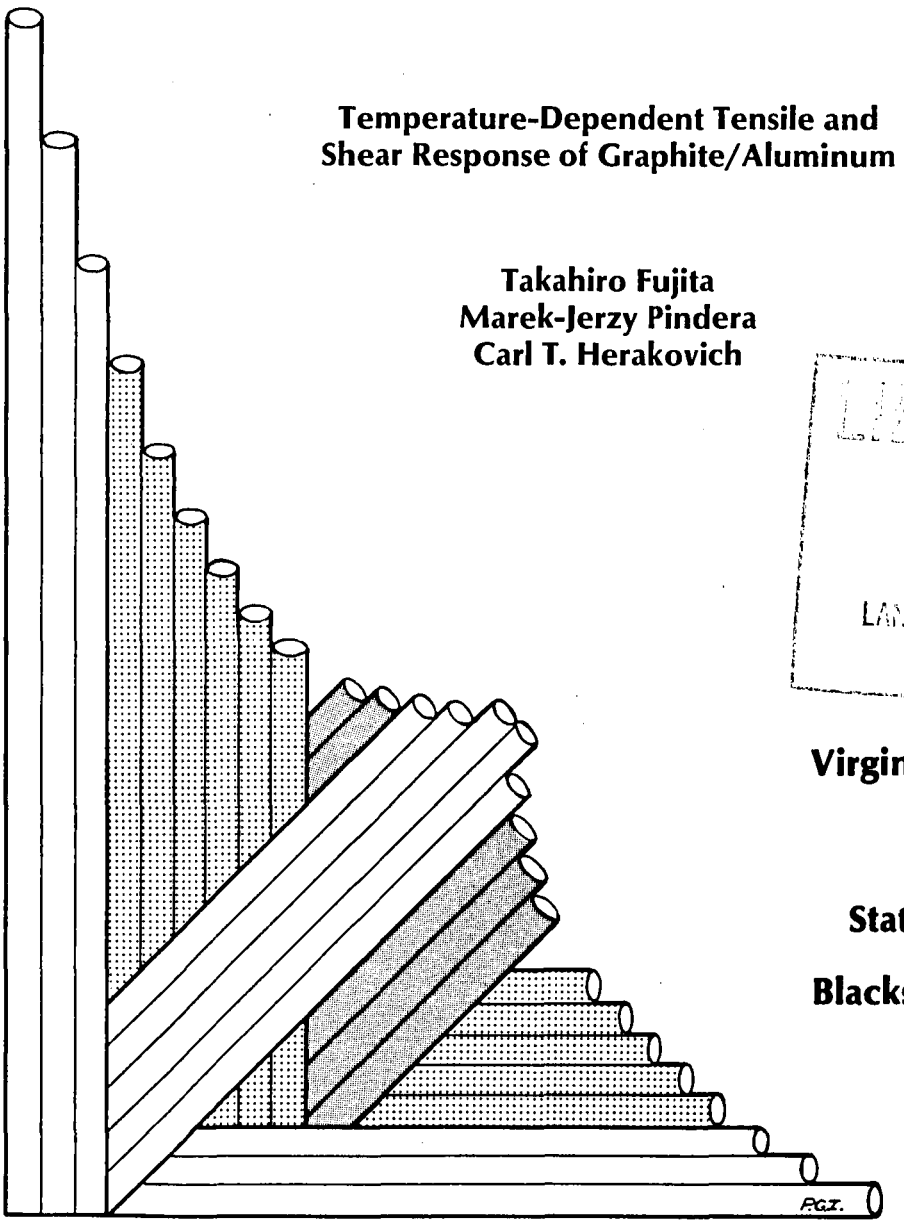

Temperature-Dependent Tensile and Shear Response of Graphite/Aluminum

Takahiro Fujita
Marek-Jerzy Pindera
Carl T. Herakovich

Virginia Polytechnic Institute and State University

Blacksburg, Virginia 24061

College of Engineering
Virginia Polytechnic Institute and State University
Blacksburg, Virginia 24061

May 1987

CCMS-87-08
VPI-E-87-8

Temperature-Dependent Tensile and Shear Response of Graphite/Aluminum

Takahiro Fujita[1]
Marek-Jerzy Pindera[2]
Carl T. Herakovich[3]

Department of Engineering Science & Mechanics

Prepared for:

National Aeronautics and Space Administration
Goddard Space Flight Center
Greenbelt, MD 20771

Materials Sciences Corporation
Gwynedd Plaza 2
Bethlehem Pike
Spring House, PA 19477

Center for Innovative Technology
Institute for Materials Science & Engineering
Virginia Polytechnic Institute & State University
Blacksburg, VA 24061

---

[1] Graduate Student, Department of Engineering Science & Mechanics

[2] Assistant Professor, Department of Engineering Science & Mechanics

[3] Professor, Department of Engineering Science & Mechanics

Temperature-Dependent Tensile and Shear Response of Graphite/Aluminum

by

Takahiro Fujita

Carl T. Herakovich, Co-Chairman

Engineering Science and Mechanics

(ABSTRACT)

The thermo-mechanical response of unidirectional P100 graphite fiber/6061 aluminum matrix composites (v_f = 0.47) was investigated at four temperatures: -150°F, +75°F, +250°F and +500°F, using test methods developed at Virginia Tech. Two types of tests, off-axis tension and Iosipescu shear, were used to obtain the desired properties. Good experimental-theoretical correlation was obtained for E_{xx}, ν_{xy} and G_{12}. It is shown that E_{11} is temperature independent, but E_{22}, ν_{12} and G_{12} generally decrease with increasing temperature. Compared with rather high longitudinal strength, very low transverse strength was obtained for the graphite/aluminum. The poor transverse strength is believed to be due to the low interfacial bond strength in this material. The strength decreases significantly with increasing temperature. The tensile response at various temperatures is greatly affected by the residual stresses caused by the mismatch in the coefficients of thermal expansion of fibers and matrix. The degradation of the aluminum matrix properties at higher temperatures has a deleterious effect on composite properties. The composite has a very low coefficient of thermal expansion in the fiber direction.

Acknowledgements

This work was supported by the Materials Sciences Corporation through a subcontract on a project funded by NASA Goddard Space Flight Center and the CIT Institute of Materials Science and Engineering. Mr. Fujita was supported by NKK Industries of Tokyo, Japan.

The authors also want to express their appreciation to Jeff Hidde, Mike Starbuck, Mark Lin and Todd Williams for their assistance with some portions of the experimental work.

Table of Contents

List of Illustrations

List of Tables

1.0 Introduction

1.1 High Temperature Composites

Metal-matrix composites (MMC) have the potential to offer many advantages of composite materials such as high strength-to-weight and stiffness-to-weight ratios at high temperatures [1-3]. Although their use has been limited because of the high cost of raw materials and manufacturing, efforts continue to be given to the development and application of metal-matrix composites. Graphite-reinforced aluminum is one type of metal matrix composite which has been studied [4-7]. Graphite fibers have many advantages such as high strength, high stiffness, low density and the potential of low-cost manufacturing. Likewise, aluminum is relatively low cost and readily available. Graphite/aluminum composites have been applied to defense endeavors such as tactical missile skins, stiffeners, rocket launch tubes, armor components, and light weight field erectable assault bridges [2]. There can be little doubt that their application will increase in the future.

In space, the temperature rises to +250°F in the sun while it drops to -250°F in the shade. Structural components in high precision space structures must be not only heat-resistant but also dimensionally stable in such an environment. Because of their low thermal expansion properties and high specific stiffnesses, graphite/aluminum composites are leading candidates for space structural applications.

1.2 Fabrication of Graphite/Aluminum Composites

Although graphite/aluminum composites are very attractive materials for many applications, there are major difficulties with their fabrication process. Molten aluminum does not normally wet as-received graphite, and when it does, aluminum carbide (Al_4C_3), which can severely degrade filament strength [8, 9], is readily formed. Thus, most studies have been devoted to improving the wettability between aluminum and graphite fibers as well as preventing the formation of Al_4C_3. There are several methods currently in use for making uniaxial graphite/aluminum composites.

An infiltration/liquid phase vacuum hot pressing technique was pioneered by Pepper et al [10, 11] and has been refined and examined by several investigators in the U.S. [12-16]. This technique consists of chemical treatment of fiber surfaces followed by infiltration of fibers by liquid aluminum and subsequent vacuum hot pressing. Figure 1 shows the surface treatment and infiltration process. As mentioned previously, surface treatment is performed in order to improve wettability. Chemical vapor deposition (CVD) of titanium-boron [6, 14, 17-19] or electroplating of nickel [14, 20, 21] are alternative methods of chemical surface treatment. They provide a coating to fi-

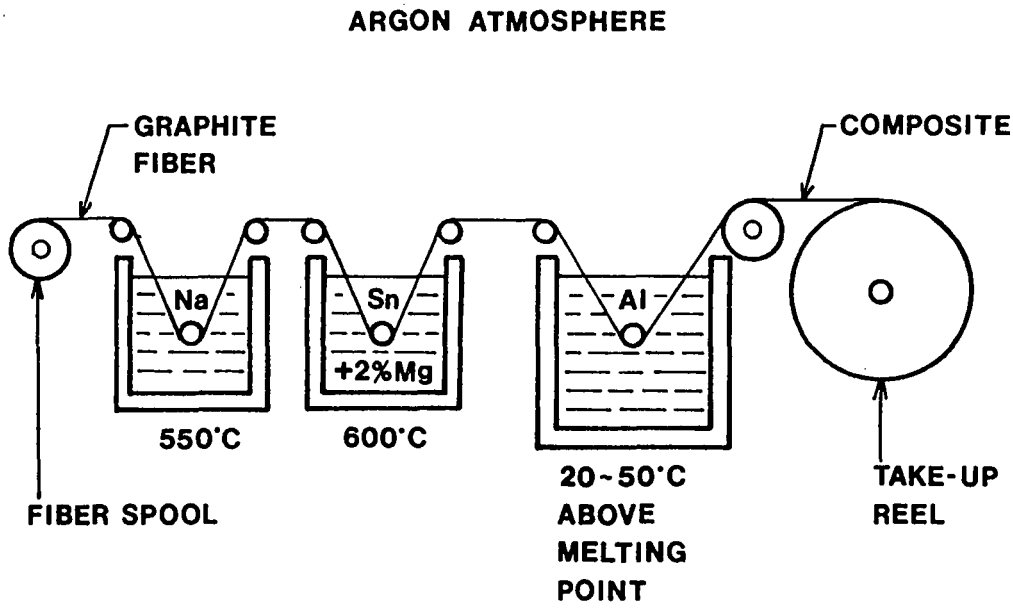

Figure 1. Liquid aluminum infiltration process [14]

bers which is intended to prevent chemical interaction as well as to promote wettability. There have been numerous other attempts to deposit aluminum on fibers other than liquid aluminum infiltration. They are electrodeposition of aluminum [22], CVD of aluminum [23, 24] and ion-plating of aluminum [25]. Coated fibers are called precursor wires.

There are various techniques to fabricate graphite/aluminum. A forced impregnation or forced infiltration, which is similar to the infiltration/liquid phase vacuum hot pressing, has been developed in the U.S.S.R. [26-28]. Plasma spray of aluminum powder on fibers to form pre-preg sheets followed by hot pressing [29, 30] or roll diffusion bonding [31, 32] was introduced in Japan. Powder metallurgy was applied to manufacture the composites in West Germany [33].

Because graphite fibers are available in yarn form rather than monofilament form, fiber distribution can be nonuniform and the maximum fiber volume fraction is limited to 50% by the above mentioned methods. Two methods of manufacturing aluminum/graphite composites with fiber volume fraction of 70% have been disclosed recently; one is the electric-discharge sintering (EDS) method [34] and the other is the squeeze casting method [35].

1.3 Material

The material used for this study was unidirectional Thornel P100 graphite fiber/6061 aluminum composite manufactured by infiltration/liquid phase hot pressing. Impor-

Table 1. Properties of P100 graphite fiber at room temperature [36]

Density	0.078	lb/in^3
Ultimate Tensile Stress	325.0	ksi
Ultimate Tensile Strain	0.31	%
Longitudinal Tensile Modulus	105.0	msj
Longitudinal Thermal Expansion Coefficient	-0.78×10^{-6}	in/in/°F

tant properties of P100 graphite fiber [36] and 6061 aluminum [7] at room temperature are listed in Tables 1 and 2. Since no particular heat treatment was given to the present material, judging from the heat history during the fabrication process, 6061-O (annealed) data are chosen as the aluminum matrix properties. Figure 2 illustrates the tensile response of aluminum 2024-T4 at +70°F, +120°F, +400°F +500°F and +700°F [37, 38]. Since no data could be found for 6061-O, available data of 2024-T4

Table 2. Properties of 6061-O aluminum at room temperature

Density*	0.098	lb/in^3
Ultimate Tensile Stress*	18.0	ksi
Ultimate Tensile Strain*	30.0	%
Yield Stress**	5.0	ksi
Tensile Modulus**	9.9	msi
Poisson's Ratio**	0.309	
Thermal Expansion Coefficient*	13.0×10^{-6}	in/in/°F
Shear Modulus**	3.78	msi

* Ref. 7
** Experiments by Mark Lin - private communication

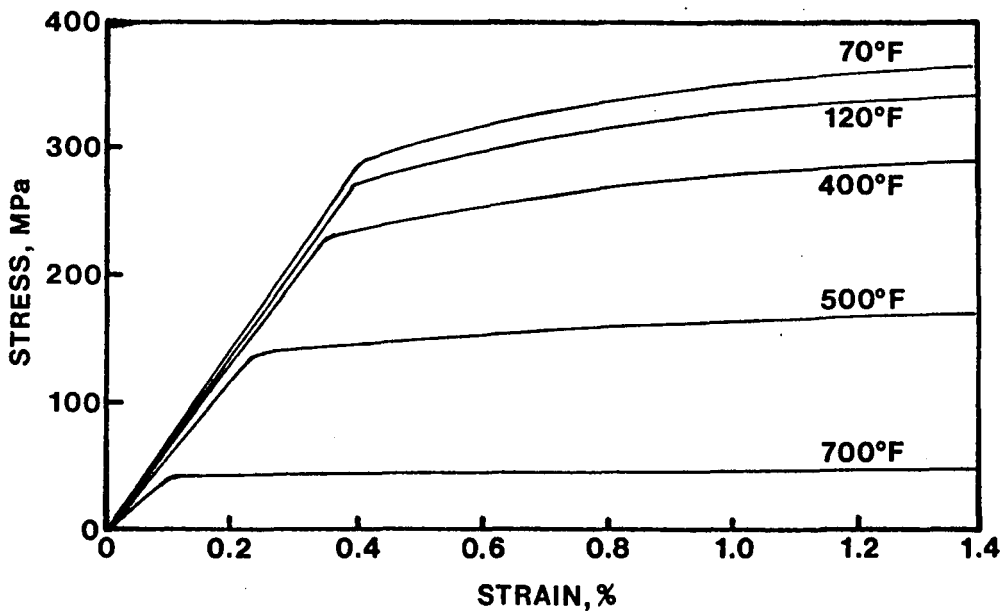

Figure 2. Tensile response of 2024-T4 aluminum at several temperatures [37, 38]

were used to show temperature-dependent aluminum properties. It is seen that stress-strain behavior of aluminum is significantly affected by temperature. On the other hand, it can be assumed that the properties of graphite fibers do not change in this temperature range.

The precursor wires used in this study were produced by Material Concepts, Inc. and provided by the U.S. Navy. The wire was manufactured by infiltrating P100 fiber bundles with molten 6061 aluminum. Each wire consisted of 2000 graphite filaments; the average wire fiber volume fraction was 50.07 %. Average wire strength was 213 ksi and average wire diameter was 0.024 in. Utilizing these precursor wires, DWA Composite Specialties, Inc. fabricated unidirectional panels using liquid phase vacuum hot pressing. The unidirectional panels consisted of 0.0018 in. thick 6061 foils on the top and bottom surfaces with two layers of the precursor wire sandwiched between these foils as illustrated in Fig. 3. The consolidated panels were 12 in. by 12 in. by 0.040 in. thick. The average fiber volume fraction of the panels was 46.57 %.

1.4 Objective of the Study

Typical stress-strain responses of P100 graphite fiber and 6061 aluminum are shown in Fig. 4; obviously, the differences are quite significant. The fiber exhibits high-stiffness, high-strength and brittle behavior whereas the aluminum exhibits low-stiffness, low-strength and ductile behavior. Although it is important to know and

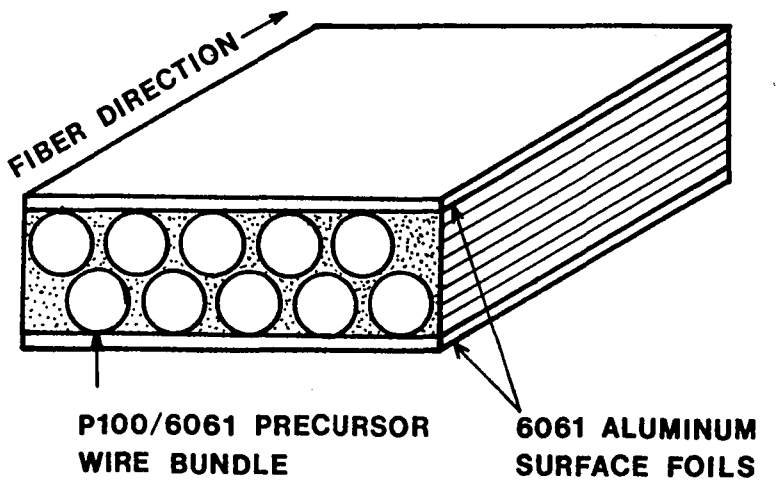

Figure 3. P100/6061 composite panel composed of precursor wires and thin aluminum foils

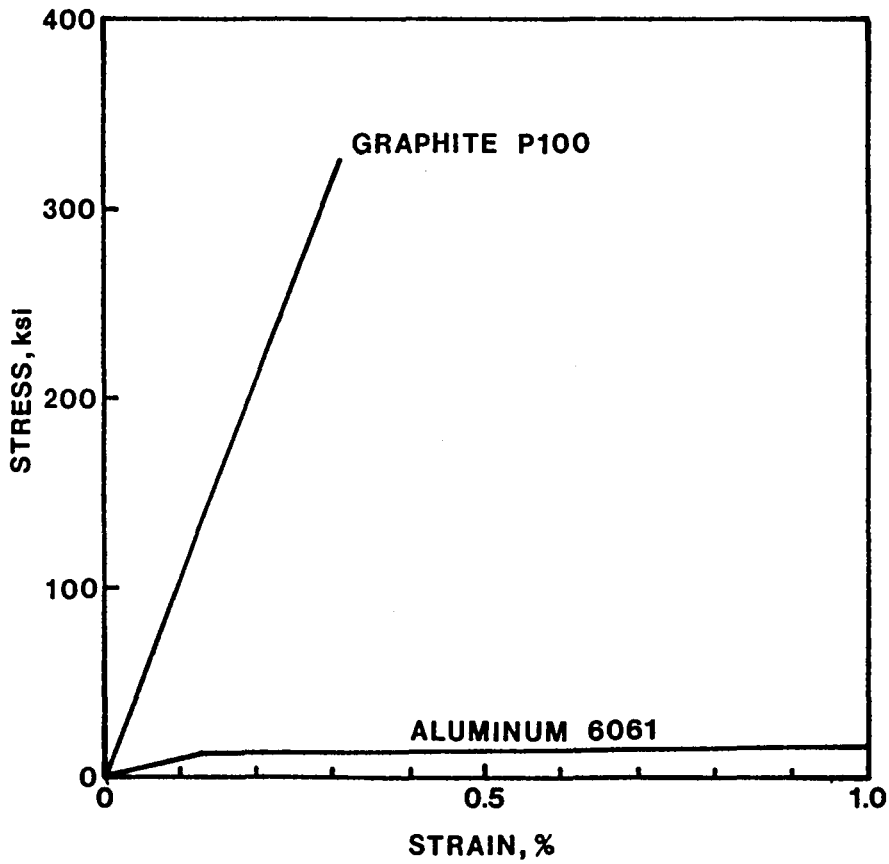

Figure 4. Stress-strain responses of P100 graphite fiber and 6061 aluminum

understand the behavior of graphite/aluminum composite composed of these quite different constituents, this material has not been well-characterized by a systematic study.

Most studies thus far have measured ultimate tensile strength and tensile moduli in the fiber direction. A few studies have obtained transverse strength, but little attention has been given to off-axis tensile and shear properties. One paper has presented tensile and shear strength variation with regard to fiber orientation [16]. Apparently, there has been no report which deals with off-axis tensile modulus. One paper reported G_{12} value using 15° off-axis tension test at room temperature [15]. A number of efforts have been devoted to the study of high temperature performance of this material. The effect of thermal cycling on ultimate strength has been a prime interest, but modulus values and nonlinear response at elevated and cold temperatures have not been well-documented.

Residual stress developed during the fabrication process is another matter of concern for this material. As shown in Tables 1 and 2, considerable mismatch of the coefficient of thermal expansion in the fiber direction exists between the graphite fibers (-0.78×10^{-6}/°F) and the aluminum matrix (13.0×10^{-6}/°F). This mismatch may result in significant residual stresses upon cool-down from the fabrication temperature. Hoover [18] suggested the presence of residual stress to explain the experimental result that T50 graphite/201 aluminum yielded in tension before it yielded in compression. A continuum theory has been applied to estimate the effect of residual stresses on the material response of graphite/aluminum. Min and Crossman [39] showed that the residual stress greatly affects the yield stress of VS0054 graphite/6061-T6 aluminum on the basis of experimental results and theoretical ana-

lyses. Aboudi [37, 38] predicted the residual stresses and their effect on the overall behavior of T50 graphite/2024-T4 aluminum under various types of applied stresses.

The present study is an investigation of the material properties of unidirectional P100/6061 graphite/aluminum composite in the temperature range from -150°F to +500°F using test methods developed at Virginia Tech. The research is divided into three phases: monotonic response, cyclic response and thermo-mechanical response. The monotonic and cyclic tests were conducted at four temperatures; -150°F, +75°F, +250°F and +500°F. Three types of tests, on-axis and off-axis tension, and Iosipescu shear were used to obtain the desired properties.

2.0 Experimental Program

Details of the experimental program are described in this chapter. First, the test methods used to obtain the material behavior of each phase are outlined. At least two tests were conducted for each test configuration. Precise strain measurement is required to characterize the thermo-mechanical properties of the material. Detailed strain gage procedures and methods of apparent strain compensation and shear strain calculation are explained. Next, each test method and the equations used to determine the material properties from the test results are described. Particular emphasis is placed on an explanation of the end-constraint effect of the off-axis tension test and the method of correcting measured values. A brief introduction is given to the Iosipescu shear test. Finally, the testing system and temperature control methods are introduced.

2.1 Testing Program

2.1.1 Monotonic Tests

Monotonic tests were conducted at -150°F, +75°F, +250°F and +500°F to obtain in-plane elastic properties such as E_{11}, E_{22}, ν_{12} and G_{12}, and subsequent nonlinear behavior including failure. Theoretically, only three specimen configurations, i.e. 0°, 90° and one off-axis specimen, are required to obtain these properties. The 15° off-axis specimen was chosen because it exhibits extensive nonlinear response. The 0° Iosipescu tests were conducted to obtain initial shear modulus, extensive nonlinear shear deformation and shear strength.

At room temperature only, 10° and 45° off-axis tension tests and 90° Iosipescu tests were conducted in addition to the above mentioned tests. The 10° off-axis specimen is often employed as the off-axis specimen rather than the 15° specimen. The change in lamina moduli near this fiber angle is so great that the several fiber angles provide a good check on the applicability of the transformation equations. The 45° off-axis specimen provides a very accurate shear modulus G_{12} [40]. The 90° Iosipescu test was used in conjunction with the off-axis and 0° Iosipescu to compare the shear response from different test methods.

Table 3 shows the test matrix for monotonic tests.

Table 3. Test matrix for monotonic tests

Fiber Orientation	Temperature			
	-150°F	+75°F	+250°F	+500°F
Tension				
0°	2	3	2	2
10°	-	2	-	-
15°	2	2	2	2
45°	-	3	-	-
90°	2	2	2	2
Iosipescu				
0°	2	3	2	2
90°	-	4	-	-

2.1.2 Cyclic Tests

Cyclic tests were performed at the same temperatures as the monotonic tests to determine the unloading and reloading response of the material. Only three specimen configurations (0°, 15° and 90°) were used for these tests. Based on the monotonic test results, load reversal levels were chosen as 80% of the tensile strength for each configuration and each temperature. Each specimen was loaded to the reversal level,

then completely unloaded (i.e. until no load was observed) and finally reloaded to failure.

Table 4 shows the test matrix for cyclic tests.

Table 4. Test matrix for cyclic tests (tension)

Fiber Orientation	Temperature			
	-150°F	+75°F	+250°F	+500°F
0°	2	2	2	2
15°	2	3	2	2
90°	2	2	2	2

2.1.3 Thermo-Mechanical Tests

The thermo-mechanical tests consisted of tensile loading up to 75% of the ultimate strength at room temperature (+75°F) followed by thermal loading to either +500°F or -150°F while maintaining constant tensile load. Two configurations, 15° and 90° specimens, were used for these thermo-mechanical tests.

Table 5 shows the test matrix for thermo-mechanical tests.

Table 5. Test matrix for thermo-mechanical tests (tension)

Fiber Orientation	Temperature	
	+75°F to +500°F	+75°F to -150°F
15°	2	2
90°	2	2

2.2 *Strain Measurement*

2.2.1 Gage Selection

Lamina Young's modulus E_{11}, Poisson's ratio ν_{12}, and the in-plane shear modulus G_{12} were determined using three-element 45° rectangular stacked rosette strain gages. For some specimens - usually off-axis specimens -, significant initial curvature was present prior to testing. A single-element longitudinal gage was installed on the back surface to measure the bending effects.

Micro-Measurements gages were used for all the tests. For tensile specimens, gages, 0.06 in. long, were employed. For Iosipescu specimens, smaller gages, 0.03 in. long, were used because the region of uniform shear stress is quite small. Self-temperature-compensating (S-T-C) gages with the S-T-C number of 06 were used for all the tests. The S-T-C number ($\times 10^{-6}$/°F) should match the approximate thermal

expansion coefficient of the material to eliminate apparent strain errors which are caused by the temperature-induced resistance change.

For the room temperature tests, constantan (A-alloy) gages (WA series) were used. The tension specimens were instrumented with a WA-06-060WR-120 rosette and a WA-06-062AP-120 uniaxial gage. The Iosipescu specimens were instrumented with a WA-06-030WR-120 rosette and a WA-06-031CF-120 uniaxial gage.

For high and low temperature tests, K-alloy gages (WK series) were employed since they provide more accurate correction for apparent strain errors at the temperature extremes. The tension specimens were instrumented with a WK-06-060WR-350 rosette and a WK-06-062AP-350 uniaxial gage. The Iosipescu specimens were instrumented with a WK-06-030WR-120 rosette and a WK-06-031CF-350 uniaxial gage. The method of correction for apparent strain errors will be described later.

2.2.2 Gage Installation

2.2.2.1 Room Temperature Specimens

Techniques presented in *M-M Instruction Bulletin B-127* were employed for gage installation. M-Bond 200 catalyst was applied to the bond surface of the gage and terminal while one or two drops of M-Bond 200 adhesive were applied to the specimen surface. Firm thumb pressure was given to the gage and terminal area for at least one minute to obtain good bonding between gage/terminal and specimen.

The soldering techniques given in *M-M TECH TIP TT-606* were followed for attaching leads to gages. After M-FLUX AR was added to the tips of the gage leads, leadwires, and terminals, with a temperature-controlled soldering iron of Mark V Soldering Station, gage leads and leadwires were soldered at the terminals using a 361-20R solder.

2.2.2.2 -150°F and +250°F Specimens

Techniques given in *M-M Instruction Bulletin B-130* were used for gage installation at -150°F and +250°F specimens. A thin layer of M-Bond 610 adhesives was applied to the backing of the gage/terminal and specimen surface and then dried in the air for 15 to 30 minutes. After the gage/terminal assembly was placed on the specimen, a piece of thin Teflon sheet, a thick silicone gum pad and a metal back plate were placed over the gage/terminal area. A spring clamp was used to apply pressure on the gage/specimen during the curing cycle. The clamped gage/specimen was placed into a cool oven and the temperature was raised to 350°F. After curing for one hour, the gage/specimen was gradually cooled to room temperature in the oven. The gage leads and lead wires were then soldered in the same way as for the room temperature specimens.

2.2.2.3 +500°F Specimens

The gage installation procedures for these elevated temperature specimens were almost the same as -150°F and +250°F specimens. The difference in procedure was that the terminals were not installed and a postcure was required. After the initial curing, the clamping fixture was removed from the gage/specimen. The specimen

was then put into the oven again and postcured for two hours at +575°F (+75°F above the test temperature).

Since the melting point of 361-20R solder is +361°F, this solder could not be used for +500°F specimens. Instead, the silver soldering technique presented in *M-M TECH TIP TT-602* was employed. First, the gage lead exit area was covered with a piece of masking tape. This was done to avoid separating the gage lead from the specimen during the following procedures. After the leadwires were anchored to the specimen surface, both gage leads and leadwires were carefully lifted. Next, each gage lead and stripped end of the corresponding lead wire were knitted together by using a pair of tweezers. A small portion of M-M 570-28R solder was then applied to the solder joint. Using the resistance soldering unit M-M WRS-1, the end of knitted gage wire/leadwire was grasped firmly with the clean electrodes. Then, the unit was energized by pressing the footswitch of the M-M WRS-1. After the water in the solder boiled away, the actual flow of solder was accomplished. Since there is no terminal for this soldering, the entire assembly should be handled very carefully during soldering and testing in order to prevent damage to the gages.

2.2.3 Temperature-Induced Apparent Strain

A strain gage on a specimen responds not only to the applied strain, but also to any temperature change. A change in the temperature causes a resistance change in the gage and a differential thermal expansion between the grid conductor and the testing material. Thus the temperature change results in *apparent strain.* If no temperature change occurs during the test, strain measurements can be accomplished without

compensating for apparent strain. For low and high temperature tests, however, it is difficult to maintain the temperature in the chamber uniformly constant. Therefore, temperature compensation should be included in the measurement procedure.

A method of compensation for apparent strain is described in *M-M TECH NOTE TN-504*. The apparent strain can be compensated by employing a compensating or "dummy" strain gage which is identical to the "active" gage. This gage is mounted on an unstrained or "dummy" specimen made from the same material as the test specimen and is subjected to the same temperature as the active gage. Since the thermal expansion of a unidirectional composite varies with the change of fiber orientation, a different type of dummy specimen should be used for each test specimen configuration. Once the dummy gage is connected in an adjacent arm of the Wheatstone bridge circuit, the apparent strain in the active and dummy gages cancel exactly since identical resistance changes in adjacent arms of the Wheatstone bridge do not cause any imbalance in the circuit. Thus, only the stress-induced strain in the active strain gage is recorded. Furthermore, as mentioned above, since the S-T-C gages were used in this research, excellent temperature compensation could be achieved over a wide temperature range.

The coefficient of thermal expansion of graphite/aluminum was measured by monitoring temperature induced strains. The strain gage output of the stress-free specimen subjected to the temperature change include apparent strain of the gage as well as thermal strain of the specimen. The apparent strain of the gage can be obtained by measuring the strain of the gage mounted on a piece of ultralow expansion glass. Subtracting the apparent strain from the total strain of the specimen gives the thermal strain of the specimen.

2.2.4 Shear Strain

Hereafter, a 1-2 coordinate system is used in the principal material directions and an *x*-*y* coordinate system is used in the lamina coordinates. The angle from the *x*-axis to the 1-axis, θ, is defined as shown in Fig. 5.

In order to obtain the in-plane shear modulus G_{12} using the off-axis tension test or the Iosipescu shear test, the shear strain in the principal material direction γ_{12} must be determined. Consider a 3-element 45° rectangular stacked rosette whose x-direction gage is oriented at the angle θ with respect to the principal material direction. If the normal strains along the gage are designated as ε_0, ε_{45} and ε_{90} as shown in Fig. 5, from elementary mechanics,

$$\varepsilon_0 = \frac{\varepsilon_1 + \varepsilon_2}{2} + \frac{\varepsilon_1 - \varepsilon_2}{2}\cos 2\theta + \frac{\gamma_{12}}{2}\sin 2\theta \tag{2.1}$$

$$\begin{aligned}\varepsilon_{45} &= \frac{\varepsilon_1 + \varepsilon_2}{2} + \frac{\varepsilon_1 - \varepsilon_2}{2}\cos 2(\theta + 45°) + \frac{\gamma_{12}}{2}\sin 2(\theta + 45°) \\ &= \frac{\varepsilon_1 + \varepsilon_2}{2} - \frac{\varepsilon_1 - \varepsilon_2}{2}\sin 2\theta + \frac{\gamma_{12}}{2}\cos 2\theta\end{aligned} \tag{2.2}$$

$$\begin{aligned}\varepsilon_{90} &= \frac{\varepsilon_1 + \varepsilon_2}{2} + \frac{\varepsilon_1 - \varepsilon_2}{2}\cos 2(\theta + 90°) + \frac{\gamma_{12}}{2}\sin 2(\theta + 90°) \\ &= \frac{\varepsilon_1 + \varepsilon_2}{2} - \frac{\varepsilon_1 - \varepsilon_2}{2}\cos 2\theta - \frac{\gamma_{12}}{2}\sin 2\theta\end{aligned} \tag{2.3}$$

From Eqs. (2.1), (2.2) and (2.3),

$$\varepsilon_0 - \varepsilon_{90} = (\varepsilon_1 - \varepsilon_2)\cos 2\theta + \gamma_{12}\sin 2\theta$$

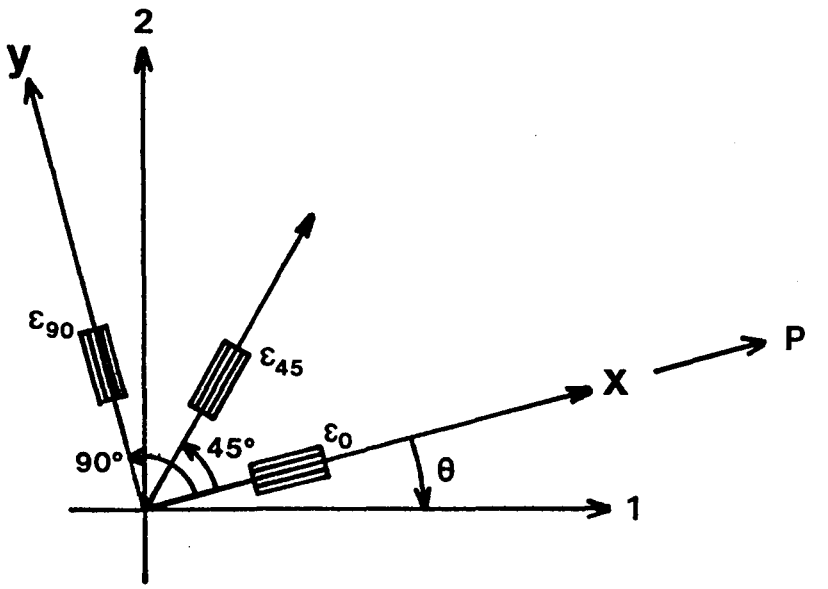

Figure 5. Definition of rotation of 1-2 axes from x-y axes and a 3-element 45° rosette for shear strain measurement

$$\varepsilon_0 + \varepsilon_{90} - 2\varepsilon_{45} = (\varepsilon_1 - \varepsilon_2) \sin 2\theta - \gamma_{12} \cos 2\theta$$

Solving for γ_{12},

$$\gamma_{12} = (\varepsilon_0 - \varepsilon_{90}) \sin 2\theta - (\varepsilon_0 + \varepsilon_{90} - 2\varepsilon_{45}) \cos 2\theta \qquad (2.4)$$

2.3 *Test Methods*

2.3.1 Tension Test

2.3.1.1 Longitudinal and Transverse Loading

Since 0° and 90° specimens are orthotropic in the plane, the so called "shear-coupling effect" does not occur even if these specimens are loaded with the ends of the specimen rigidly gripped and prevented from rotation. Thus Instron grips which rigidly grip the specimen were used for room temperature test. However, for the low and high temperature tests in a chamber, the Instron grips were too large. Therefore, small rotating end grips (Fig. 6), originally designed for off-axis tension tests, were used. Typical specimen size for the 0° and 90° tests was 0.5 in. wide and 6 in. long with 1.5 in. at either end reserved for gripping. Rather short specimens can be used since stress and strain distributions are uniform throughout the specimen even if their ends are rigidly gripped.

Since there is no shear deformation for this specimen configuration, only tensile response and Poisson's response of the material were obtained. The axial stress σ_{xx} in the loading direction is calculated as

$$\sigma_{xx} = \frac{P}{A_t} \tag{2.5}$$

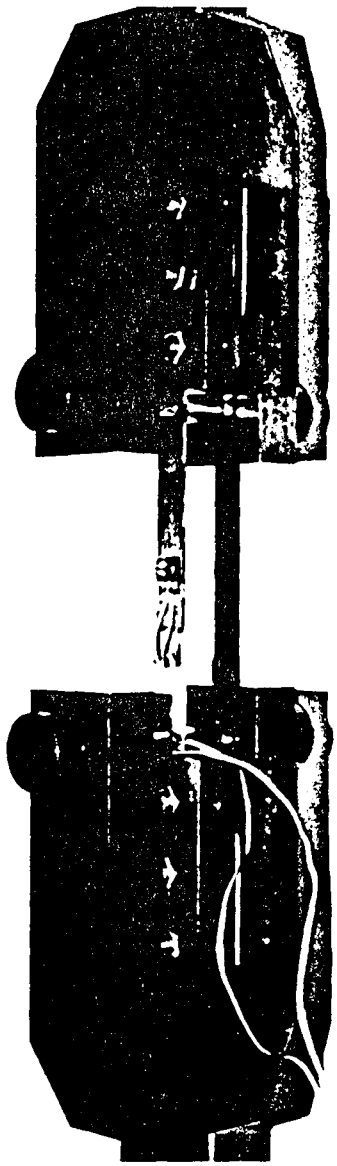

Figure 6. Rotating end-grip test fixture assembly

where P is the axial load and A_t is the cross-sectional area of the specimen. The strain in the longitudinal (loading) direction and that in the transverse direction are designated as ε_{xx} and ε_{yy}, respectively. Then, Young's modulus in the x-direction and Poisson's ratio are defined as

$$E_{xx} = \frac{\sigma_{xx}}{\varepsilon_{xx}} \tag{2.6}$$

$$\nu_{xy} = -\frac{\varepsilon_{yy}}{\varepsilon_{xx}} \tag{2.7}$$

For 0° test, E_{xx} and ν_{xy} correspond to E_{11} and ν_{12}, respectively, and for 90° test, E_{xx} and ν_{xy} correspond to E_{22} and ν_{21}, respectively.

2.3.1.2 Off-Axis Test

If a unidirectional composite is subjected to tension under off-axis loading conditions, the specimen behavior is not orthotropic. Instead, coupling between normal stress and shear strain is introduced. If the specimen is stressed without any lateral constraint, it distorts into a parallelogram (Fig. 7a). However, it is almost impossible to pull the specimen under such ideal conditions. In most cases, the ends of the specimens are firmly gripped during the test. This prevents free deformation, induces shear force at the ends and results in in-plane bending as schematically shown in Fig. 7b. This has been called the *end-constraint effect* [41]. Its extent is a function of aspect ratio of the specimen, material properties and off-axis orientation.

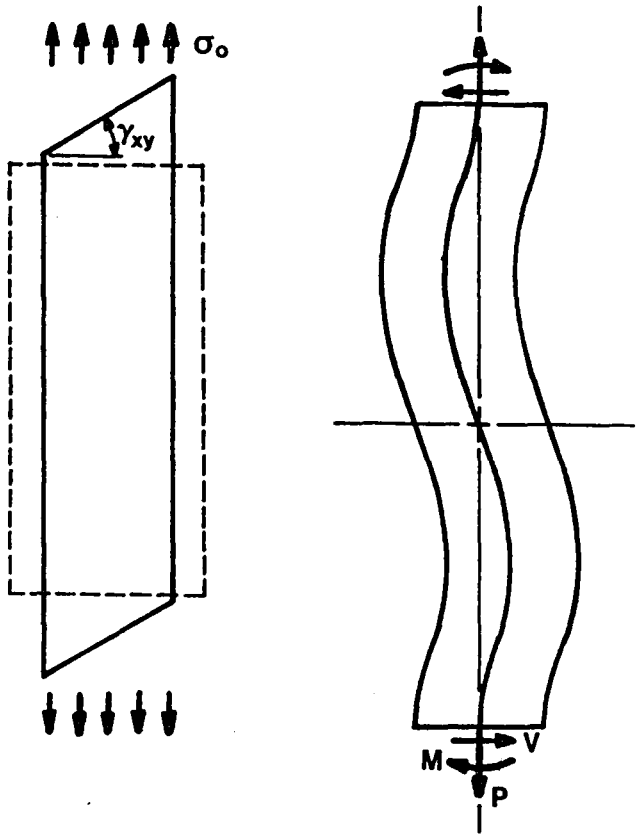

(a) Uniform state of stress

(b) Effect of clamped ends

Figure 7. Influence of end constraint in the testing of anisotropic body

Pagano and Halpin [41] gave a closed-form approximate solution to the end-constraint problem. They introduced the apparent Young's modulus E^*_{xx} which is erroneously estimated under end-constraint conditions. In a later paper, Pindera and Herakovich [42] discussed the apparent shear modulus G^*_{12} and the apparent Poisson's ratio ν^*_{xy}.

In the end-constrained specimen, stress and strain distributions are non-uniform. At the midpoint of the specimen, the relationship between stresses and strains is expressed as

$$\begin{Bmatrix} \varepsilon_{xx} \\ \varepsilon_{yy} \\ \gamma_{xy} \end{Bmatrix} = \begin{bmatrix} \bar{S}_{11} & \bar{S}_{12} & \bar{S}_{16} \\ \bar{S}_{12} & \bar{S}_{22} & \bar{S}_{26} \\ \bar{S}_{16} & \bar{S}_{26} & \bar{S}_{66} \end{bmatrix} \begin{Bmatrix} \sigma_{xx} \\ 0 \\ \tau_{xy} \end{Bmatrix} \tag{2.8}$$

with σ_{xx} and τ_{xy} given by

$$\sigma_{xx} = C_2 \tag{2.9}$$

$$\tau_{xy} = \beta\sigma_{xx} \tag{2.10}$$

where

$$C_2 = \frac{\bar{S}_{11} + 6\left(\frac{h}{l}\right)^2\bar{S}_{66}}{\bar{S}^2_{11} + 6\left(\frac{h}{l}\right)^2(\bar{S}_{11}\bar{S}_{66} - \bar{S}^2_{16})}\varepsilon_0 \tag{2.11}$$

$$\beta = -\frac{6\left(\frac{h}{l}\right)^2\frac{\bar{S}_{16}}{\bar{S}_{11}}}{1 + 6\left(\frac{h}{l}\right)^2\frac{\bar{S}_{66}}{\bar{S}_{11}}} \tag{2.12}$$

ε_0 is the applied center-line strain, $\bar{S}_{ij}$ are the transformed compliances in the lamina coordinates and h and l are the half-width and length of the specimen, respectively. In the experiment, though, we measure the average axial stress $\bar{\sigma}_{xx}$ which is defined as Eq. (2.5). In Pagano and Halpin's solution, this is expressed in terms of σ_{xx} as

$$\bar{\sigma}_{xx} = \left(1 - \frac{2}{3}\eta\right)\sigma_{xx} \tag{2.13}$$

where

$$\eta = -\frac{6\left(\frac{h}{l}\right)^2\left(\frac{\bar{S}_{16}}{\bar{S}_{11}}\right)^2}{1 + 6\left(\frac{h}{l}\right)^2\frac{\bar{S}_{66}}{\bar{S}_{11}}} \tag{2.14}$$

Noting that

$$\eta = -\frac{\bar{S}_{16}}{\bar{S}_{11}}\beta \tag{2.15}$$

from Eqs. (2.8), (2.10) and (2.15),

$$\begin{aligned}\varepsilon_{xx} &= (\bar{S}_{11} + \beta\bar{S}_{16})\sigma_{xx} \\ &= \bar{S}_{11}(1 - \eta)\sigma_{xx}\end{aligned} \tag{2.16}$$

$$\varepsilon_{yy} = (\bar{S}_{12} + \beta\bar{S}_{26})\sigma_{xx} \tag{2.17}$$

Equation (2.16) can be rewritten as

$$\frac{\sigma_{xx}}{\varepsilon_{xx}} = \frac{1}{\bar{S}_{11}(1 - \eta)} = \frac{E_{xx}}{1 - \eta} \tag{2.18}$$

By using Eqs. (2.13) and (2.18), the expression for the apparent Young's modulus E^*_{xx} becomes

$$E^*_{xx} = \frac{\bar{\sigma}_{xx}}{\varepsilon_{xx}} = \left(1 - \frac{2}{3}\eta\right)\frac{\sigma_{xx}}{\varepsilon_{xx}} = \frac{1 - \frac{2}{3}\eta}{1 - \eta}E_{xx} \tag{2.19}$$

Finally, the ratio of the true modulus to the apparent modulus is obtained as

$$\frac{E_{xx}}{E^*_{xx}} = \frac{1 - \eta}{1 - \frac{2}{3}\eta} \tag{2.20}$$

Similarly, from Eqs. (2.16) and (2.17), the apparent Poisson's ratio can be expressed as

$$\nu^*_{xy} = -\frac{\varepsilon_{yy}}{\varepsilon_{xx}} = -\frac{\bar{S}_{12}}{\bar{S}_{11}}\frac{1 + \beta\frac{\bar{S}_{26}}{\bar{S}_{12}}}{1 + \beta\frac{\bar{S}_{16}}{\bar{S}_{11}}} = \nu_{xy}\frac{1 + \beta\frac{\bar{S}_{26}}{\bar{S}_{12}}}{1 + \beta\frac{\bar{S}_{16}}{\bar{S}_{11}}} \tag{2.21}$$

Then the ratio of ν_{xy} to ν^*_{xy} becomes

$$\frac{\nu_{xy}}{\nu^*_{xy}} = \frac{1 + \beta\frac{\bar{S}_{16}}{\bar{S}_{11}}}{1 + \beta\frac{\bar{S}_{26}}{\bar{S}_{12}}} \tag{2.22}$$

By using the stress transformation equations, the shear stress τ_{12} in the 1-2 coordinate system at the midpoint of the end-constraint specimen is

$$\tau_{12} = -\sigma_{xx}\sin\theta\cos\theta + \tau_{xy}(\cos^2\theta - \sin^2\theta) \tag{2.23}$$

Substituting Eqs. (2.10) and (2.13) in (2.23),

$$\tau_{12} = -\frac{\bar{\sigma}_{xx}}{1-\frac{2}{3}\eta}[\sin\theta\cos\theta - \beta(\cos^2\theta - \sin^2\theta)] \tag{2.24}$$

However, in the experiment, the shear stress τ_{xy} induced by the end-constraint effect is generally ignored and only the average axial stress $\bar{\sigma}_{xx}$ is used to obtain the apparent shear stress τ_{12}^* as follows:

$$\tau_{12}^* = -\bar{\sigma}_{xx}\sin\theta\cos\theta \tag{2.25}$$

If the apparent shear modulus is defined by $G_{12}^* = \frac{\tau_{12}^*}{\gamma_{12}}$, dividing Eq. (2.24) by Eq. (2.25) gives

$$\frac{G_{12}}{G_{12}^*} = \frac{\tau_{12}}{\tau_{12}^*} = \frac{1}{1-\frac{2}{3}\eta}\left[1 - \beta\frac{(\cos^2\theta - \sin^2\theta)}{\sin\theta\cos\theta}\right] \tag{2.26}$$

In this research, the average stress $\bar{\sigma}_{xx}$ defined by Eq.(2.5) was obtained and the apparent shear stress τ_{12}^* defined by Eq. (2.25) was computed for all the off-axis tension tests. Then, $\bar{\sigma}_{xx}$ vs ε_{xx}, ε_{yy} vs ε_{xx} and τ_{12}^* vs γ_{12} relations were plotted for each test. Estimating initial tangents of these curves graphically, E_{xx}^* , ν_{xy}^* and G_{12}^* were obtained. Finally, by the use of Eqs. (2.20), (2.22) and (2.26), the true modulus values E_{xx}, ν_{xy} and G_{12} were determined, respectively.

In the experiment, in order to reduce the end-constraint effect, two important measures were employed: the use of high aspect ratio specimens, and the use of a rotating, fixed-grip fixture. It has been shown that the end-constraint effect decreases with the increase in specimen aspect ratio [40, 41]. Therefore, specimens with gage

length of 7 in. were used for all the off-axis tension tests. As the specimen width was 0.5 in., the specimen aspect ratio was 14. The rotating end grips used in the experiments were originally designed by Pindera and Herakovich [40]. The grips not only reduce the end-constraint effects but also eliminate alignment problems.

2.3.2 Iosipescu Test

It has been shown that the 45° specimen is the best off-axis tension specimen to determine the in-plane shear modulus G_{12} [40, 42]. However, the 45° off-axis specimen is not good for determination of shear strength. It has been reported by several investigators that an excellent test method to determine both the initial shear modulus and ultimate shear strength is the Iosipescu test [43-47]. The Iosipescu shear test was originally proposed by Nicolae Iosipescu of Bucharest, Rumania in the early 1960's. Although his primary interest was to test isotropic materials, several investigators have applied this test method to composite materials. Complete details are described by Walrath and Adams [45].

Figure 8 shows the Iosipescu specimen configuration which was proposed by Walrath and Adams [46] and used by Pindera et al [47]. It is 3 in. long and 0.75 in. wide with an 'as-received' thickness of 0.040 ± 0.001 in. A 110° notch is cut on each edge of the specimen at the midlength to a depth of 0.15 in. Notch tips are rounded to avoid the complex stress state which may contribute to failure, as suggested by Herakovich et al [43, 44]. Specimens with fibers oriented parallel and perpendicular to the longitudinal axis were designated as 0° and 90° Iosipescu specimen, respectively. The test fixture used for the Iosipescu test is shown in Fig. 9. This is a modification of the

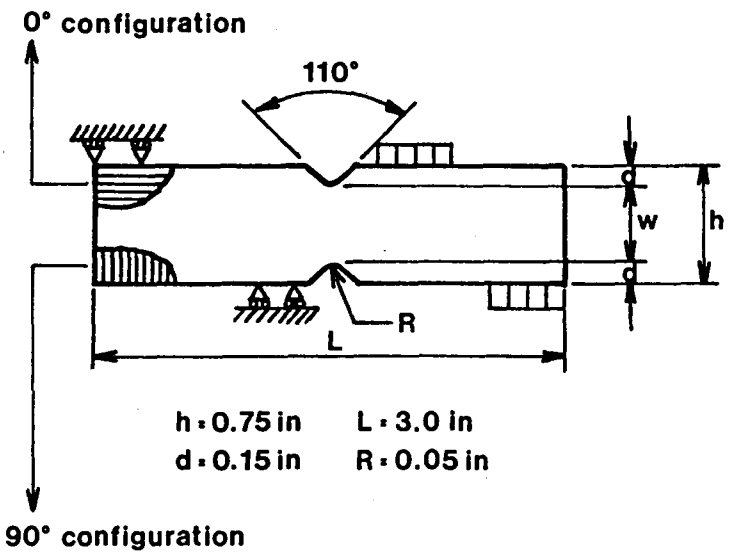

Figure 8. Iosipescu shear test configuration

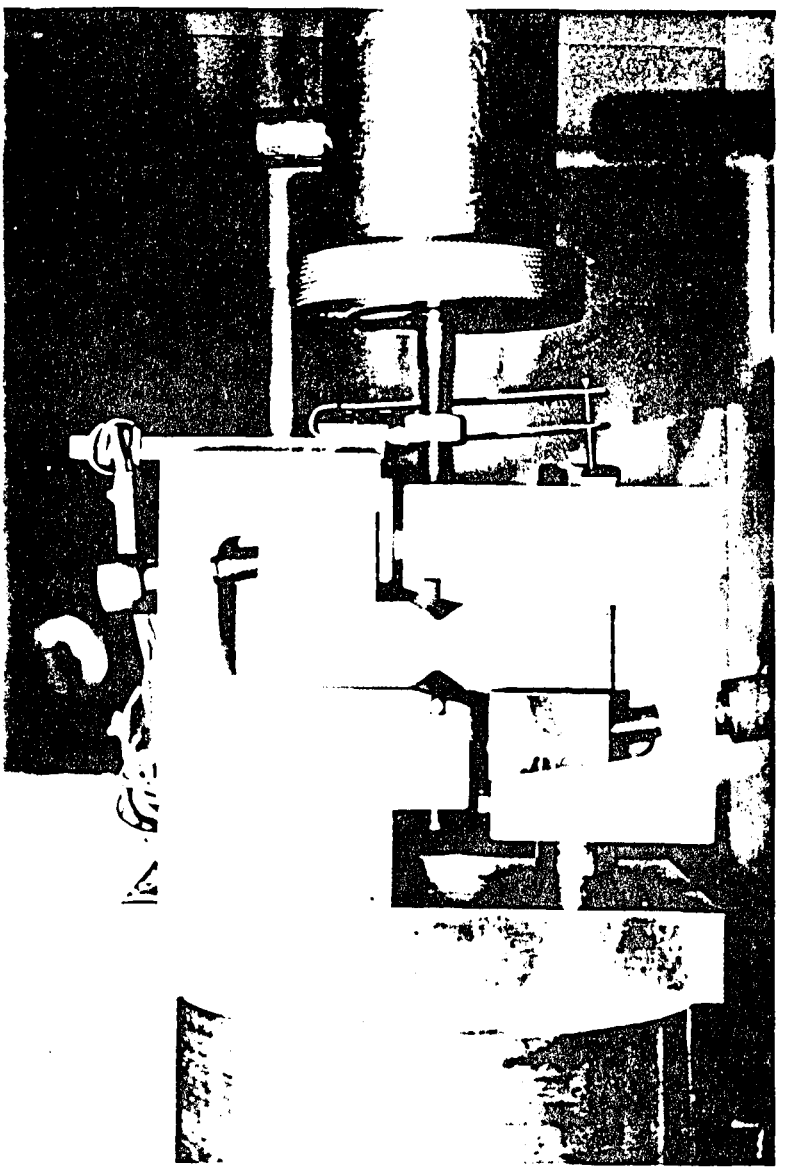

Figure 9. Iosipescu test fixture assembly

original model designed by Walrath and Adams [46]. A state of nearly pure shear stress can be obtained at specimen mid-length by application of two counteracting moments produced by two force couples. During the test, the average shear stress $\bar{\tau}_{12}$ is obtained by

$$\bar{\tau}_{12} = \frac{P}{A_l} \tag{2.27}$$

where P is the vertical force applied to the Iosipescu specimen and A_l is the cross-sectional area between the V-notches. The shear strain γ_{12} is obtained from the three normal strains as indicated by Eq. (2.4). The apparent shear modulus G^*_{12} is defined by

$$G^*_{12} = \frac{\bar{\tau}_{12}}{\gamma_{12}} \tag{2.28}$$

Pindera et at [47] have carried out finite element calculations for aramid/epoxy and graphite/polyimid Iosipescu specimens and obtained shear stress distributions along the test section. For the 0° specimen, it was shown that the shear stress at the center of the specimen is lower than the average shear stress $\bar{\tau}_{12}$ for both materials and that the apparent shear modulus G^*_{12} becomes seven percent higher than the true G_{12} obtained from the 45° off-axis tension test. For the 90° specimen, on the other hand, the opposite results are obtained; the shear stress at the center is higher than $\bar{\tau}_{12}$ and G^*_{12} is 17% lower than G_{12}. The 0° specimen was recommended as the preferred specimen because the 90° specimen gives very low apparent shear strength. To confirm this for the present material, several 90° Iosipescu tests were conducted at room temperature.

2.4 *Testing Procedure*

2.4.1 Testing System

All the tests were conducted on a United Testing System (UTS) screw-driven, displacement controlled testing machine. Load was introduced at a constant crosshead speed and measured by a load cell. An IBM-XT personal computer with a Data Translation DT 2805/5716 board controlled the tests and acquired the data from load cell and strain gages. Computer control was accomplished using the software program MATPAC2 [48]. This program also has a post processor which enables calculation of stresses and strains, and display of several types of graphs. After local processing, the data were transferred to the IBM main frame computer for additional plotting and data analysis. The entire testing system is shown in Fig. 10.

2.4.2 Temperature Control

All the room temperature tests were performed at ambient room conditions. The laboratory was air-conditioned and the temperature was maintained at approximately 75°F. All high and low temperature tests were conducted using an environmental chamber capable of controling the temperature range from -300°F to +800°F. The load cell was located outside the chamber and isolated from temperature variations.

For high temperature tests, an electric heater and an internal fan were used to raise the temperature at a rate of about +5°F/min. As mentioned previously, the rotating

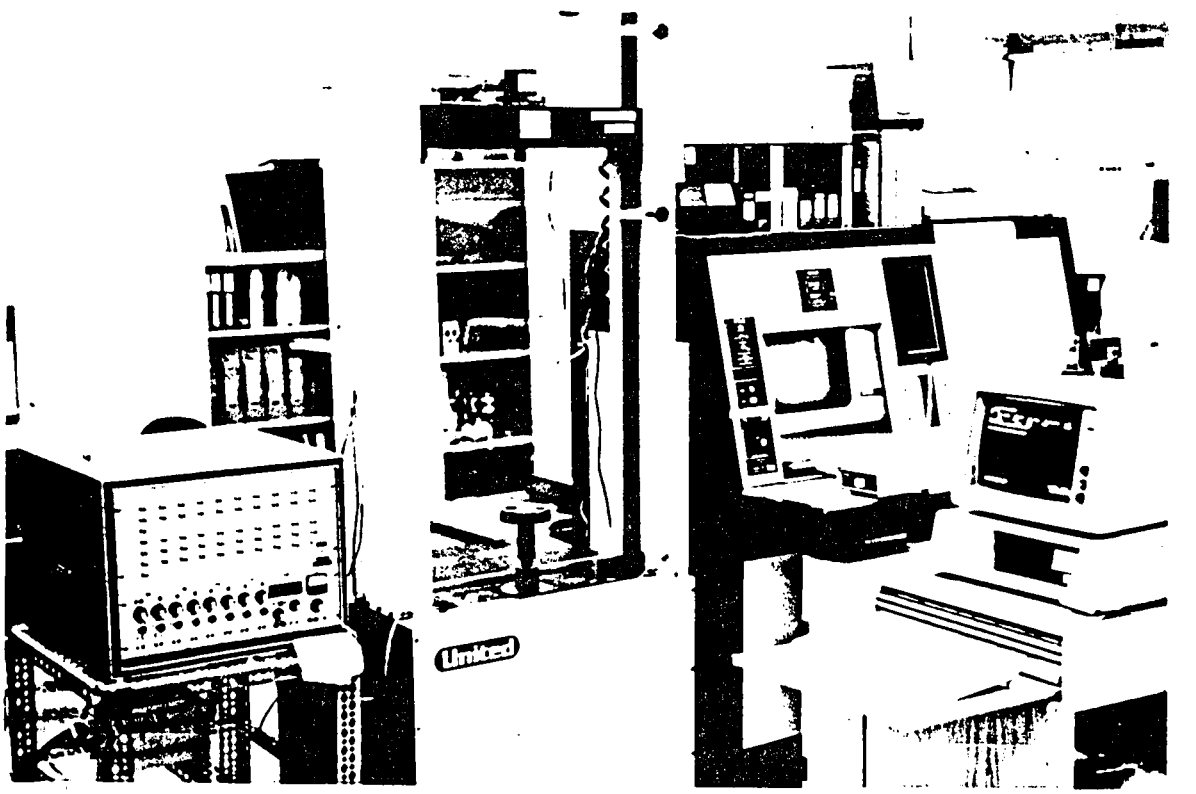

Figure 10. Test system consisting of UTS machine, IBM-XT computer and signal conditioner

grips were used for the tests in the chamber. These grips were tightened by bolts and nuts which were made from high strength steels. Because the bolts expand in their axial direction when heated, the gripping force decreases remarkably for high temperature tests. This may result in slipping between test specimen and grips. In fact, all the 0° specimens started to slip at a stress level of 60 to 70 ksi which is far lower than the ultimate tensile strength. All the 15° and 90° specimens failed prior to slippage because their ultimate strengths are rather low. To overcome the problem for 0° tests, the grips/specimen assembly, tightened at room temperature, was heated up to the test temperature in the chamber, removed from the chamber and retightened quickly while still hot. By employing this procedure, all the 0° tension specimens failed successfully at high temperature.

For low temperature tests, liquid nitrogen was used to cool the specimen at a rate of -5°F/min. Since steel bolts shrink when they are cooled, grips/specimen assembly tightened at room temperature would be further tightened at lower temperature. Thus all the low temperature tests were conducted without any difficulty.

As mentioned in the previous section, correction for apparent strain errors was made for high and low temperature tests. The "dummy" specimen was placed on a portion of the grips nearest to the specimen in order to ensure that the temperature of both specimens was the same. The temperature was monitored by means of a thermocouple placed on the grip surface near the specimen. The thermocouple was not attached directly to the specimen because if attached it sometimes resulted in significant noise to the output.

3.0 Results and Discussion

Experimental results are discussed in the following three parts:

- Room temperature properties: the variation of moduli and strengths with the fiber angle (Section 3.1).
- The effect of temperature on moduli and strengths: the effect of residual stress on material behavior (Section 3.2).
- Thermo-mechanical response: the effect of thermo-mechanical history on material behavior (Section 3.3).

Average values of experimental data and some representative data are presented in this chapter. Individual data are summarized in Appendix A. Although stress and modulus are expressed in terms of ksi and msi, respectively, in the text and tables, MPa and GPa are used in the figures together with ksi and msi. Strain scales of cyclic test results at different temperatures given in 3.2 are shifted for the comparison.

3.1 *Modulus and Strength at Room Temperature*

3.1.1 Modulus

Figures 11 and 12 show representative tensile responses (σ_{xx} vs. ε_{xx}) and Poisson's responses (ε_{yy} vs. ε_{xx}) of different off-axis specimens. Figure 13 shows representative shear responses (τ_{12} vs. γ_{12}) obtained from 10°, 15° and 45° off-axis tension tests and 0° and 90° Iosipescu shear tests. Initial slopes of each curve corresponds to laminate Young's modulus E_{xx}, Poisson's ratio ν_{xy} and shear modulus G_{12}, respectively. These modulus values were estimated graphically. The average values of these moduli as well as ultimate stresses and strains are listed in Tables 6 and 7. Average modulus values include the results of the initial loading of cyclic tests and all the moduli listed here are apparent values. However, only monotonic data are included in average ultimate stress and strain because in general ultimate strength increases after a loading/unloading cycle.

Lamina moduli E_{11}, ν_{12}, E_{22} and G_{12} can be defined by E_{xx} for 0°, ν_{xy} for 0°, E_{xx} for 90° and G_{12} for 45°, respectively. The determination of G_{12} from 45° tests is based on the discussion that the error in G_{12} caused by the end-constraint effect (Eq. (2.26)) is negligible for this configuration (Pindera and Herakovich [42]).

Longitudinal tensile modulus E_{11} can be estimated by the rule of mixture

$$E_{11} = v_f E_f + (1 - v_f) E_m \tag{3.1}$$

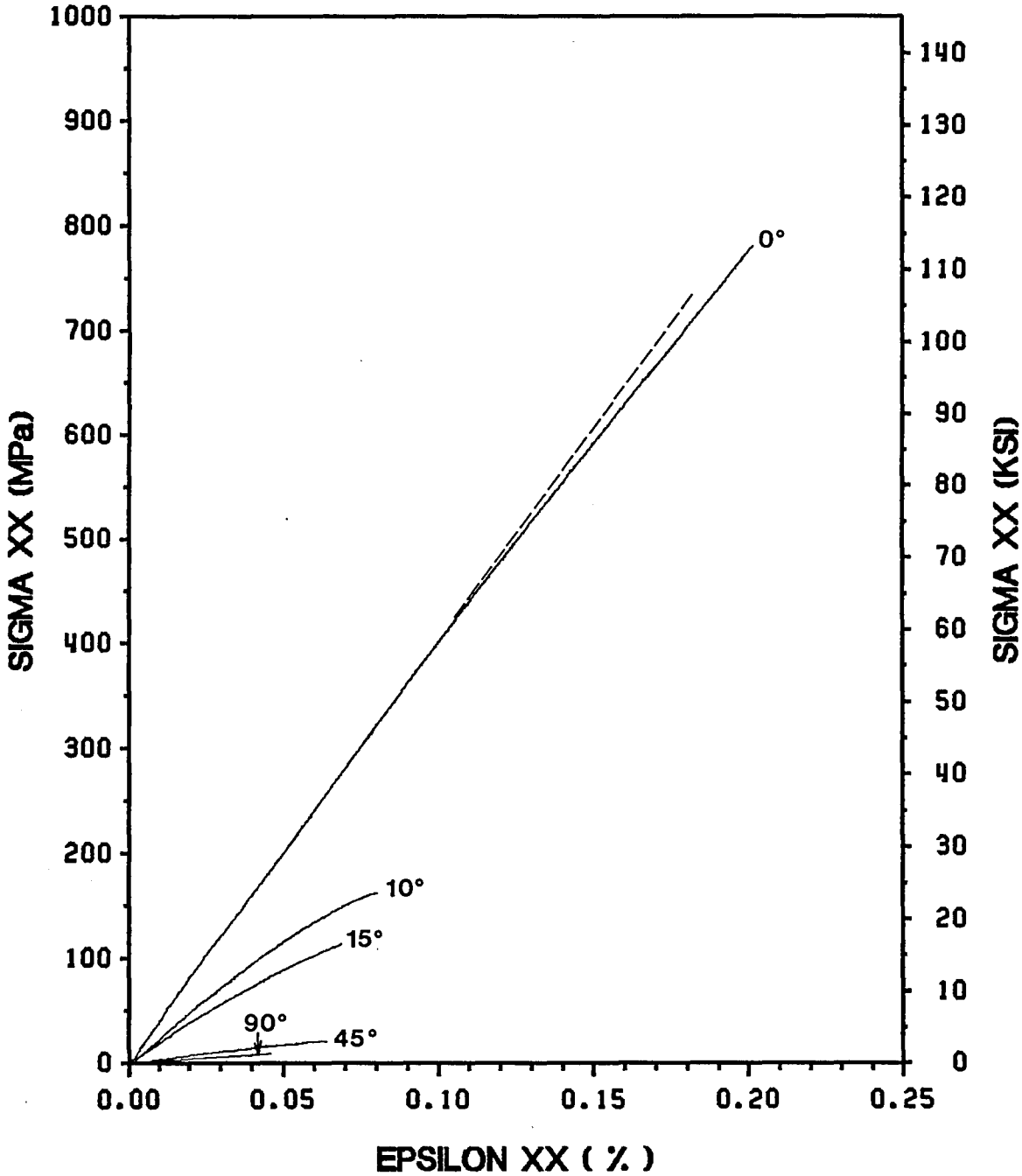

Figure 11. Tensile response of different off-axis specimens under monotonic loading at room temperature

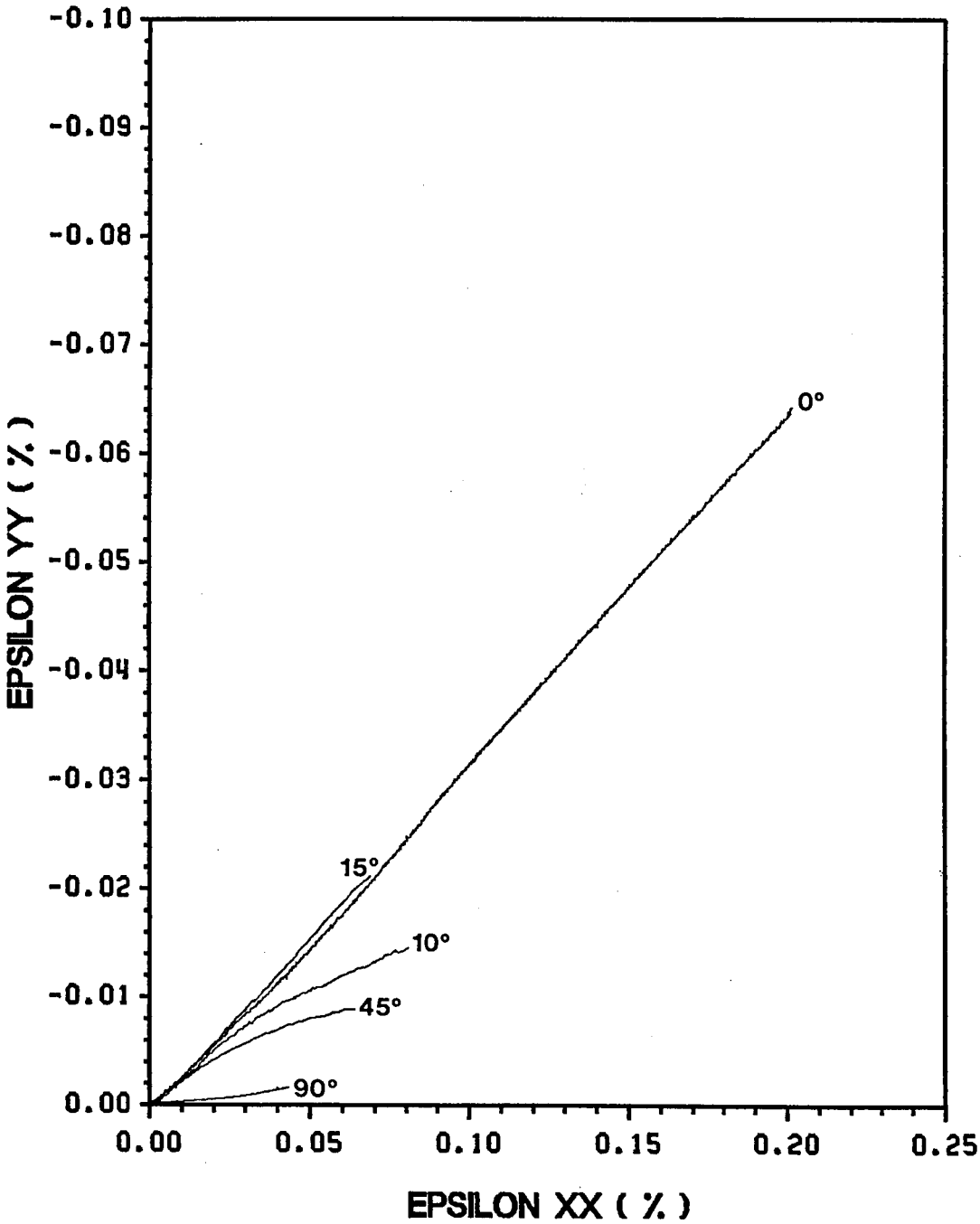

Figure 12. Poisson's response of different off-axis specimens under monotonic loading at room temperature

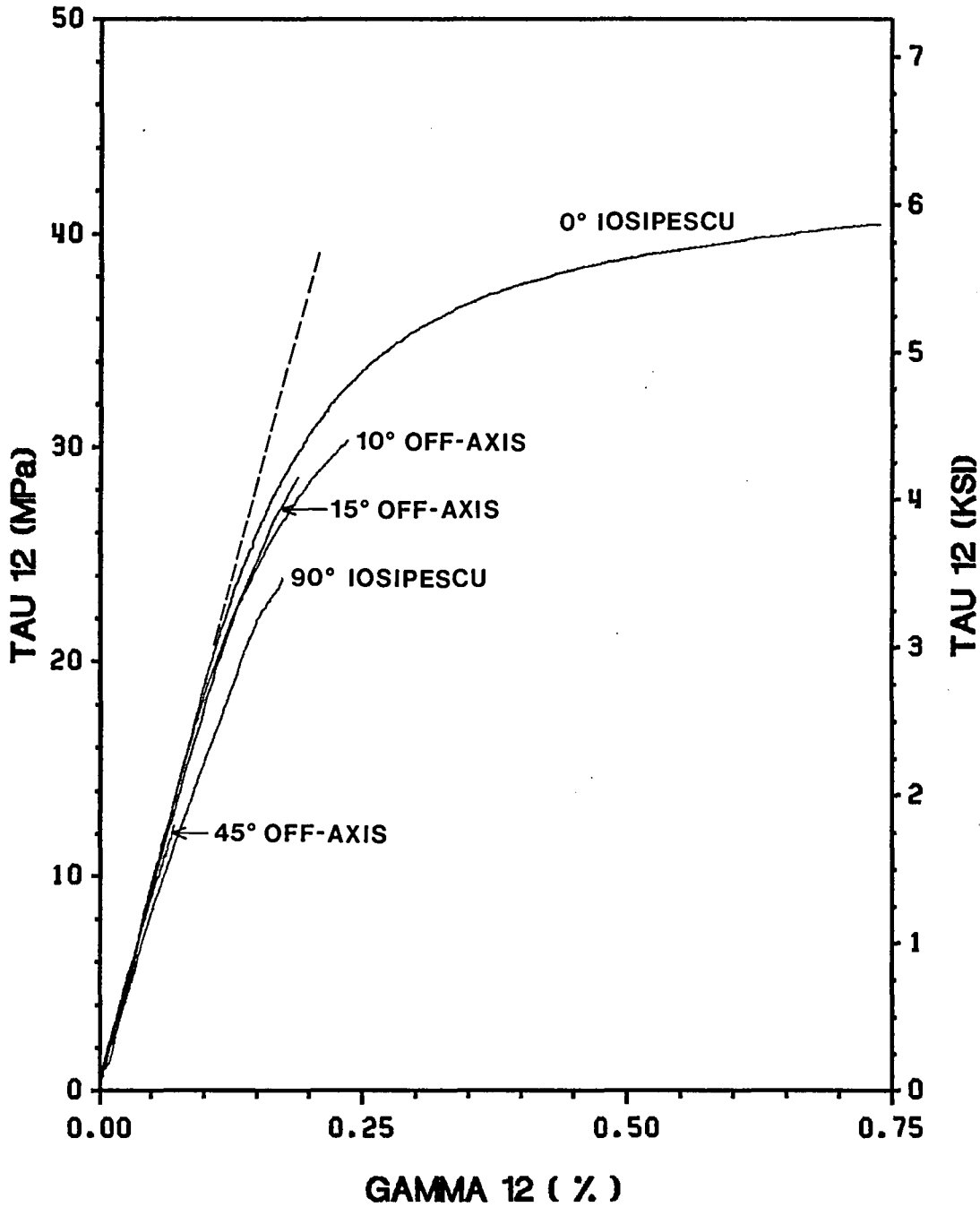

Figure 13. Shear response of different specimens under monotonic loading at room temperature

Table 6. Tensile properties at room temperature

Fiber Orientation	Elastic Modulus, E_{xx}(msi)	Poisson's Ratio, ν_{xy}	Ultimate Stress, σ_{xx}(ksi)	Ultimate Strain, ε_{xx}(%)
0°	58.4	0.291	118.1	0.205
10°	36.6	0.267	23.7	0.086
15°	27.9	0.263	15.6	0.065
45°	6.0	0.175	3.4	0.066
90°	3.5	0.028	1.3	0.042

Table 7. Shear properties at room temperature

Fiber Orientation	Shear Modulus, G_{12}(msi)	Ultimate Stress, τ_{12}(ksi)	Ultimate Strain, γ_{12}(%)
Tension			
10°	2.73	4.4	0.221
15°	2.80	4.0	0.176
45°	2.46	1.7	0.074
Iosipescu			
0°	2.76	5.1	0.484
90°	1.78	2.9	0.184

where v_f, E_f and E_m are the fiber volume fraction, the longitudinal tensile modulus of fiber and the tensile modulus of matrix, respectively. From Tables 1 and 2,

$$E_f = 105.0\ msi$$

$$E_m = 9.9\ msi$$

and

$$v_f = 0.4657$$

Substituting these values in Eq. (3.1),

$$E_{11} = 54.2\ msi$$

It can be said that the prediction of E_{11} by the rule of mixture agrees with the experimental value of 58.4 msi fairly well.

Using the lamina moduli, $E_{11}, E_{22}, \nu_{12}, G_{12}$, off-axis moduli can be predicted by the transformation law:

$$E_{xx}(\theta) = \frac{1}{\frac{1}{E_{11}}\cos^4\theta + \left(\frac{1}{G_{12}} - \frac{2\nu_{12}}{E_{11}}\right)\sin^2\theta\cos^2\theta + \frac{1}{E_{22}}\sin^4\theta} \tag{3.2}$$

$$\nu_{xy}(\theta) = E_{xx}(\theta)\left[\frac{\nu_{12}}{E_{11}}(\sin^4\theta + \cos^4\theta) - \left(\frac{1}{E_{11}} + \frac{1}{E_{22}} - \frac{1}{G_{12}}\right)\sin^2\theta\cos^2\theta\right] \tag{3.3}$$

These off-axis moduli can be converted to correct values using Eqs.(2.20) and (2.22). Figures 14 and 15 show E_{xx} and ν_{xy} as a function of the off-axis angle, respectively. Vertical lines with tick marks, solid lines and dotted lines designate experimental values, predicted values by Eqs. (3.2) and (3.3), and corrected values by Eqs. (2.20)

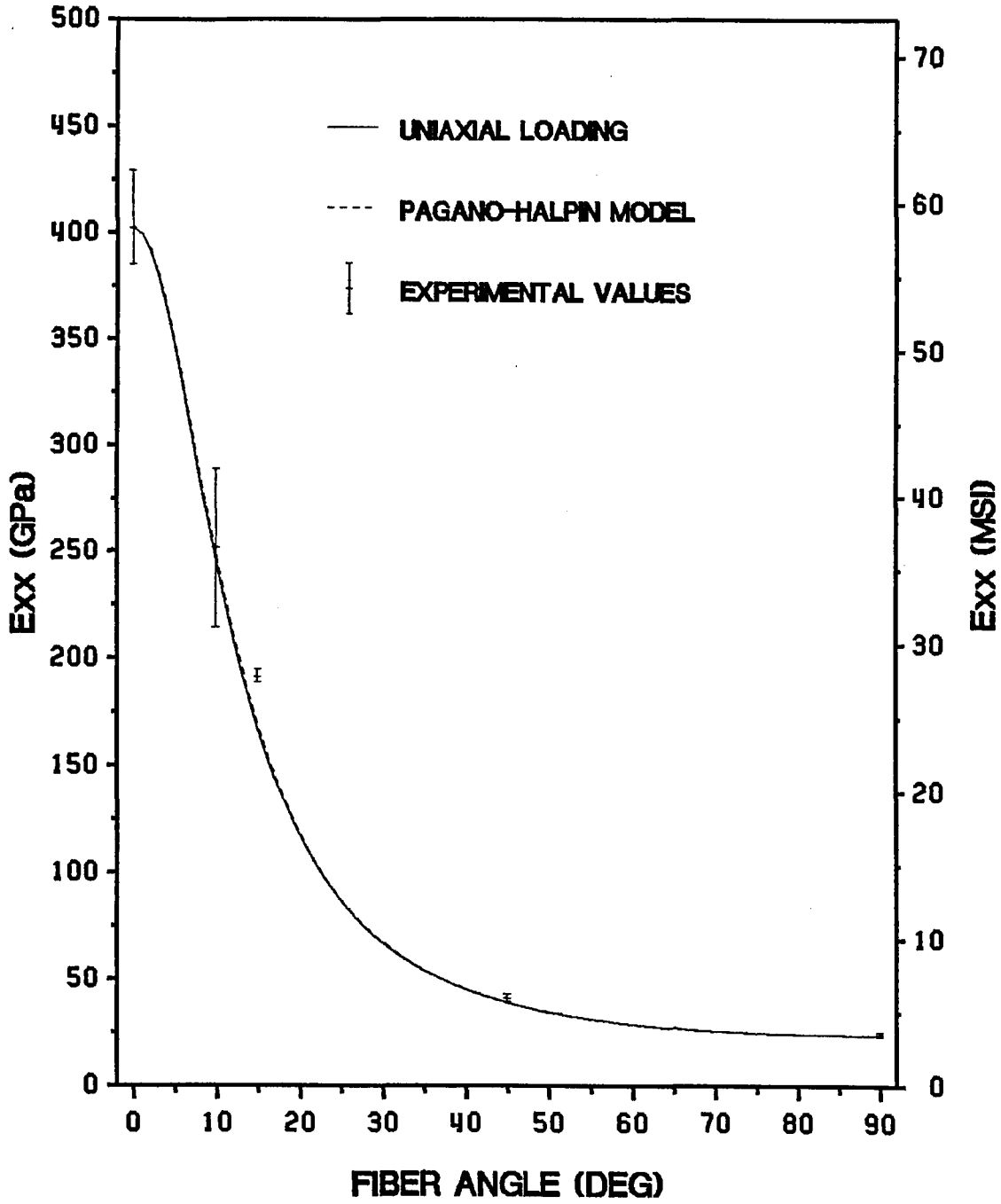

Figure 14. Off-axis elastic modulus as a function of fiber orientation at room temperature

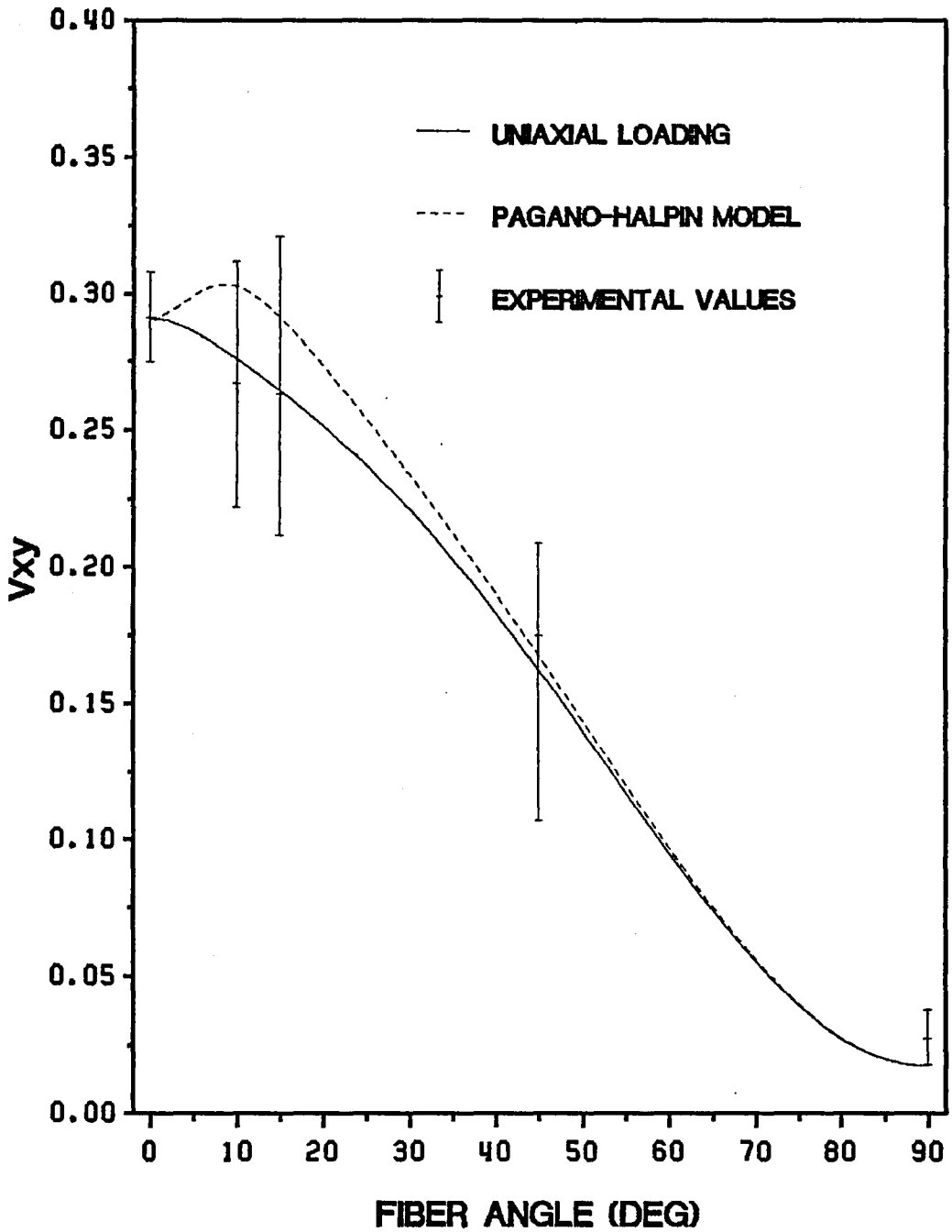

Figure 15. Off-axis Poisson's ratio as a function of fiber orientation at room temperature

and (2.22), respectively. The end-constraint effect is negligible for E_{xx} whereas it is significant for ν_{xy} at the angle between 0° and 30°. Although data scatters exist especially for ν_{xy}, experimental values agree with theoretical ones very well.

Unlike E_{xx} and ν_{xy}, G_{12} is a material constant; in other words, G_{12} should not depend on the off-axis angle. Figure 16 shows measured values of G_{12} as a function of the off-axis angle. The vertical lines with tick marks and solid line indicate experimental values and the theoretical prediction by Pagano-Halpin model (Eq. (2.26)), respectively. It is seen that the end-constraint effect is not insignificant for the low off-axis angle between 0° and 15°. Although G_{12} for the 15° tests exhibit higher values than theoretical predictions, as a whole, discrepancies in G_{12} values obtained by different types of off-axis tests are explained by the end-constraint effect. The 0° and 90° Iosipescu shear test results are also included in Fig. 16. The 0° Iosipescu test gives a high G_{12} value while the 90° Iosipescu test results in very low G_{12} . The result coincides with the discussion obtained by Pindera et al [47]. The correct value of G_{12} could be obtained from both Iosipescu tests through the use of correction factors obtained from finite element analysis [47].

3.1.2 Strength

Figure 17 shows the variation of failure stresses of tension tests as a function of fiber orientation. The strength decreases dramatically with the increase in fiber angle. Transverse strength is very low; the average value is 1.3 ksi. The recent work on P100/6061 composites by Dries and Tompkins [49] has reported average transverse strength of 2.6 ksi. It is most likely that this poor transverse strength is due to low

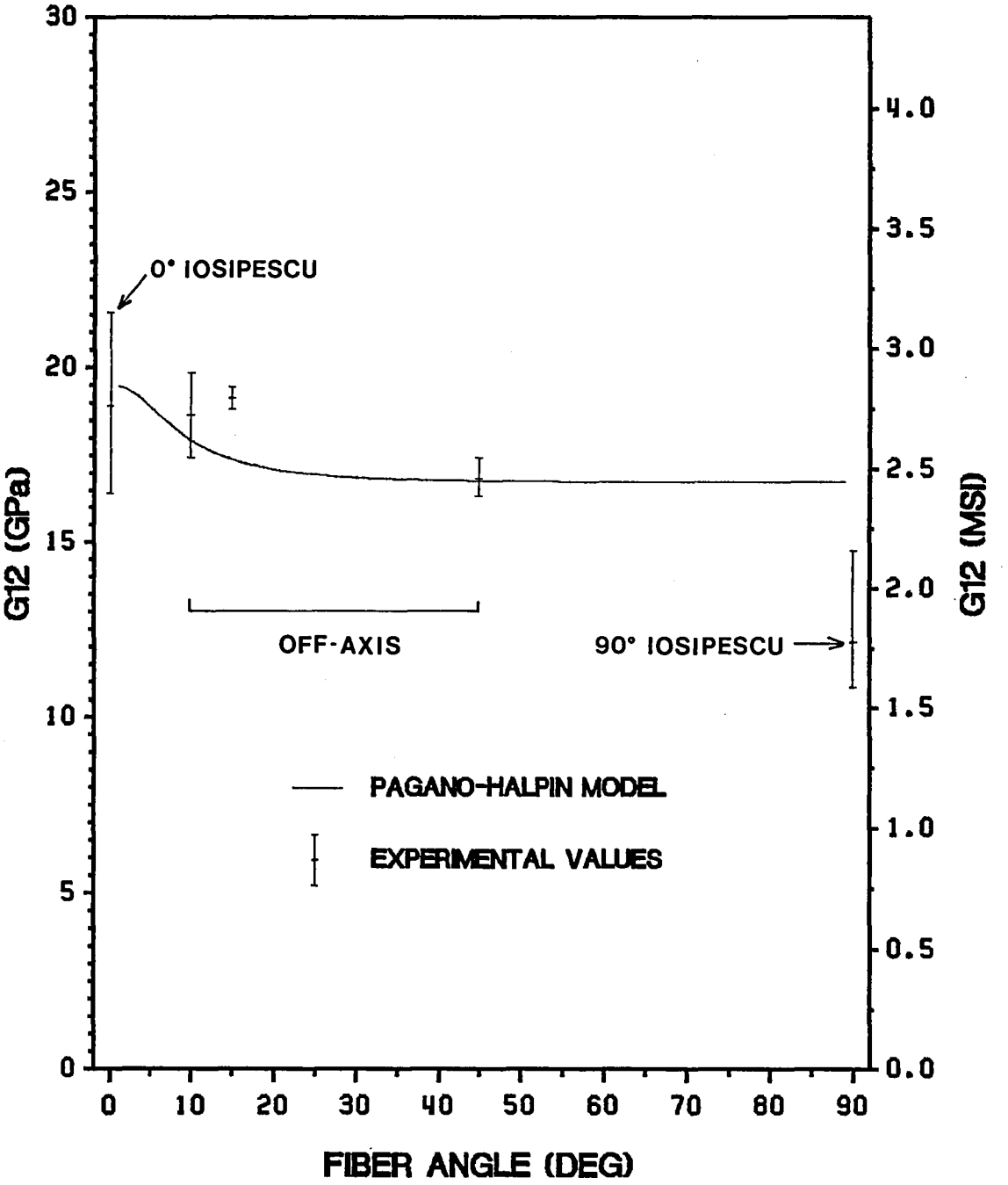

Figure 16. Shear modulus as a function of fiber orientation at room temperature

interfacial bond strength. The improvement of transverse strength has been a prime concern for aluminum/graphite composites.

The maximum stress theory and the Tsai-Wu tensor polynomial are often applied to predict the failure stress of unidirectional off-axis composite. The strength data used from this study are listed in Table 8. In the maximum stress theory, failure occurs if one of the stresses in the principal material directions satisfies one of

$$\begin{aligned} \sigma_1 &= X_t \\ \sigma_2 &= Y_t \\ |\tau_{12}| &= S \end{aligned} \tag{3.4}$$

By the Tsai-Wu theory, an orthotropic lamina under plane stress condition fails if

$$F_1\sigma_1 + F_2\sigma_2 + F_{11}\sigma_1^{\,2} + F_{22}\sigma_2^{\,2} + F_{66}\tau_{12}^{\,2} + 2F_{12}\sigma_1\sigma_2 = 1 \tag{3.5}$$

where

$$\begin{aligned} F_1 &= \frac{1}{X_t} + \frac{1}{X_c} \\ F_2 &= \frac{1}{Y_t} + \frac{1}{Y_c} \\ F_{11} &= -\frac{1}{X_t X_c} \\ F_{22} &= -\frac{1}{Y_t Y_c} \\ F_{66} &= \frac{1}{S^2} \\ F_{12} &= -\frac{\sqrt{F_{11}F_{22}}}{2} \end{aligned} \tag{3.6}$$

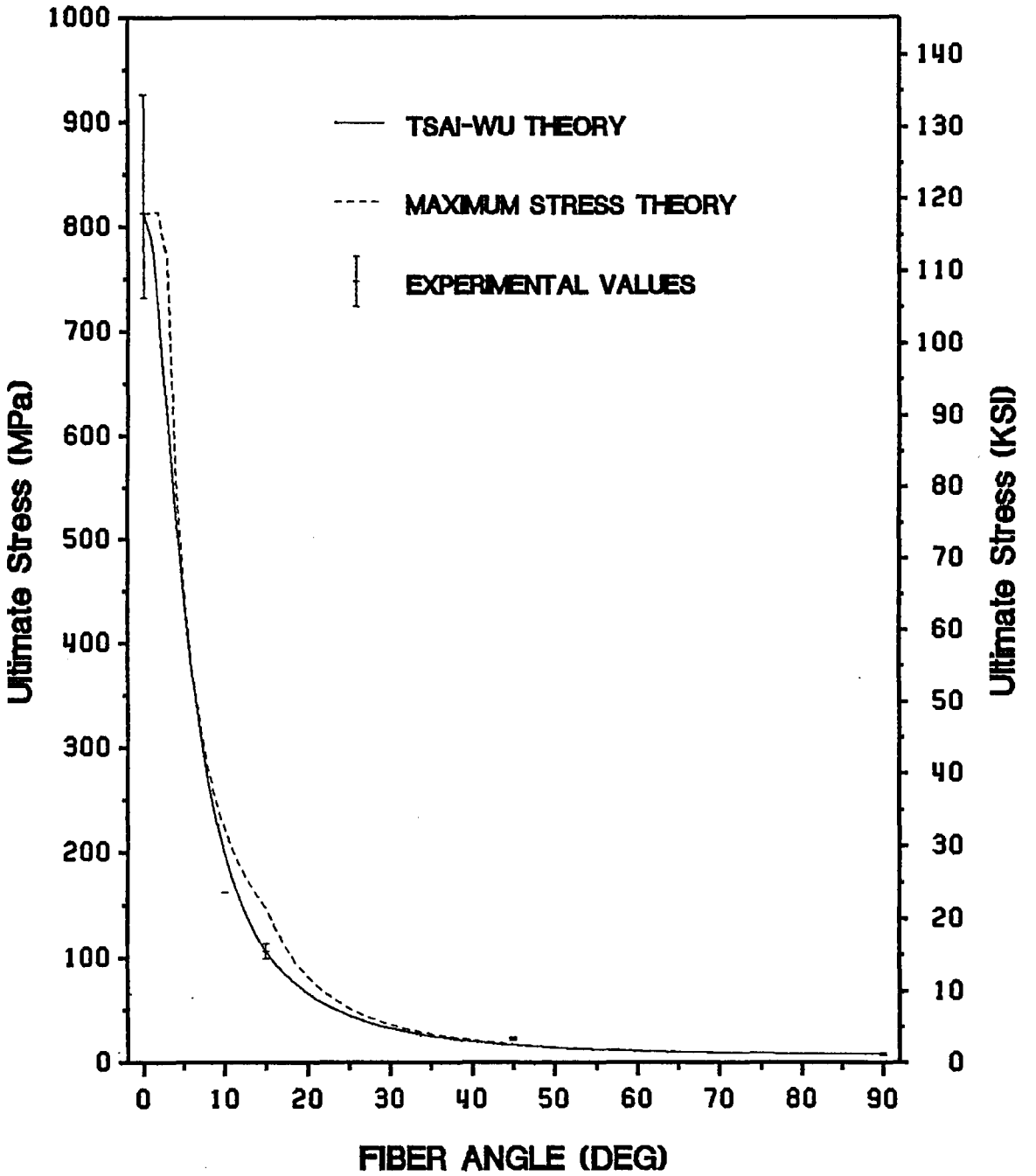

Figure 17. Off-axis tensile strength as a function of fiber orientation at room temperature

Table 8. **Strength at room temperature**

X_t	=	118.1	ksi
Y_t	=	1.3	ksi
X_c*	=	-42.1	ksi
Y_c*	=	-14.8	ksi
S**	=	5.1	ksi

* Experiments by James M. Starbuck - private communication
** 0° Iosipescu test results

The last relation in Eq. (3.6) is obtained by assuming the criterion (3.5) is a generalization of the von Mises criterion. In the end-constrained specimen, as discussed in 2.3.1.2, the stresses in the principal material directions are obtained as

$$\begin{Bmatrix} \sigma_1 \\ \sigma_2 \\ \tau_{12} \end{Bmatrix} = \begin{bmatrix} \cos^2\theta & \sin^2\theta & 2\sin\theta\cos\theta \\ \sin^2\theta & \cos^2\theta & -2\sin\theta\cos\theta \\ -\sin\theta\cos\theta & \sin\theta\cos\theta & \cos^2\theta - \sin^2\theta \end{bmatrix} \begin{Bmatrix} \sigma_{xx} \\ 0 \\ \tau_{xy} \end{Bmatrix} \tag{3.7}$$

where τ_{xy} is the shear stress induced by the end-constraint effect. Using Eq. (2.10) with Eq. (2.12), Eq. (3.7) can be rewritten as

$$\begin{aligned} \sigma_1 &= \sigma_{xx}[\cos^2\theta + 2\beta\sin\theta\cos\theta] \\ \sigma_2 &= \sigma_{xx}[\sin^2\theta - 2\beta\sin\theta\cos\theta] \\ \tau_{12} &= \sigma_{xx}[-\sin\theta\cos\theta + \beta(\cos^2\theta - \sin^2\theta)] \end{aligned} \tag{3.8}$$

Then, the maximum stress theory (3.4) becomes

$$\sigma_{xx} = \frac{X_t}{\cos^2\theta + 2\beta \sin\theta \cos\theta}$$

$$\sigma_{xx} = \frac{Y_t}{\sin^2\theta - 2\beta \sin\theta \cos\theta} \qquad (3.9)$$

$$\sigma_{xx} = \frac{S}{\sin\theta \cos\theta - \beta(\cos^2\theta - \sin^2\theta)}$$

Substituting Eq. (3.8), the Tsai-Wu criterion (3.5) is expressed as

$$A\sigma_{xx}^{\ 2} + B\sigma_{xx} - 1 = 0 \qquad (3.10)$$

where

$$A = F_{11}(\cos^4\theta + 4\beta \sin\theta \cos^3\theta + 4\beta^2 \sin^2\theta \cos^2\theta)$$
$$+ F_{22}(\sin^4\theta - 4\beta \sin^3\theta \cos\theta + 4\beta^2 \sin\theta \cos\theta)$$
$$+ F_{66}[\sin^2\theta \cos^2\theta - 2\beta \sin\theta \cos\theta(\cos^2\theta - \sin^2\theta) + \beta^2(\cos^2\theta - \sin^2\theta)^2]$$
$$+ 2F_{12}[\sin^2\theta \cos^2\theta - 2\beta \sin\theta \cos\theta(\cos^2\theta - \sin^2\theta) - 4\beta^2 \sin^2\theta \cos^2\theta]$$

$$B = F_1(\cos^2\theta + 2\beta \sin\theta \cos\theta) + F_2(\sin^2\theta - 2\beta \sin\theta \cos\theta)$$

Solving Eq. (3.10),

$$\sigma_{xx} = \frac{-B + \sqrt{B^2 + 4A}}{2A} \qquad (3.11)$$

Predictions by two failure theories are included in Fig. 17. The solid line and the dotted line designate Tsai-Wu and maximum stress theory, respectively. It is seen that the Tsai-Wu theory predicts very accurate failure stresses while the maximum stress theory gives higher - in other words, unconservative - values at fiber angles of 10° and 15°.

Figure 18 shows shear stresses at failure obtained by 10°, 15° and 45° off-axis tension tests and 0° and 90° Iosipescu shear tests. Although the edges of specimens were crushed at some stage of the test, the 0° Iosipescu test shows the highest average shear strength. Also, this test exhibits extensive nonlinear response as shown in Fig. 13. On the other hand, the 90° Iosipescu test results in low shear strength. The 45° off-axis test, which is the best off-axis test to obtain G_{12} values [42], shows the lowest strength. Therefore, it is concluded that the 0° Iosipescu test is the best test method to obtain shear strength.

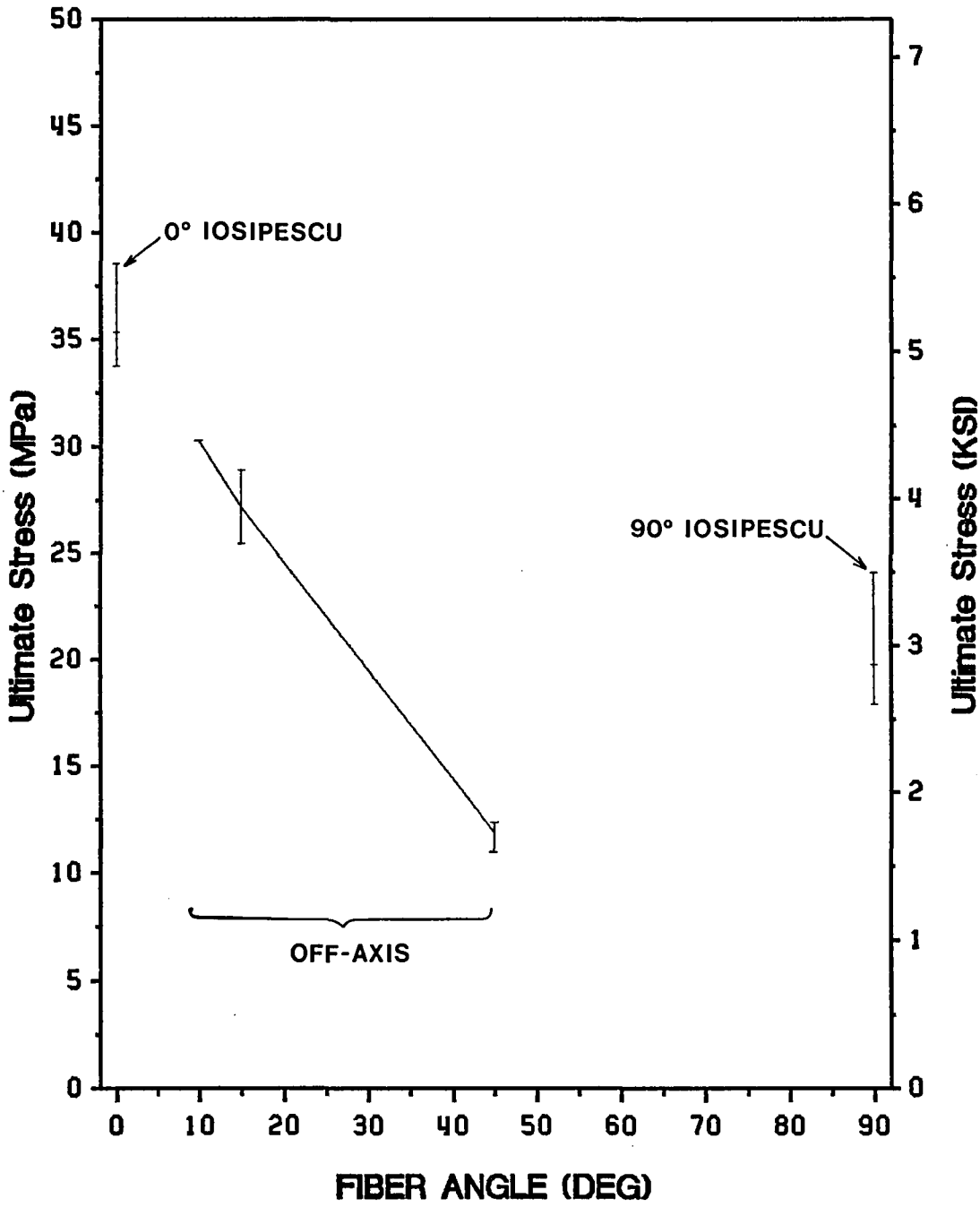

Figure 18. Shear strength as a function of fiber orientation at room temperature

3.2 *Effect of Temperature on Modulus and Strength*

3.2.1 Elastic Modulus

3.2.1.1 0° Specimen

Representative tensile response of 0° specimens under monotonic loading for all temperatures are shown in Fig. 19. It is seen that the initial slope of -150°F test result is remarkably low compared with those of other higher temperature results. The initial modulus E_{11} of -150°F test is 83% of +75°F test. Each result is so consistent that this reduction in E_{11} at -150°F may not be explained by experimental errors.

Figure 20 shows representative tensile response of 0° specimens under cyclic loading for all temperatures. Again, it is observed that the slope of the first loading curve of -150°F test is low. However, the slope of the subsequent unloading/loading curve is quite different from that of the first loading curve; it is almost parallel to the unloading/loading curves of other higher temperature tests. It is assumed that unless the material has yielded before loading, the unloading/loading curve in a cyclic test is parallel to the initial elastic portion of the first loading curve. Although this behavior is observed for other high temperature results, there is not such a portion parallel to the unloading/loading curve in the first loading curve of -150°F test. The only meaningful explanation for this -150°F test result is that the specimen had yielded prior to mechanical loading and that it exhibited strain hardening behavior

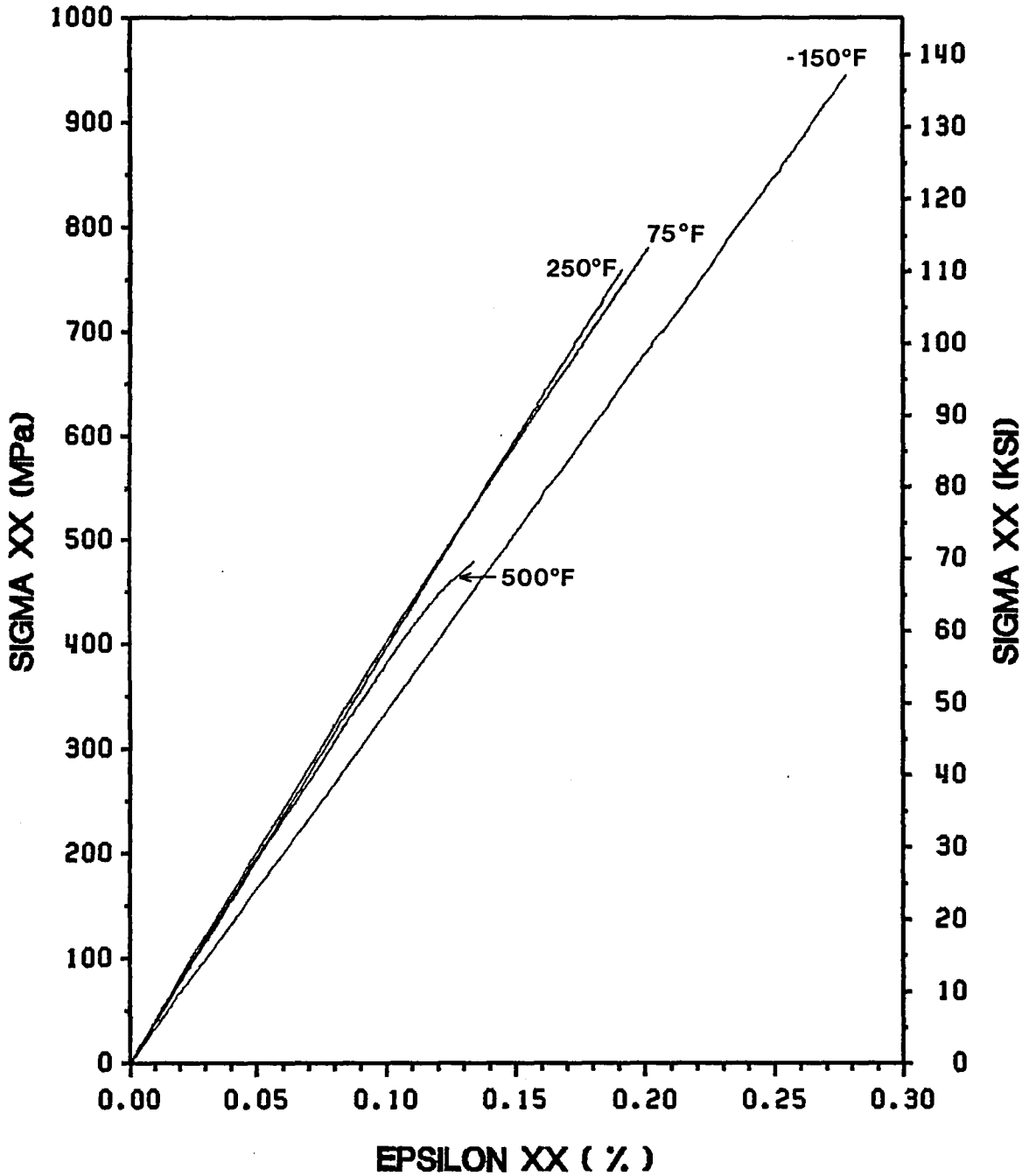

Figure 19. Tensile response of 0° tension specimens under monotonic loading for all temperatures

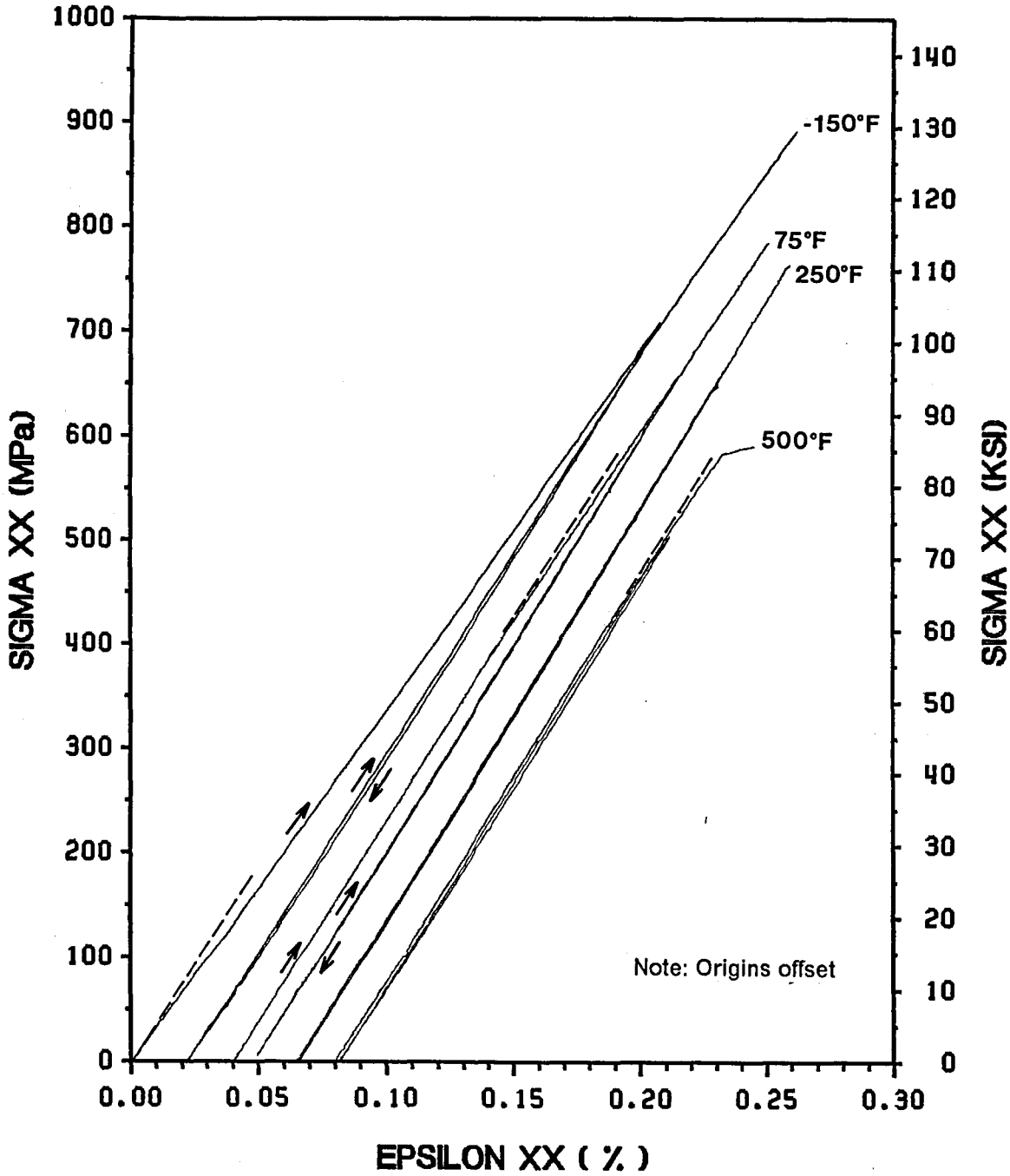

Figure 20. Tensile response of 0° tension specimens under cyclic loading for all temperatures

immediately after being subjected to load. In other words, the specimens had yielded in the cooling process.

Using a continuum theory, Min and Crossman [39] and Aboudi [37, 38] predicted the development of tensile residual stress in the aluminum matrix when being cooled down from the fabrication temperature. As stated in Section 1.4, this residual stress is caused by the mismatch in the coefficient of thermal expansion of fiber and matrix. The tensile residual stress in the matrix lowers the yield point of the composite when subjected to tensile load. The predicted tensile responses in the above references are quite similar to the present experimental results.

At +75°F, the initial portion of the first loading curve is parallel to the unloading/loading curve up to 54.8 ksi. Beyond this stress, the material exhibits nonlinear or strain hardening behavior. Thus, this stress can be defined as the yield stress of the composite. At +250°F, the initial loading and the subsequent unloading/loading curves are almost overlaid, which means the specimen exhibited elastic behavior and did not yield prior to the reversal point. Moreover, the specimen continued to exhibit elastic behavior until it failed. Thus, it is concluded that the yield stress is larger than failure stress at 250°F. At +500°F, a small amount of permanent strain is observed after unloading. As shown in Fig. 2, the properties of aluminum do not change much in the temperature range from +70°F to +400°F, but they exhibit very ductile behavior above +500°F. Although the residual stress becomes smaller at this higher temperature, the matrix properties are so deteriorated that the composite exhibits yielding at 60.5 ksi.

3.2.1.2 15° Specimen

Almost the same tensile response as 0° specimen is observed for 15° off-axis specimen as shown in Fig. 21. At -150°F, the material exhibits elastic behavior over a small portion of the first loading curve. However, due to the tensile residual stress developed in the matrix, the material soon yields at 1.8 ksi and strain hardens thereafter. At +75°F, where the residual stress are smaller, the material exhibits more elastic behavior than -150°F; the yield stress is 4.8 ksi at +75°F. At +250°F, the material exhibits the smallest permanent strain, indicating that the material yields just prior to the reversal stress. The yield stress is estimated to be 7.4 ksi for this case. At +500°F, the properties of aluminum are deteriorated so that the composite exhibits strain hardening earlier. The material yields at 2.6 ksi.

3.2.1.3 90° Specimen

Figure 22 shows representative tensile responses of 90° specimens under cyclic loading for all temperatures. As is the case with 0° and 15° specimens, changes in residual stress and aluminum properties with regard to temperature affect tensile response of 90° specimens. Since residual stress is high at -150°F, the material yields at an early stage: 0.18 ksi. As the temperature increases, the residual stress decreases, which results in an increase in yield stress. The yield stress is 0.32 ksi at +75°F and 0.62 ksi at +250°F. Although the residual stress becomes much smaller at 500°F, aluminum matrix properties are so deteriorated, as stated above, that the yield stress drops to 0.35 ksi.

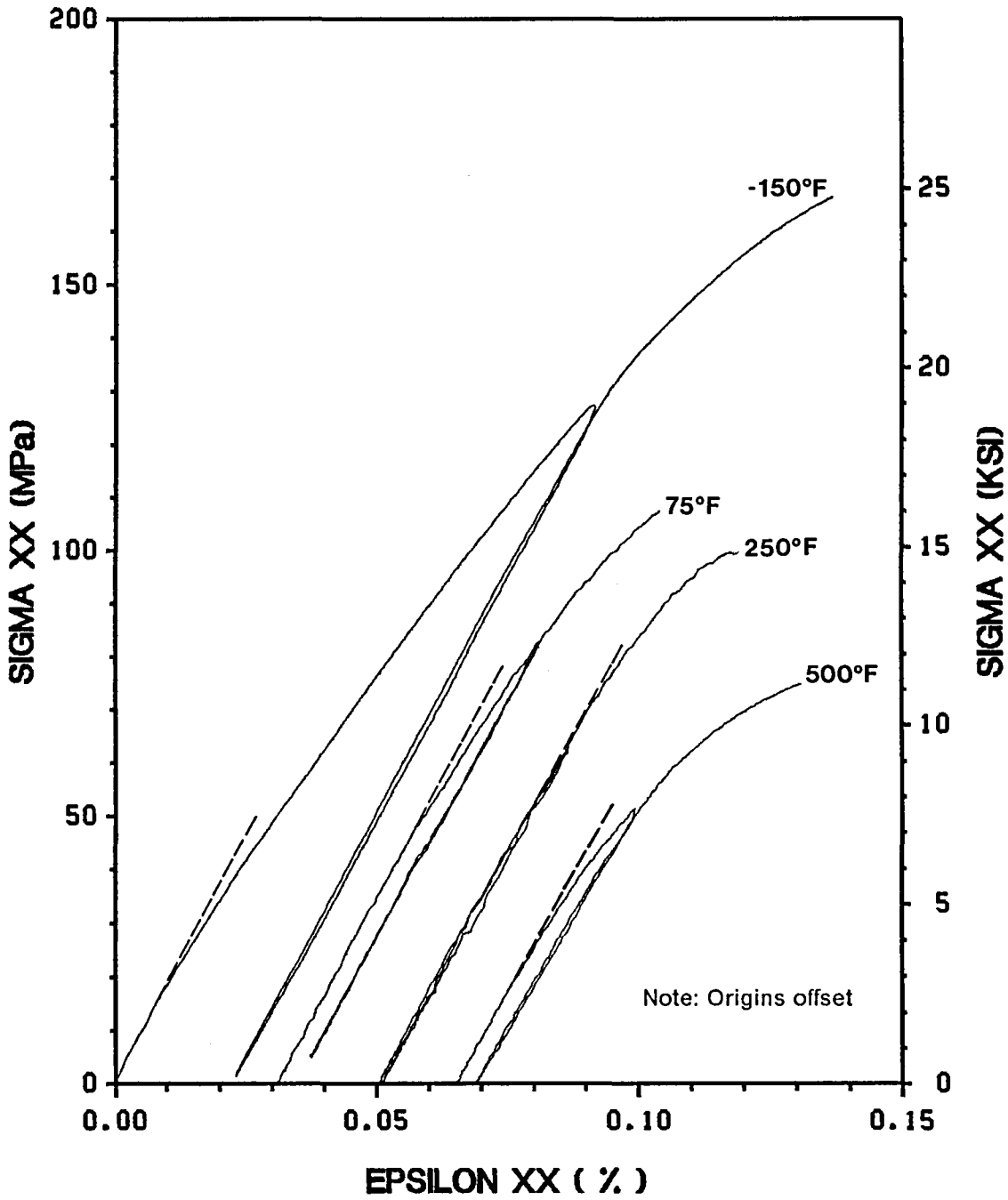

Figure 21. Tensile response of 15° tension specimens under cyclic loading for all temperatures

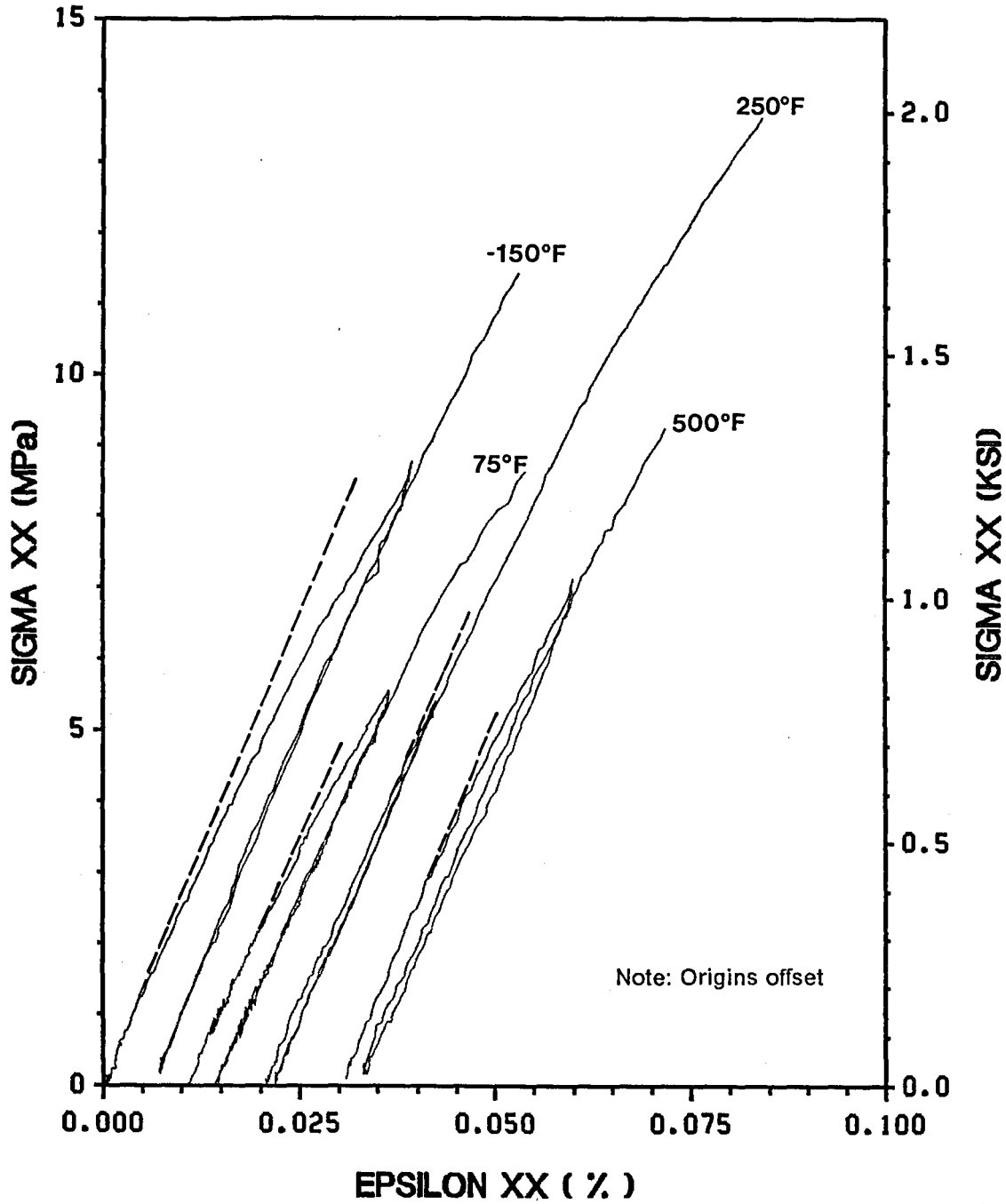

Figure 22. Tensile response of 90° tension specimens under cyclic loading for all temperatures

Table 9. Effect of temperature on yield stress

Temperature (°F)	Yield Stress, σ^{Y}_{xx}(ksi)		
	0°	15°	90°
-150	0.0	1.8	0.18
+75	54.8	4.8	0.32
+250	>116.5*	7.4	0.62
+500	60.5	2.6	0.35

* Failure stress

3.2.1.4 Yield Stress

Table 9 summarizes the axial stress at yield for each tensile test configuration. Figures 23 - 25 show yield stresses of 0°, 15° and 90° specimen as a function of temperature, respectively. As explained in 3.2.1.1, for the 0° specimen, the composite exhibits thermal yielding at -150°F and does not exhibit yielding prior to failure at +250°F. Thus, zero and failure stresses are plotted at these temperatures in Fig. 23. The highest yield stress is obtained at +250°F for all three configurations. Figure 26 illustrates the yield stress as a function of fiber angle for all temperatures. Drastic effects of residual stress and aluminum matrix properties are clearly seen in these figures. Due to the residual stress caused by the mismatch in coefficient of thermal expansion, the lowest yield stress is obtained at -150°F. As the temperature increases to +250°F, the residual stress becomes smaller and the yield stress in-

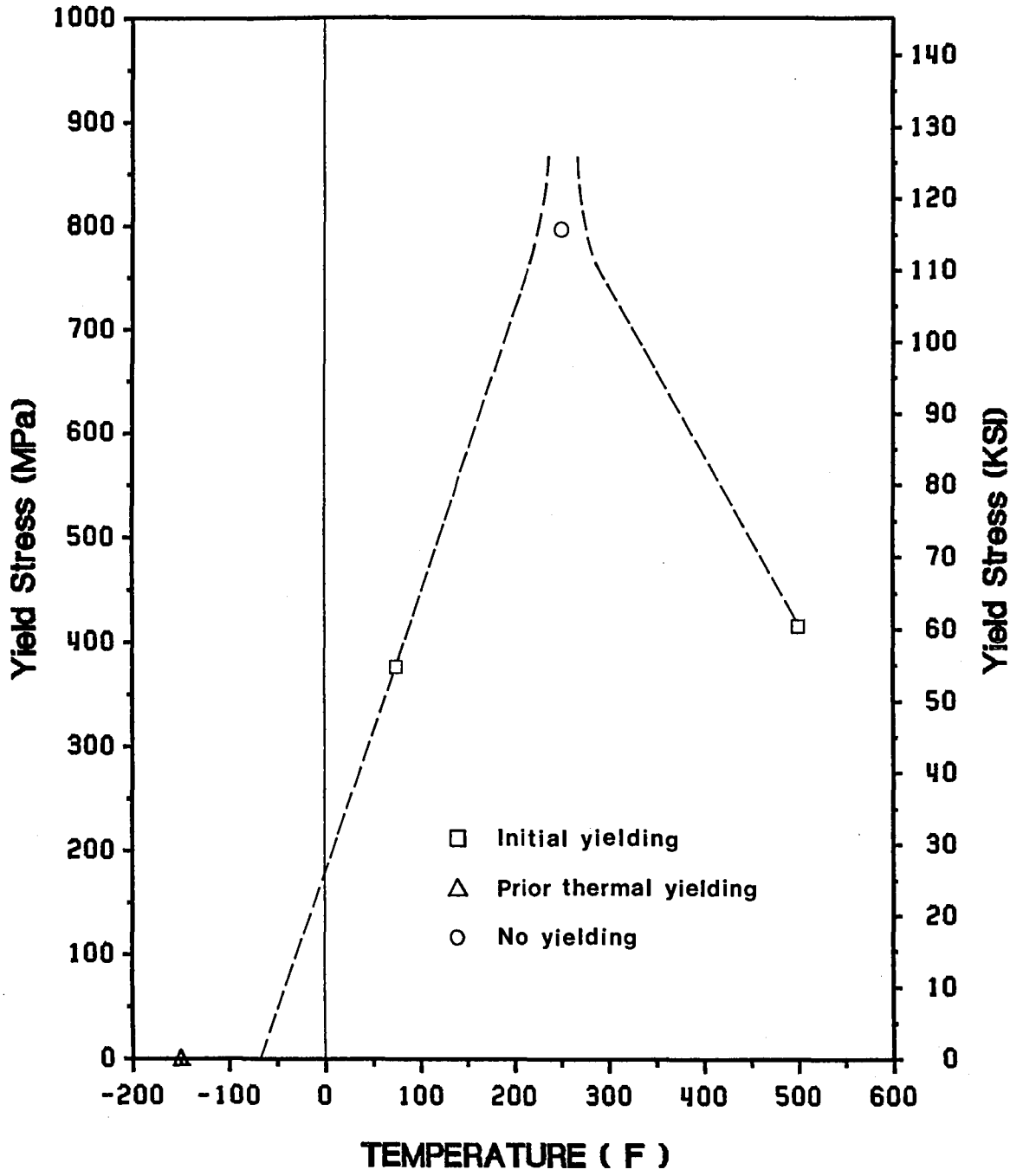

Figure 23. Yield stress of 0° tension specimens as a function of temperature

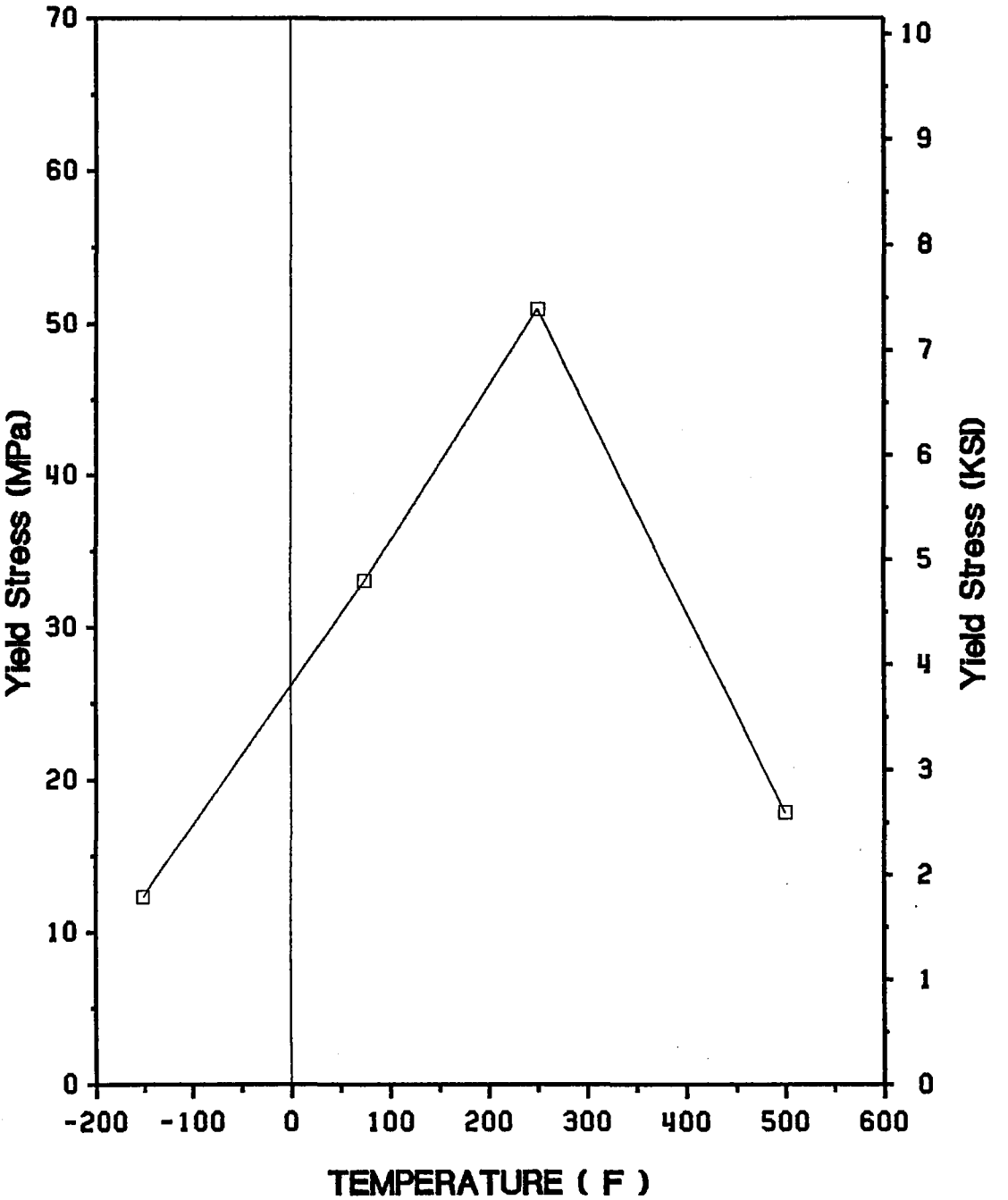

Figure 24. Yield stress of 15° tension specimens as a function of temperature

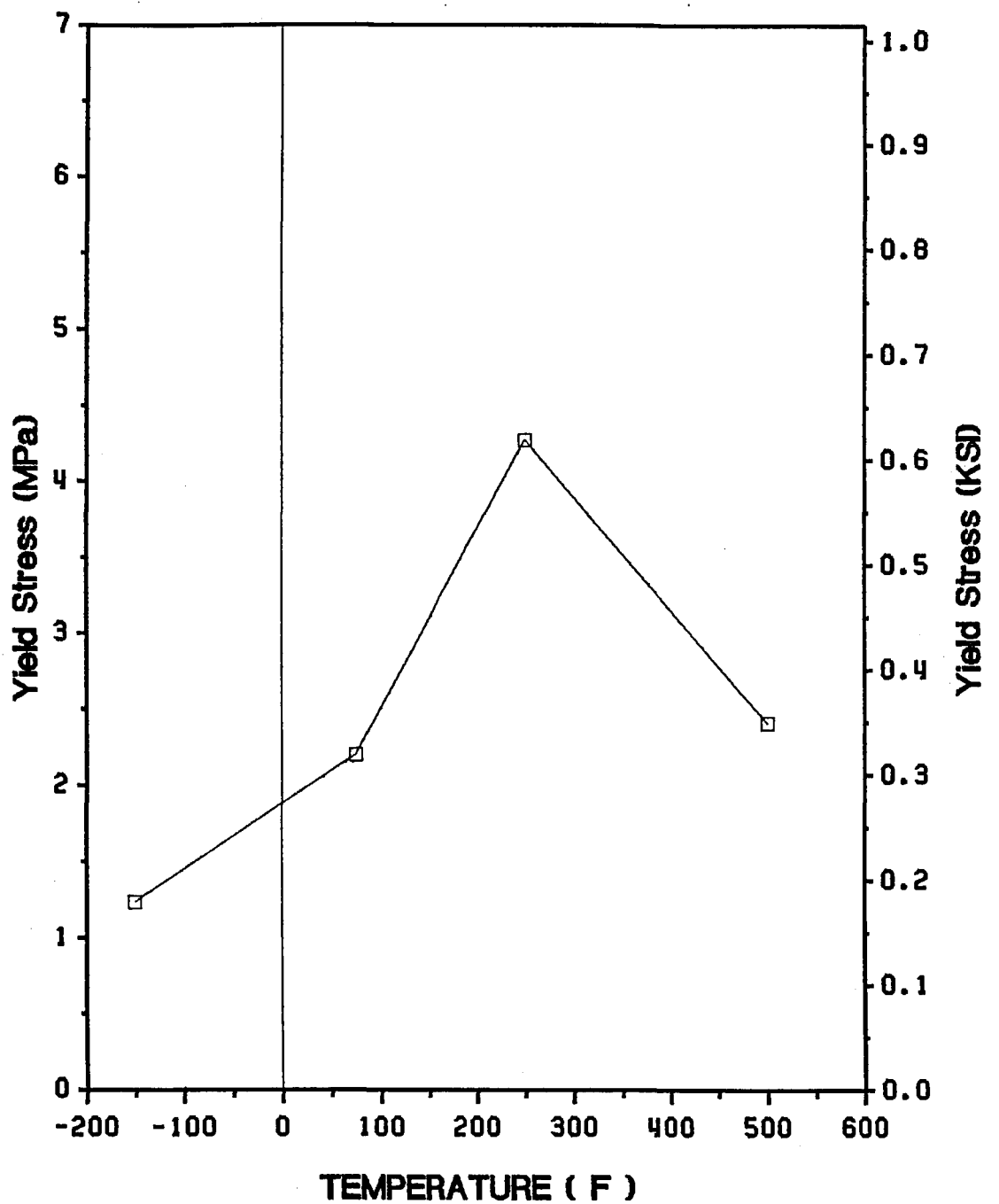

Figure 25. Yield stress of 90° tension specimens as a function of temperature

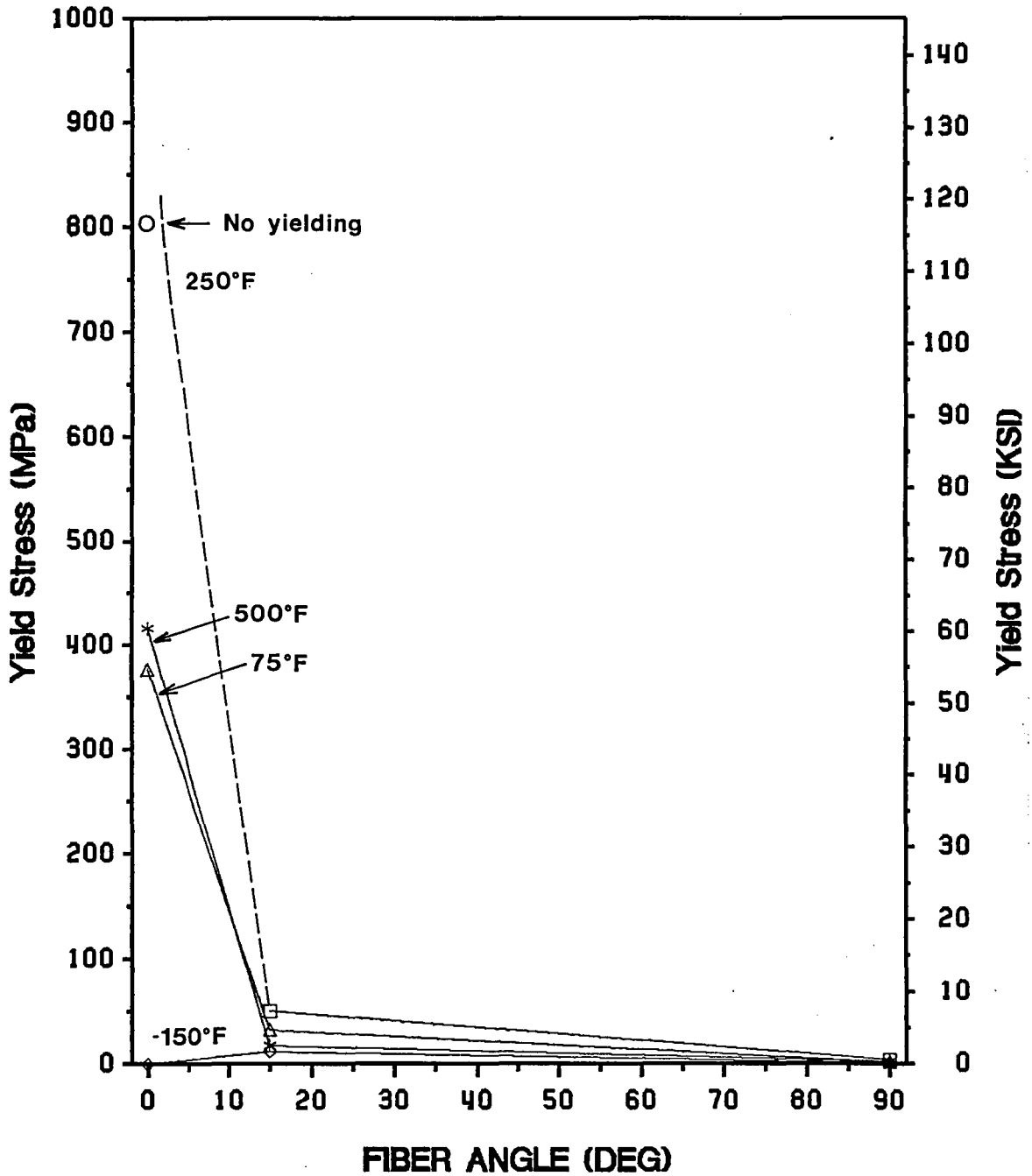

Figure 26. Yield stress as a function of fiber orientation for all temperatures

creases rapidly. After showing a maximum value at +250°F, however, the yield stress starts to decrease although the residual stress becomes further smaller. This is assumed to be due to deterioration of the aluminum matrix properties.

3.2.1.5 Summary

Table 10 summarizes tensile modulus of each specimen configuration. For 0° specimen at -150°F only, the slope of loading/unloading curve was estimated other than the initial slope of the first loading. Figures 27 - 29 illustrate elastic moduli of 0°, 15° and 90° specimen as a function of temperature, respectively. It is seen that little temperature dependency is observed for each configuration.

Table 10. Effect of temperature on elastic modulus

Temperature (°F)	Elastic Moduli, E_{xx}(msi)		
	0°	15°	90°
-150	55.1	27.3	4.3
+75	58.4	27.9	3.5
+250	56.9	26.4	4.1
+500	57.0	26.1	3.5

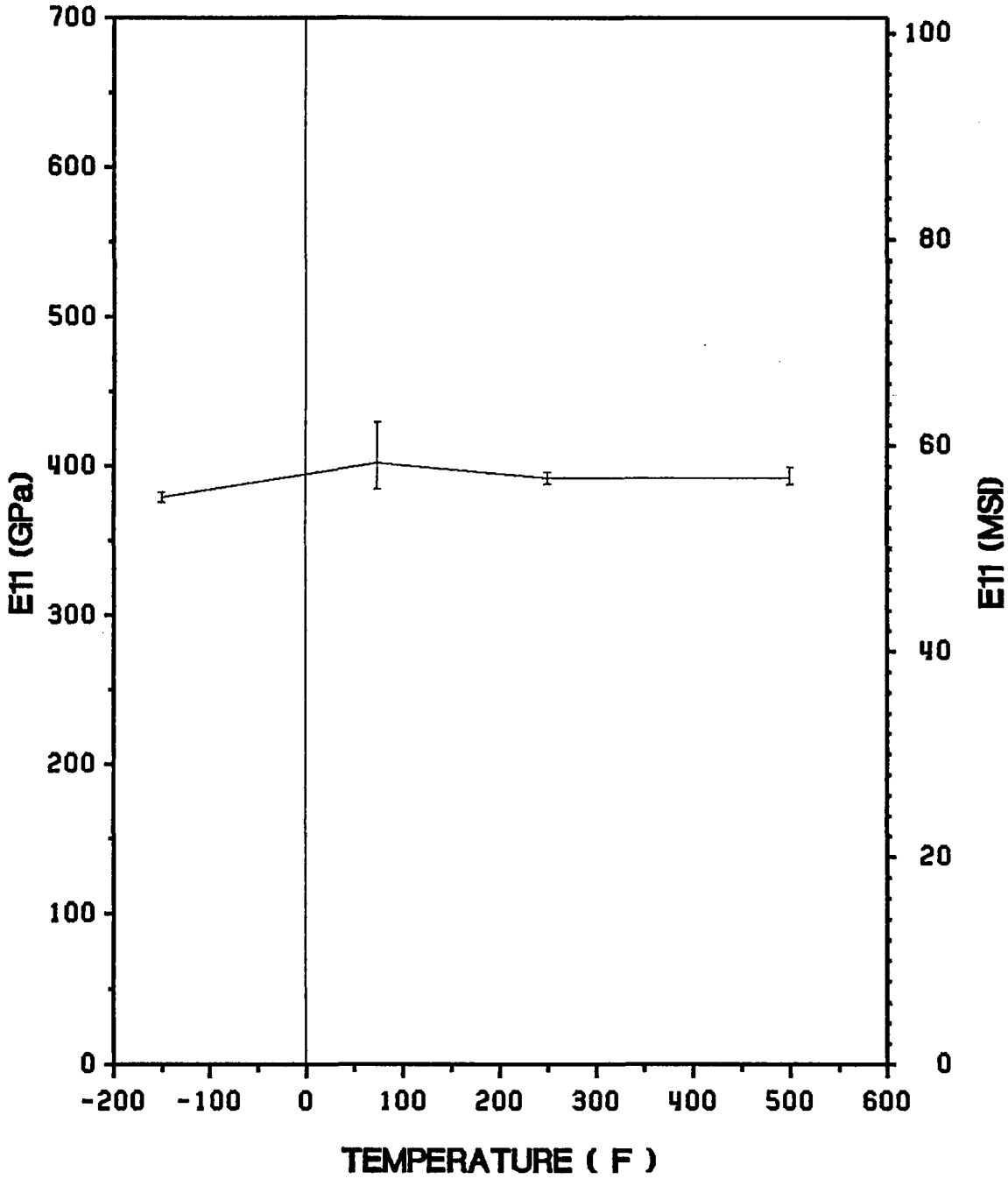

Figure 27. Elastic modulus of 0° tension specimens as a function of temperature

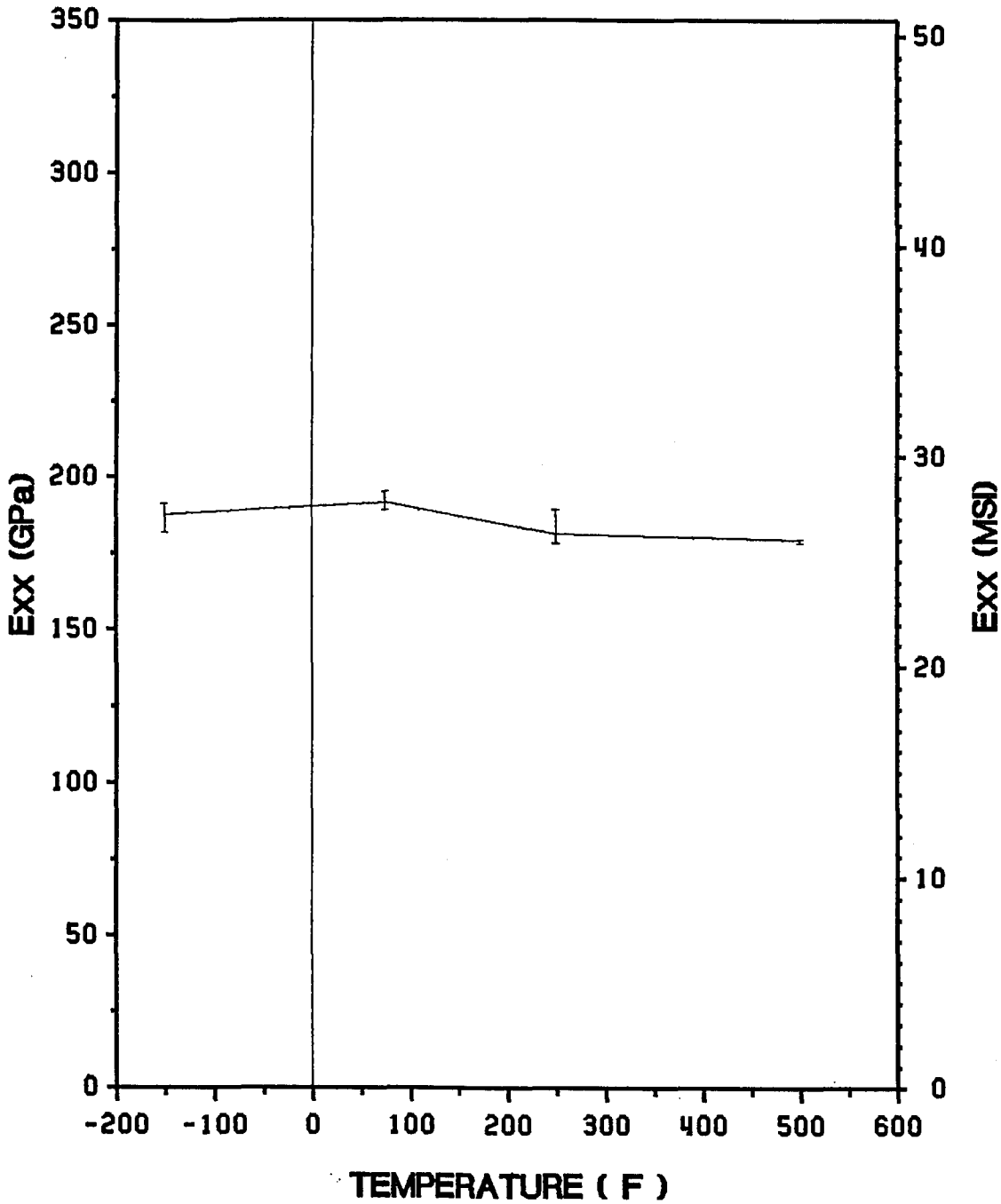

Figure 28. Elastic modulus of 15° tension specimens as a function of temperature

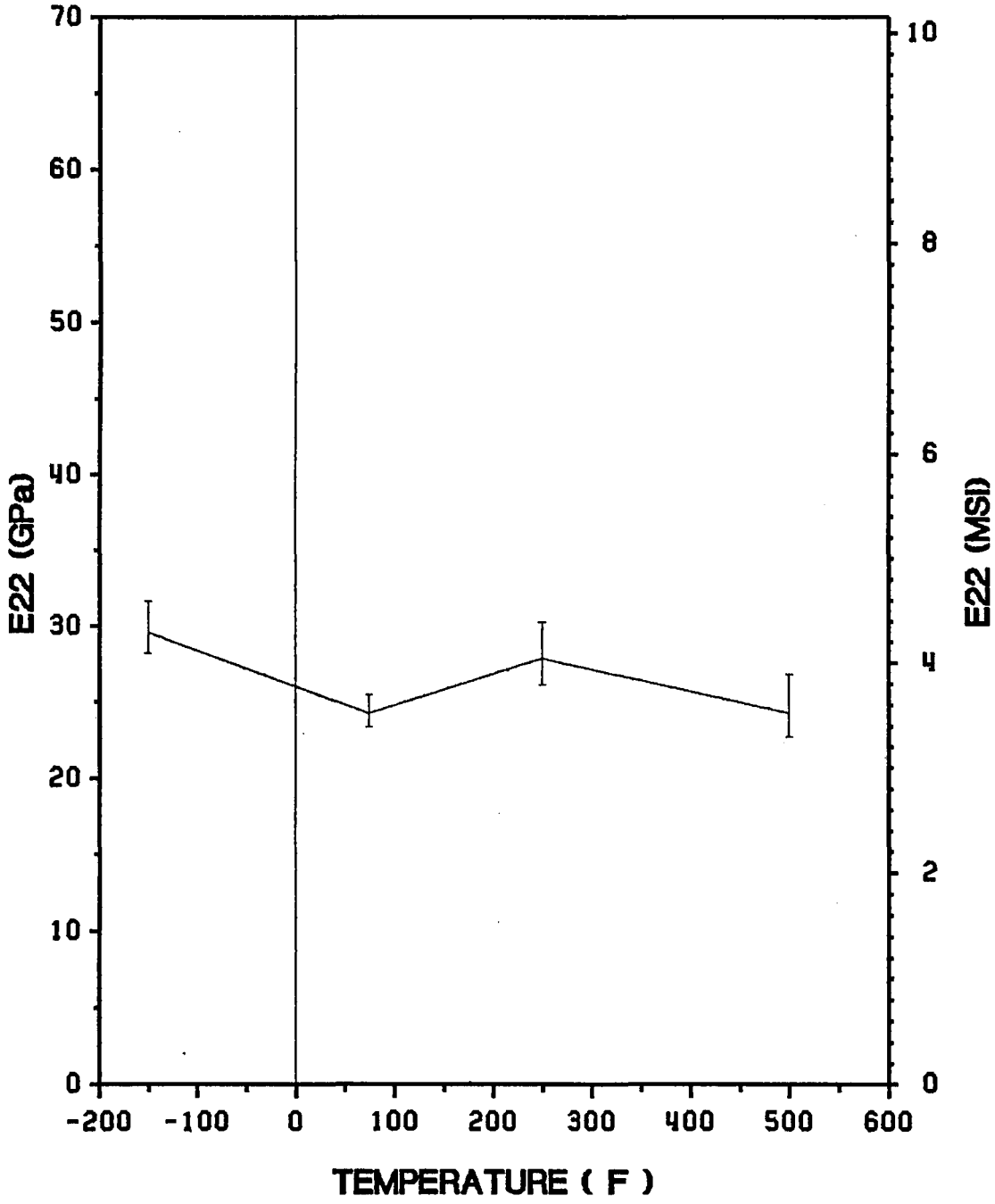

Figure 29. Elastic modulus of 90° tension specimens as a function of temperature

3.2.2 Poisson's Ratio

3.2.2.1 0° Specimen

Figure 30 shows representative Poisson's response of 0° specimens under cyclic loading for all temperatures. The effect of residual stress is clearly seen and confirmed by this figure. At -150°F, since the material already yielded prior to loading as described in 3.2.1.1, the first loading and the subsequent unloading/loading curves have no parallel part. At +75°F, the first loading curve up to ε_{yy} of -0.028% is parallel to the unloading/loading curve and the slope of the curve starts to increase beyond this point, which means that the material yields and starts strain hardening. This yield point exactly corresponds to the yield point obtained by the tensile response in Fig. 20. At +250°F, since the material did not yield up to the stress reversal point, the first loading curve exactly matches the unloading/loading curve. At +500°F, a small amount of permanent strain is observed, which means that the material yielded just below the reversal point. As is the case for tensile response, this is because aluminum properties are deteriorated at this temperature. As a whole, it seems that Poisson's ratio ν_{12} decreases slightly with the increase in temperature.

3.2.2.2 15° Specimen

Poisson's response of 15° specimens, as shown in Fig. 31, also can be explained by temperature dependent residual stress and aluminum properties as is the case of

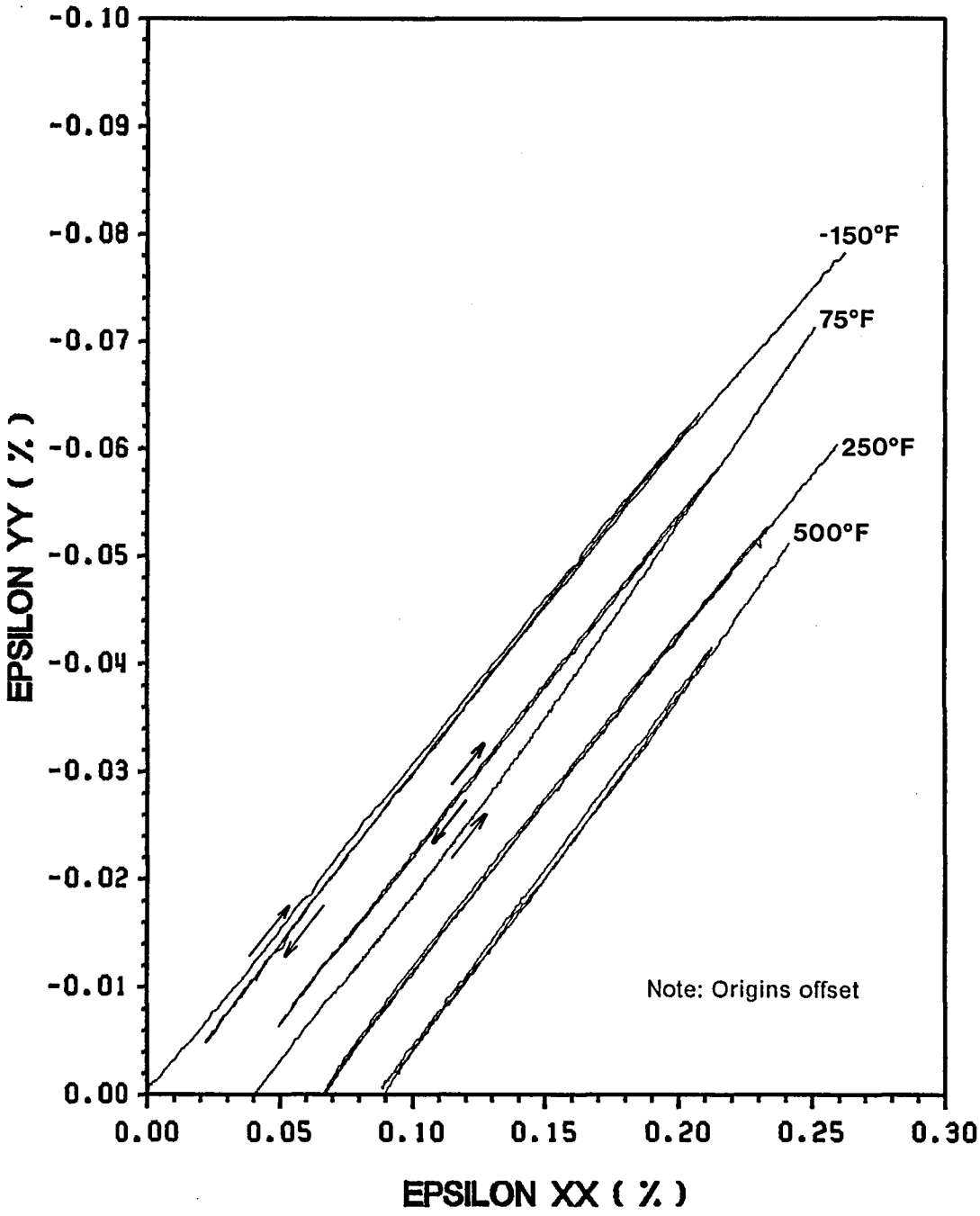

Figure 30. Poisson's response of 0° tension specimens under cyclic loading for all temperatures

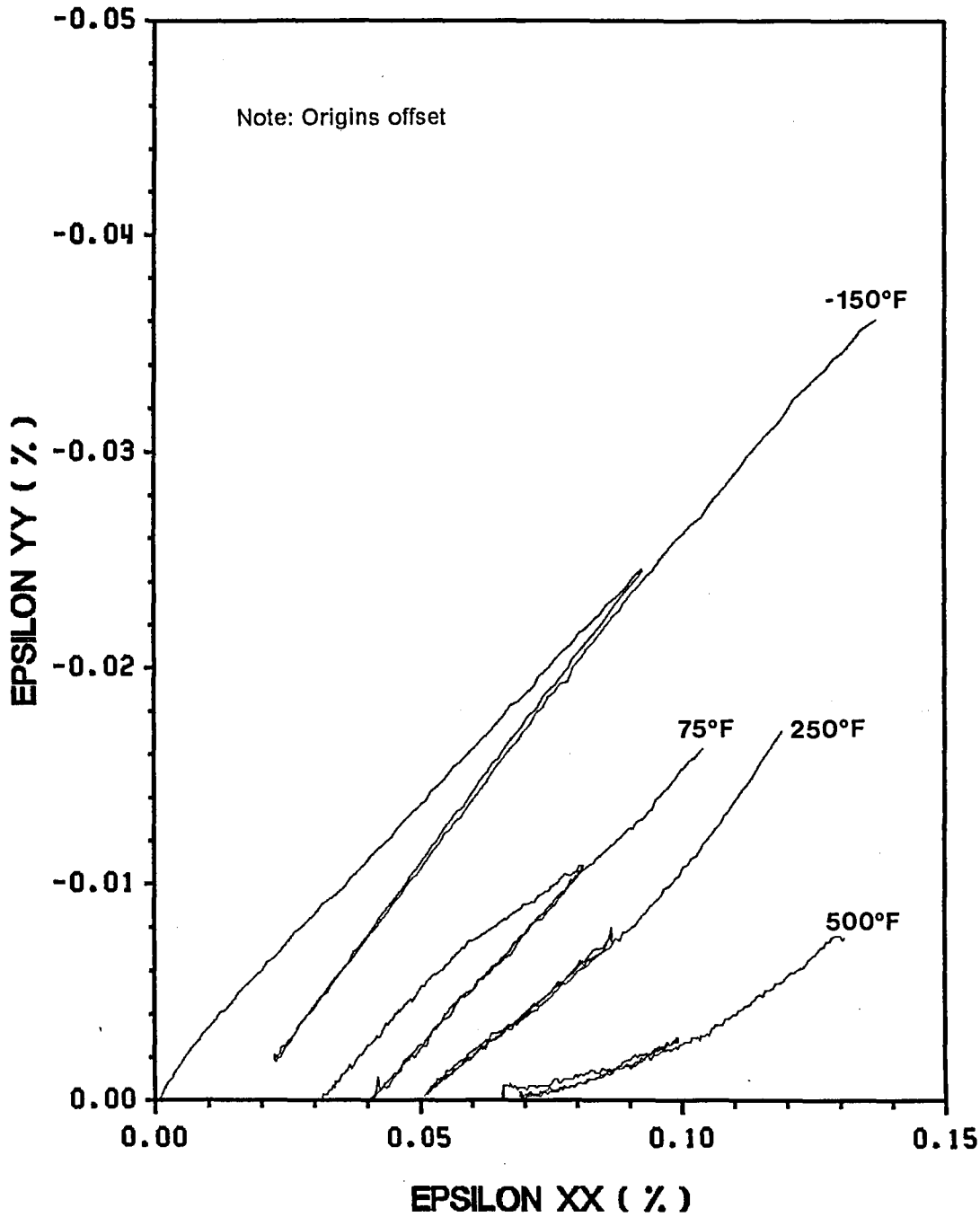

Figure 31. Poisson's response of 15° tension specimens under cyclic loading for all temperatures

tensile response. For -150°F test, the tensile residual stress is large. The material yields at an early stage and the linear elastic portion is small. For +75°F test, as the residual stress becomes smaller with increasing temperature, the material exhibits more elastic behavior. For +250°F test, the material did not yield up to the reversal stress and the first loading curve overlaid the subsequent unloading/loading curve. For +500°F test, a small amount of permanent strain indicates that the material yielded below the reversal point. This is due to deterioration of aluminum matrix property.

All the facts shown above are consistent with the tensile responses stated in 3.2.1.2. As a whole, Poisson's ratio of 15° specimen decreases with increasing temperature.

3.2.2.3 90° Specimen

Figure 32 shows representative Poisson's response of 90° specimens under cyclic loading for all temperatures. All the curves are not as smooth as those of 0° and 15° tests. The ε_{yy} value is so small that the output is easily affected by noise and amplifier resolution level. As stated before, transverse strength is so low that it is difficult to discuss the effect of residual stress and aluminum properties by this figure. In general, however, it is observed that Poisson's ratio ν_{21} decreases as the temperature increases.

3.2.2.4 Summary

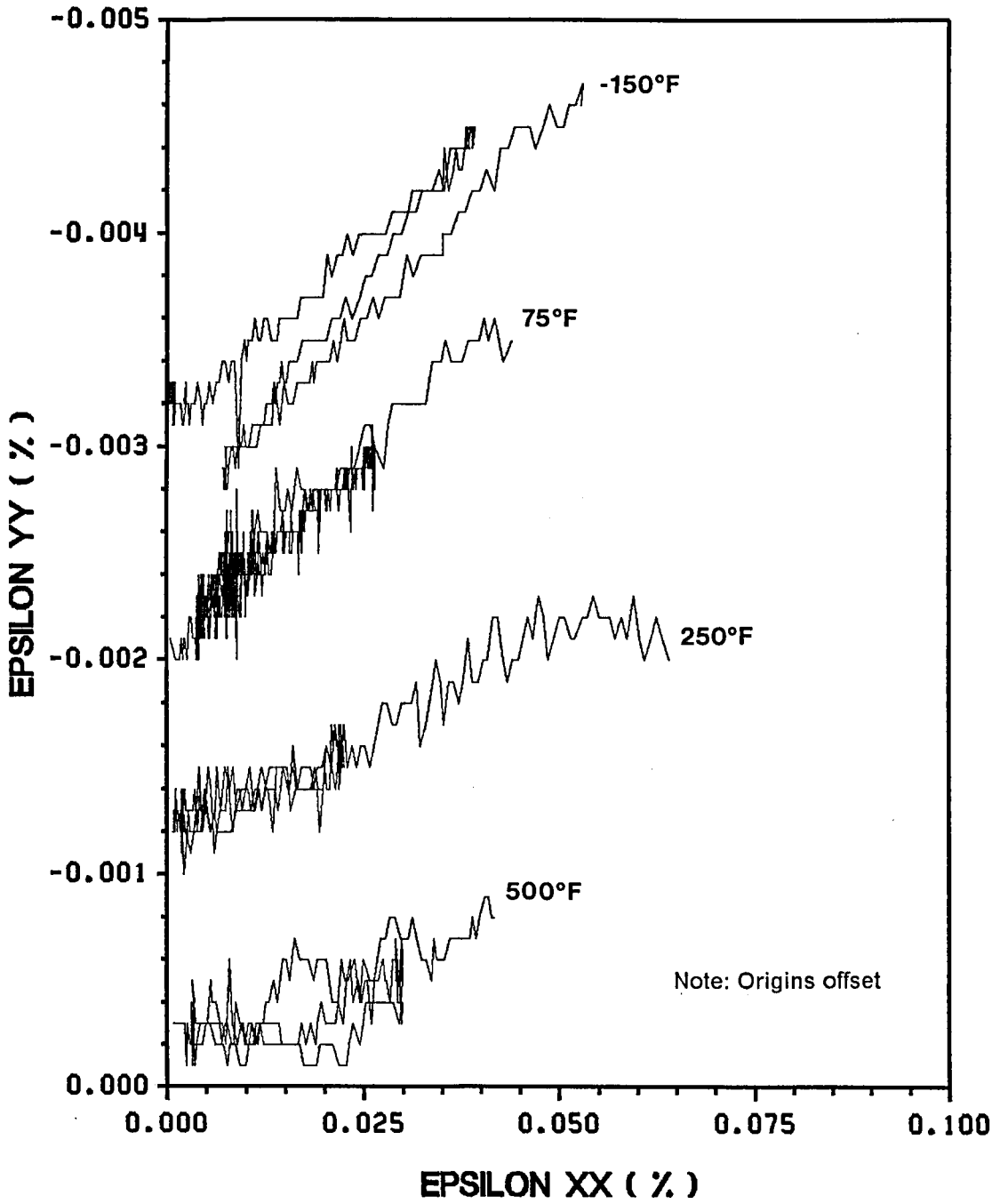

Figure 32. Poisson's response of 90° tension specimens under cyclic loading for all temperatures

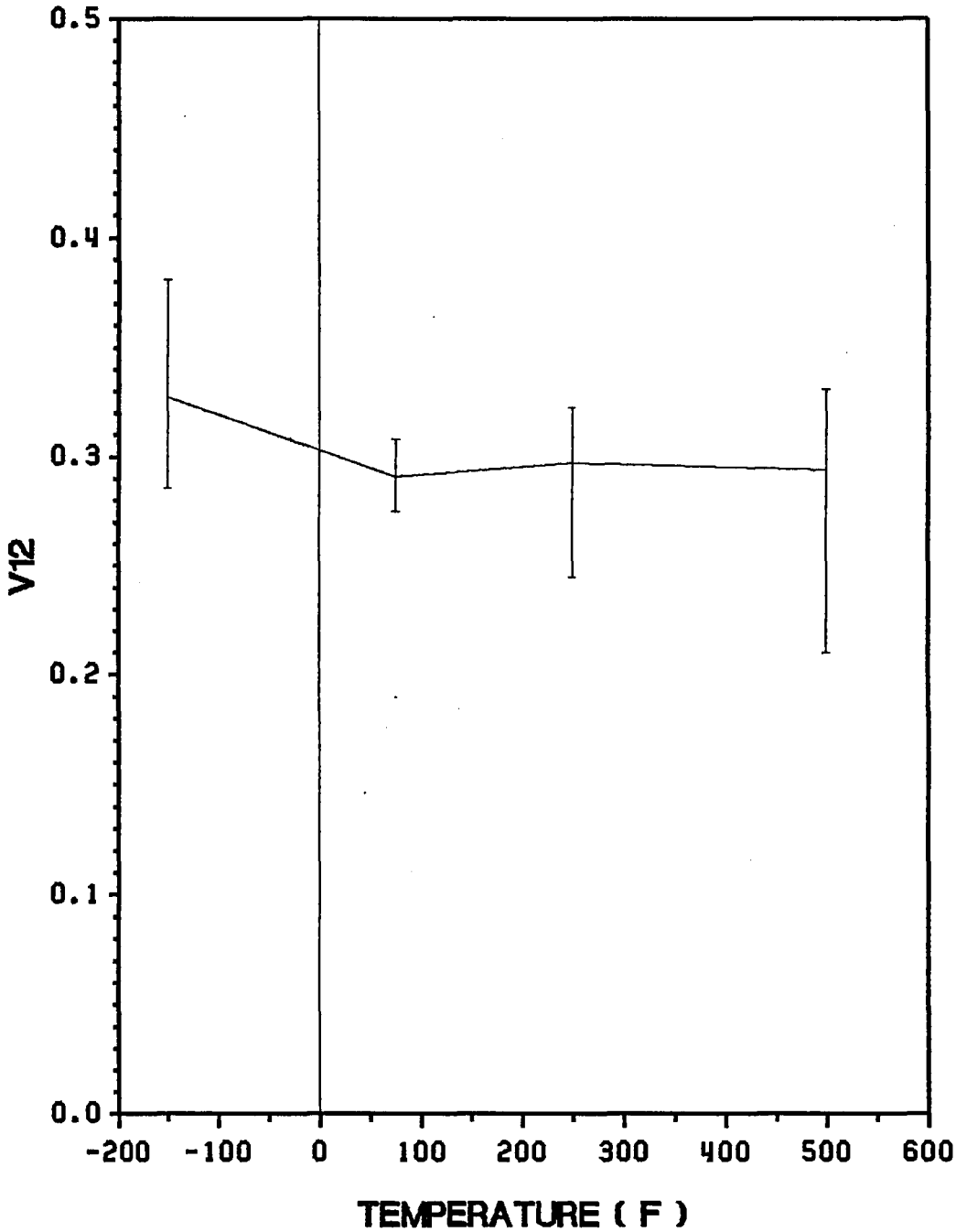

Figure 33. Poisson's ratio of 0° tension specimens as a function of temperature

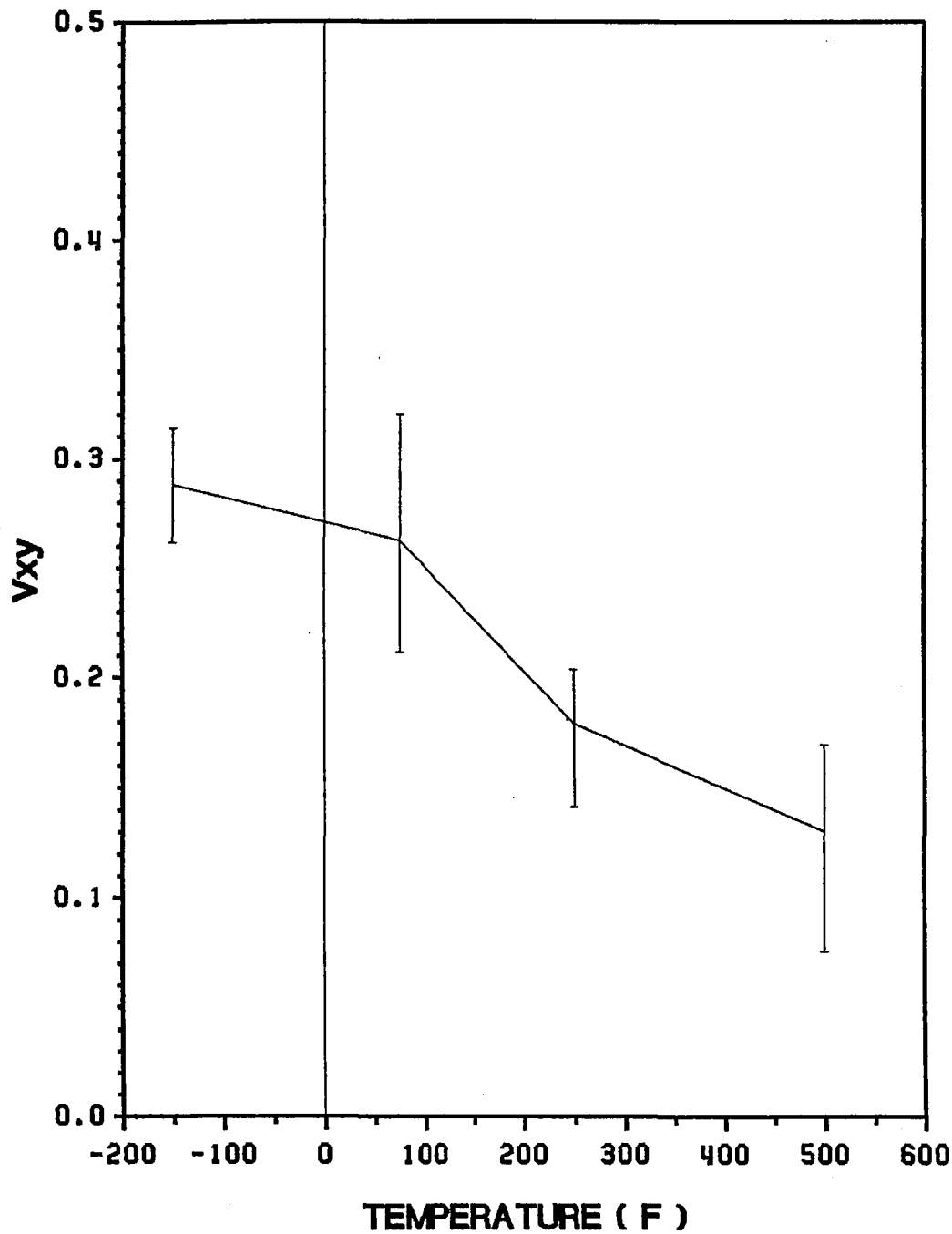

Figure 34. Poisson's ratio of 15° tension specimens as a function of temperature

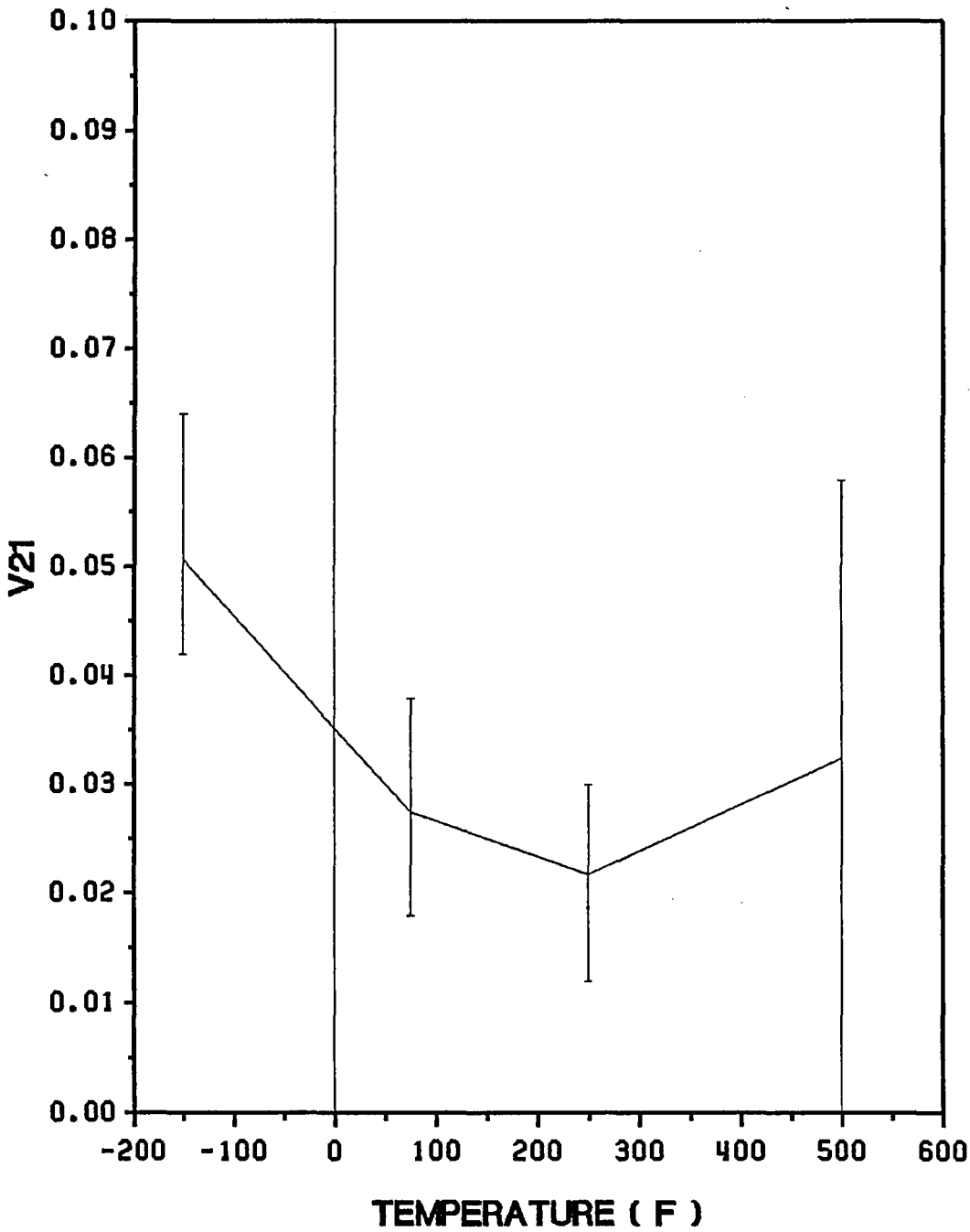

Figure 35. Poisson's ratio of 90° tension specimens as a function of temperature

Average values of Poisson's ratio of different specimens are listed in Table 11. Variations of Poisson's ratio of 0°, 15° and 90° specimens with regard to temperature are shown in Figs. 33 - 35, respectively. Although large scatters are observed for Poisson's ratio, it is seen that Poisson's ratio decreases with the increase in temperature especially for 15° and 90° tests.

Table 11. Effect of temperature on Poisson's ratio

Temperature (°F)	Poisson's Ratio		
	0°	15°	90°
-150	0.328	0.288	0.051
+75	0.291	0.263	0.028
+250	0.297	0.180	0.022
+500	0.294	0.130	0.033

3.2.3 Shear Modulus

3.2.3.1 15° Off-Axis

Representative shear response of 15° off-axis tension tests under cyclic loading for all temperatures are shown in Fig. 36. The characteristics of shear response are almost the same as tensile response as described in 3.2.1.2. The material has already yielded prior to loading at -150°F. The yield point increases significantly and the

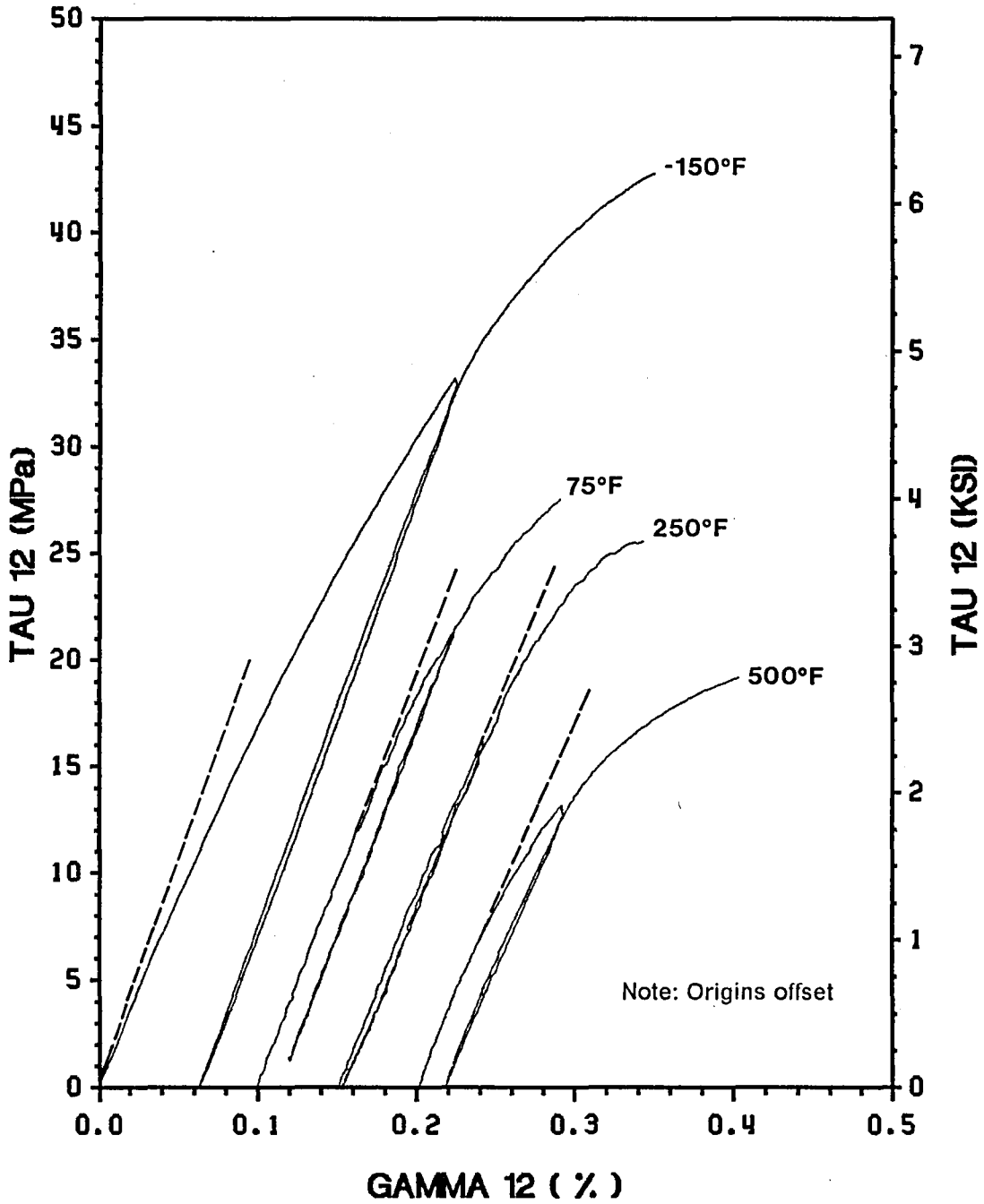

Figure 36. Shear response of 15° tension specimens under cyclic loading for all temperatures

material exhibits a large amount of elastic behavior at +75°F. Overlap of the loading and unloading/loading curves of +250°F test indicates that the material does not yield prior to the reversal point. There exists a certain amount of permanent strain at +500°F, which indicates that the material yields below the reversal stress. All the phenomena may be explained by variation of residual stress and aluminum matrix properties with regard to temperature as is the case with tensile response.

When obtaining modulus values, it is sometimes difficult to find an initial linear elastic portion of the stress-strain curve. On the first loading curves of Fig. 36, for example, a linear elastic range is limited to a small portion for the -150°F test and it is hard to define a linear region from nonlinear initial response of +500° test. In these cases, the unloading/loading curve in a cyclic test can be used as an alternative for determining the elastic modulus. Compared with the first loading curve, the subsequent unloading/loading curve usually has a longer linear portion, which results in more precise modulus determination. This is demonstrated in the shear modulus of cyclic test results (Tables A.9 - A.12 in Appendix A). It is obvious that the modulus values obtained by the unloading/loading curves are very reproducible whereas those by the first loading curves have large scatter.

3.2.3.2 0° Iosipescu

Representative shear response of 0° Iosipescu shear tests under monotonic loading for all temperatures are shown in Fig. 37. The Iosipescu tests give quite different results from the 15° off-axis test. Unlike 15° off-axis tension tests, the specimens exhibit much more extensive nonlinear behavior especially at elevated temperatures. Two results of 500° tests are included in Fig. 37; the first test exhibits over 2% shear

strain at failure. In the 15° off-axis tension tests, on the other hand, the highest ultimate shear strain is only 0.13%. Based on these experimental results, it can be concluded again that the 0° Iosipescu test is an excellent test method to obtain nonlinear shear response.

Figure 38 illustrates an enlargement of initial shear response of 0° Iosipescu tests. The effect of temperature on G_{12} is profound. It is seen from Fig. 38 that as the temperature increases, G_{12} decreases significantly, but not monotonically. Although there exists significant data scatter, a small increase in G_{12} is observed as the temperature increases from +75°F to +250°F. Similar results were predicted theoretically by Aboudi [37]. In Aboudi's predictions, as the temperature increases, not only initial modulus decreases monotonically but, also, the specimen exhibits nonlinear behavior at a lower stress level; these are almost the same phenomena obtained in the present Iosipescu tests. It can be presumed that this temperature effect is characterized by change in residual stresses as well as aluminum properties. Unlike E_{11} expressed by Eq. (3.1), the matrix shear modulus is the dominant term in G_{12} of the composite. For the isotropic material, shear modulus can be expressed in terms of Young's modulus E and Poisson's ratio ν,

$$G = \frac{E}{2(1 + \nu)}$$

Assuming that Poisson's ratio is temperature independent, the shear modulus of the aluminum is proportional to Young's modulus at each temperature. As shown in Fig. 2, Young's modulus of aluminum decreases as the temperature increases. Therefore, it is likely that a decrease in elastic modulus of aluminum at high temperature

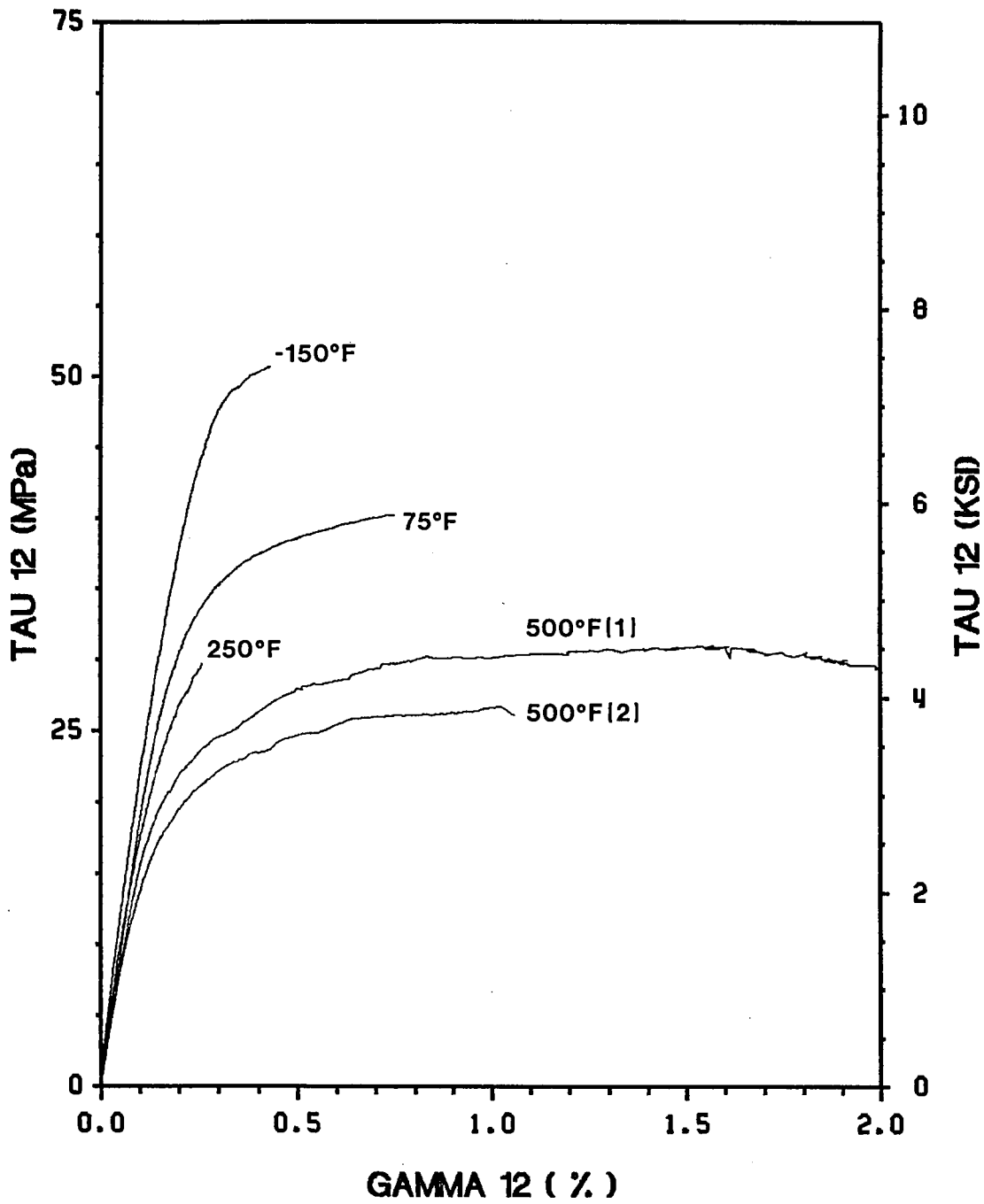

Figure 37. Overall shear response of 0° Iosipescu specimens under monotonic loading for all temperatures

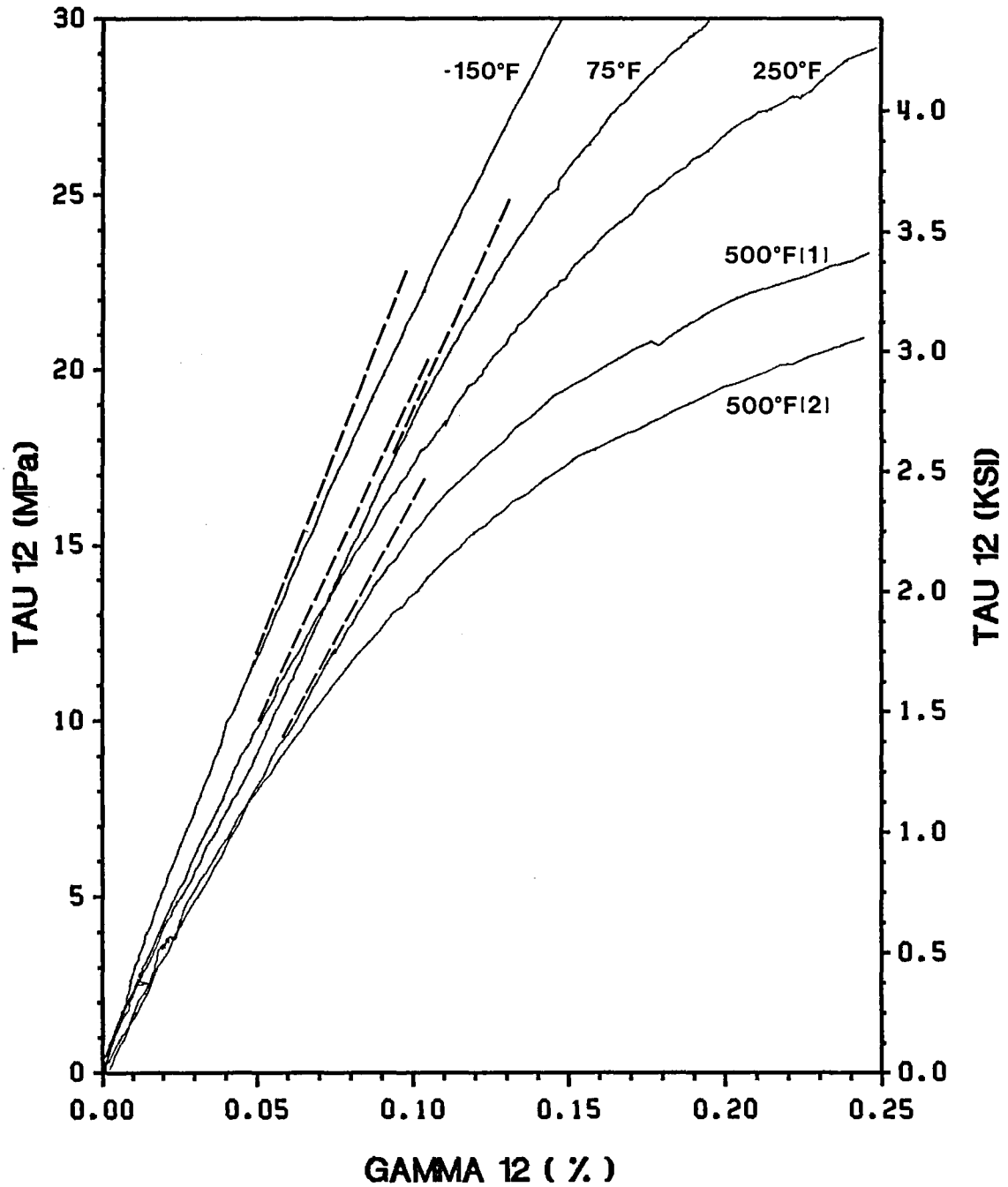

Figure 38. Initial shear response of 0° Iosipescu specimens under monotonic loading for all temperatures

is related to the present decrease in shear modulus of the composite, as shown in Fig. 38.

The cause of a small increase in G_{12} with increasing temperature from +75°F to +250°F, which is obtained in the present experiments, is uncertain. Although conflicting with 15° Off-axis results and Aboudi's predictions, this trend is also observed for E_{22} (Fig. 29) and ν_{12} (Fig. 33). Considering that they are all matrix dominated properties, it is probable that some phenomenon takes place inside the material in the temperature range between +75°F and +250°F.

3.2.3.3 Yield Stress

Table 12 summarizes the results for yield stresses obtained from the 15° off-axis and 0° Iosipescu tests. Figure 39 illustrates yield shear stress of both specimens as a function of temperature. The 15° off-axis test result shows almost the same behavior as tensile yield stress shown in Fig. 24, whereas the Iosipescu test exhibits a different trend; the yield stress is rather high at -150°F and the maximum value appears at +75°F instead of +250°F. It is possible that this difference is caused by stress interaction of the 15° off-axis specimen, but further experiments and analyses are necessary to confirm this.

3.2.3.4 Summary

Average values of shear modulus obtained by both test methods are listed in Table 13. Results of 15° off-axis tension tests are estimated by the unloading/loading curve

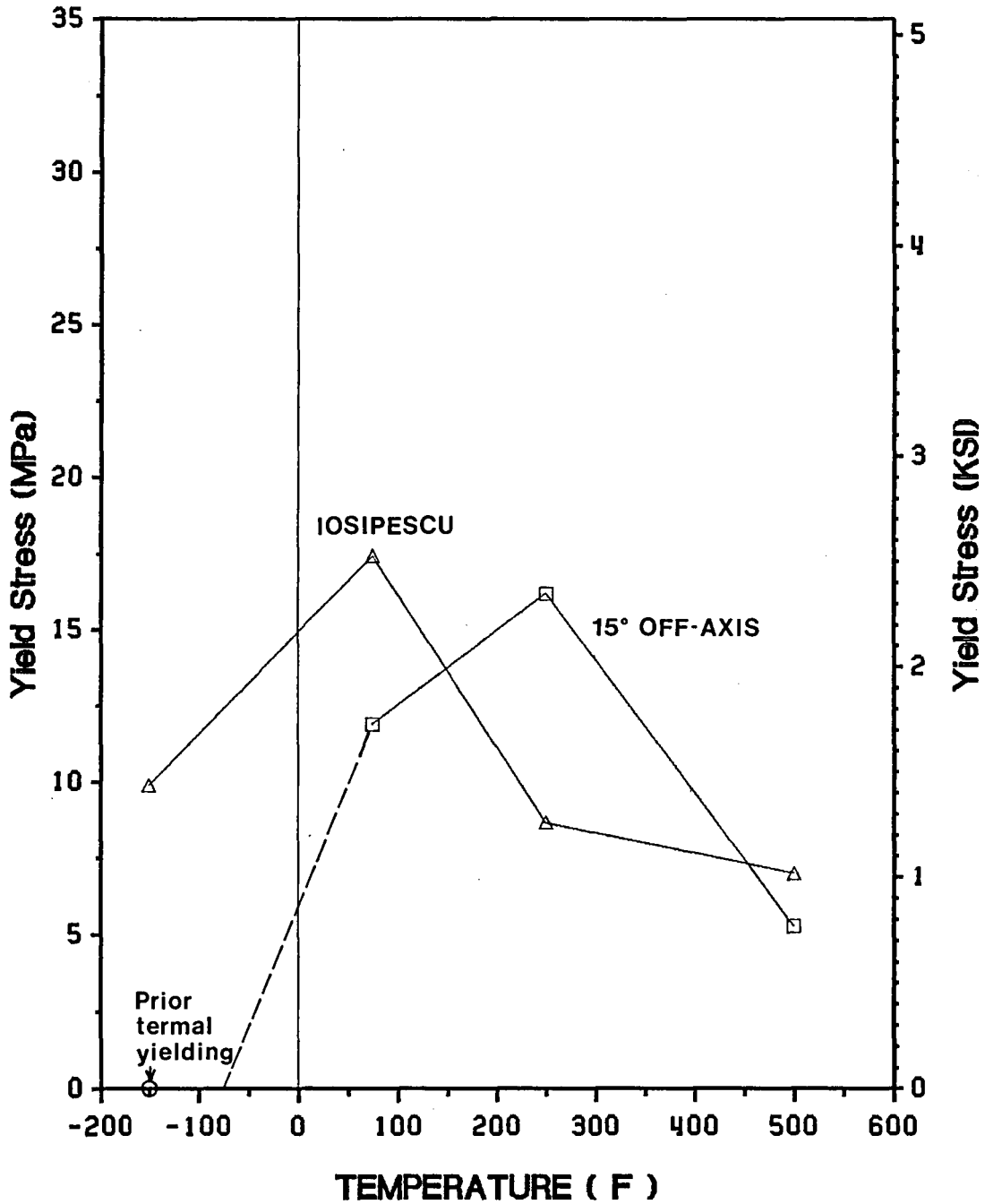

Figure 39. Yield stress of shear specimens as a function of temperature

Table 12. Effect of temperature on yield shear stress

Temperature (°F)	Yield Stress, τ_{12}^{Y}(ksi)	
	15° Off-Axis	0° Iosipescu
-150	0.0	1.44
+75	1.73	2.53
+250	>2.35	1.26
+500	0.77	1.02

of cyclic tests whereas those of 0° Iosipescu shear tests are obtained from monotonic tests.

Variations of shear modulus from 15° off-axis tension and 0° Iosipescu specimens as a function of temperature are shown in Figs. 40 and 41, respectively. It is seen in Fig. 40 that the shear modulus from the off-axis test decreases almost linearly with the

Table 13. Effect of temperature on shear modulus

Temperature (°F)	Shear Modulus, G_{12}(msi)	
	15° Off-Axis	0° Iosipescu
-150	3.07	3.45
+75	2.87	2.76
+250	2.75	3.03
+500	2.52	2.56

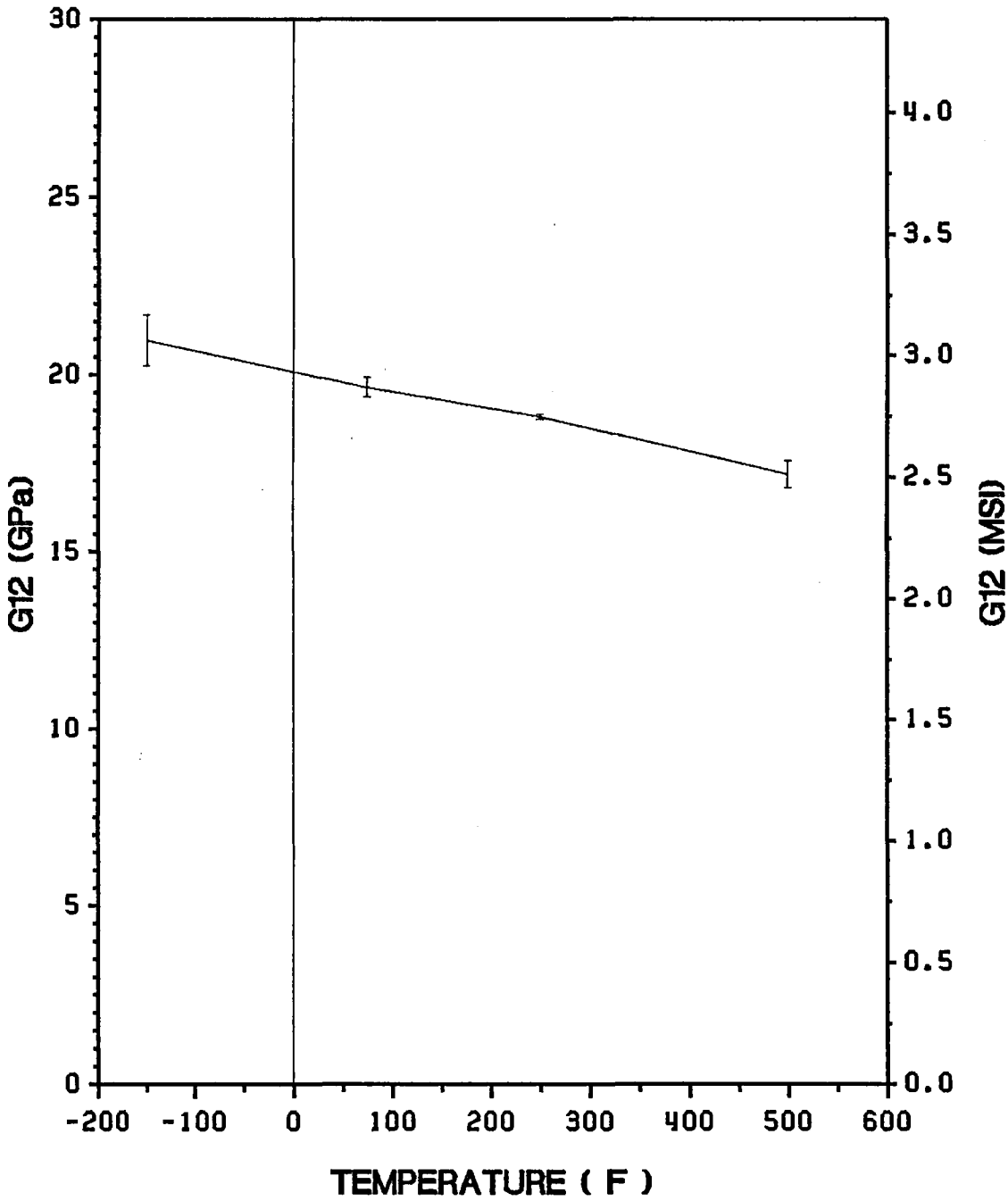

Figure 40. Shear modulus of 15° tension specimens as a function of temperature

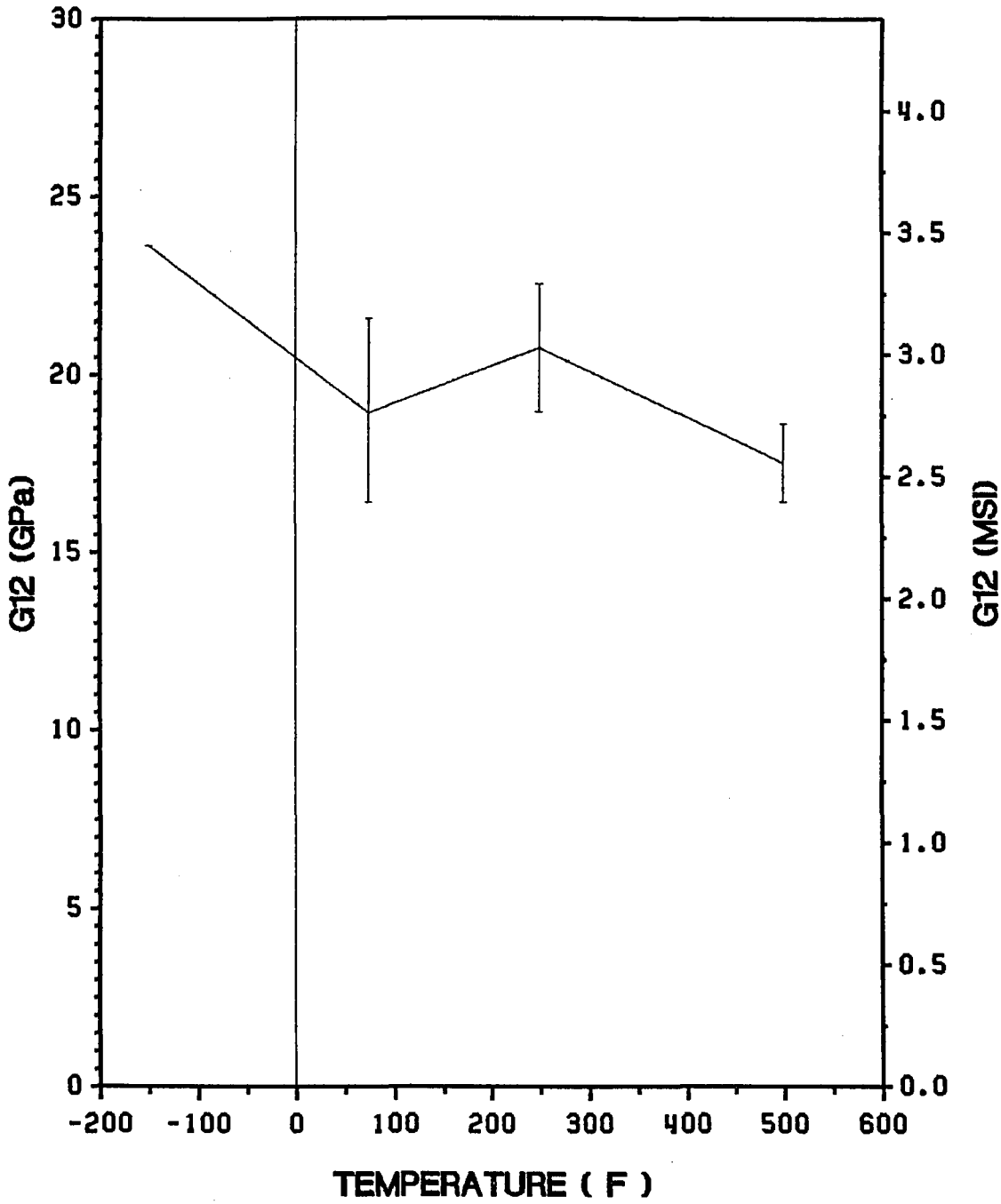

Figure 41. Shear modulus of 0° Iosipescu specimens as a function of temperature

increase in temperature and that there is little data scatter. The unloading/loading curves of the 15° tension tests are used to estimate these moduli. On the other hand, the monotonic 0° Iosipescu test results are used to obtain the results in Fig. 41. As pointed out in 3.2.3.1, it is difficult to determine the elastic portion of the stress-strain curve in monotonic Iosipescu test. As a result, there is significant data scatter in Fig. 41. However, decrease in G_{12} with increasing temperature is also generally observed. It is desirable to conduct cyclic Iosipescu tests to obtain more precise modulus and yield stress.

3.2.4 Strength

3.2.4.1 Tensile Strength

Monotonic Loading: Average values of tensile strength in monotonic loading are listed in Table 14. Variations of tensile strength of 0°, 15° and 90° specimens with regard to temperature are shown in Figs. 42 - 44, respectively. The effect of temperature on strength is significant for 0° and 15° specimens. Although there exists considerable data scatter for 0° specimens, significant reduction in strength is observed at +500°F. One of the specimens failed at 69.7 ksi which is almost half the highest strength of 137.2 ksi obtained at -150°F. It is suspected that this degradation of ultimate strength at +500°F is closely related to the deterioration of aluminum matrix property as shown in Fig. 2. The temperature effect is more significant for the 15 ° tests. The ultimate strength decreases sharply as the temperature increases. The ultimate strength at -150°F is more than two and one half times that at +500°F.

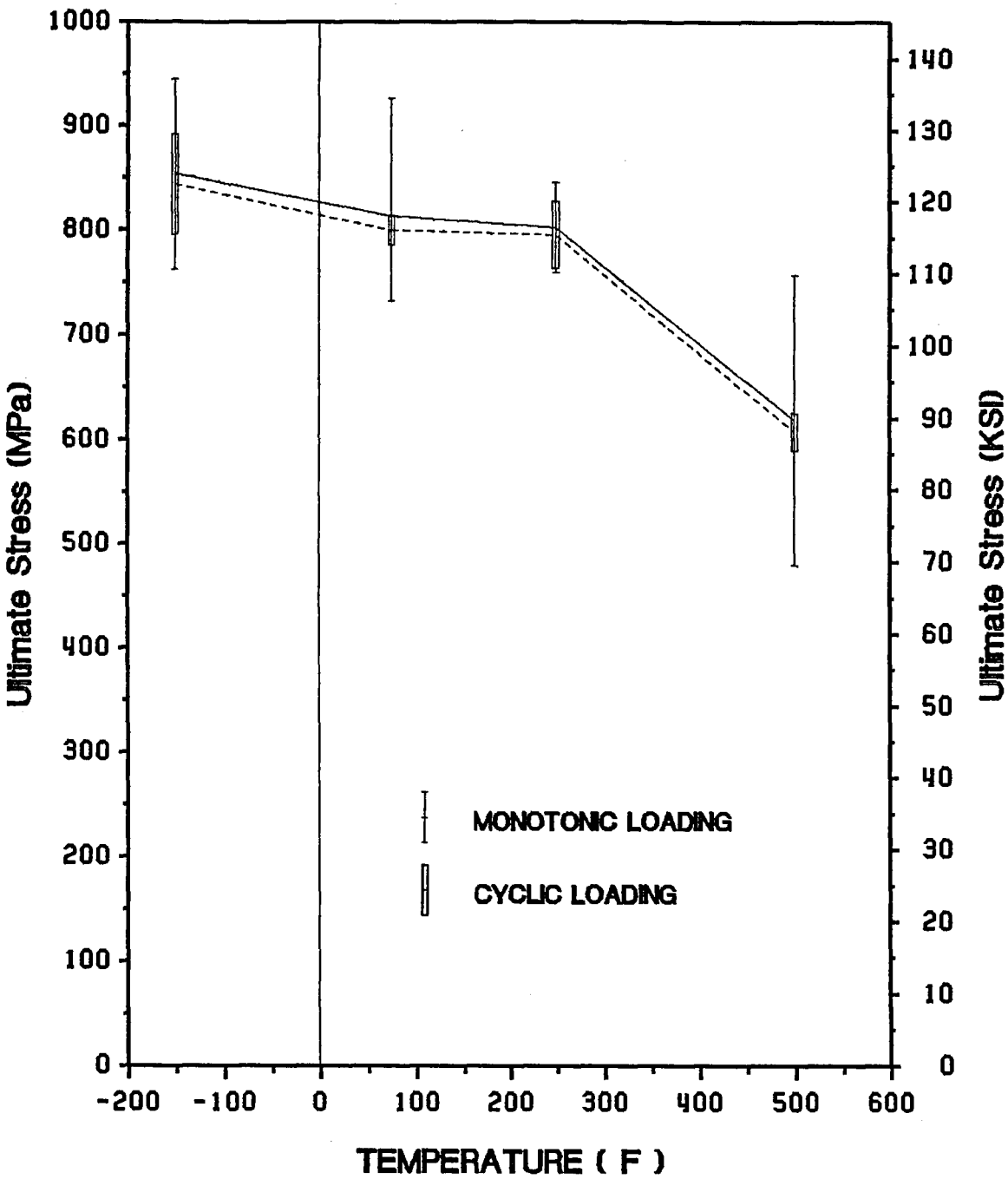

Figure 42. Tensile strength of 0° tension specimens as a function of temperature

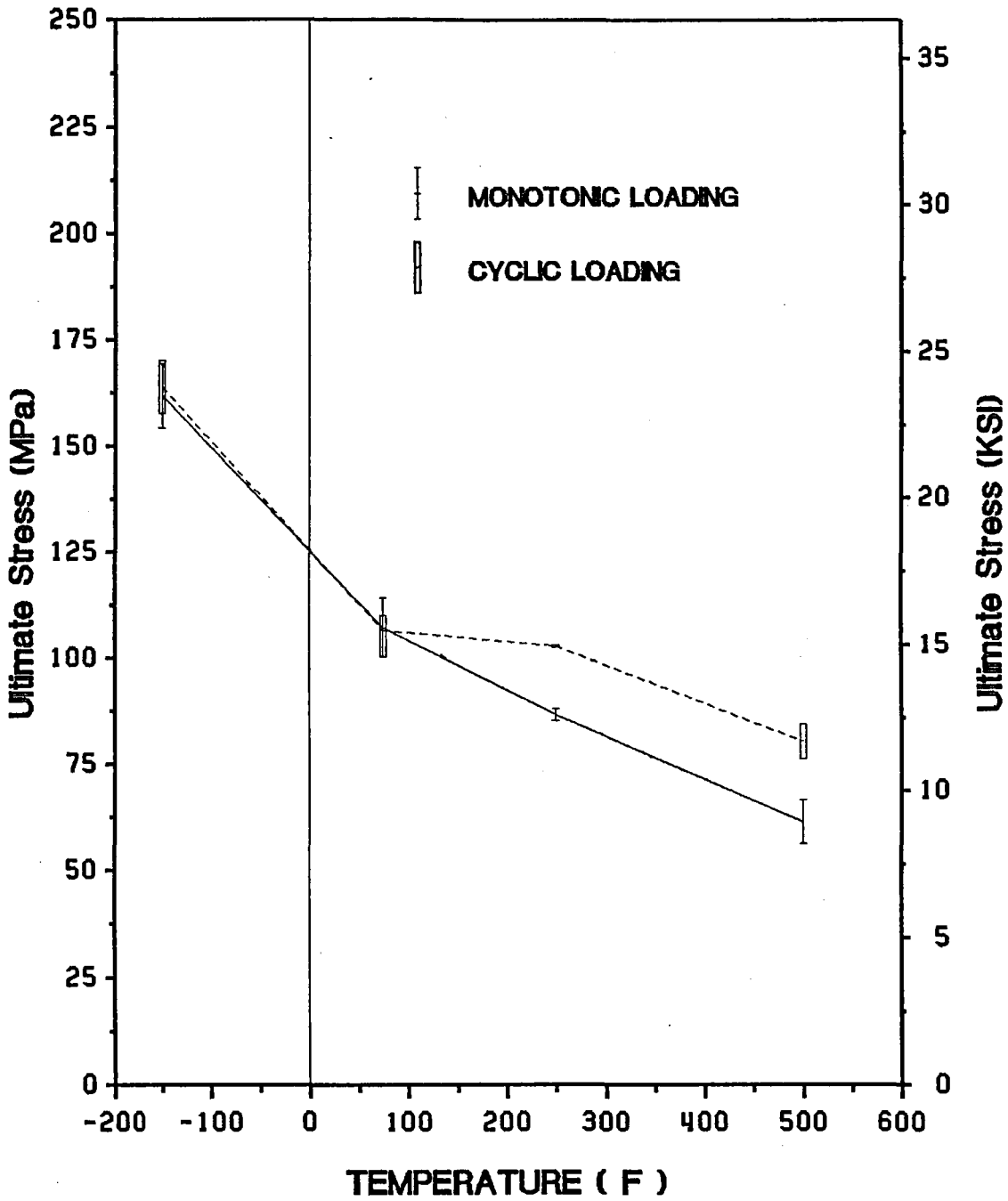

Figure 43. Tensile strength of 15° tension specimens as a function of temperature

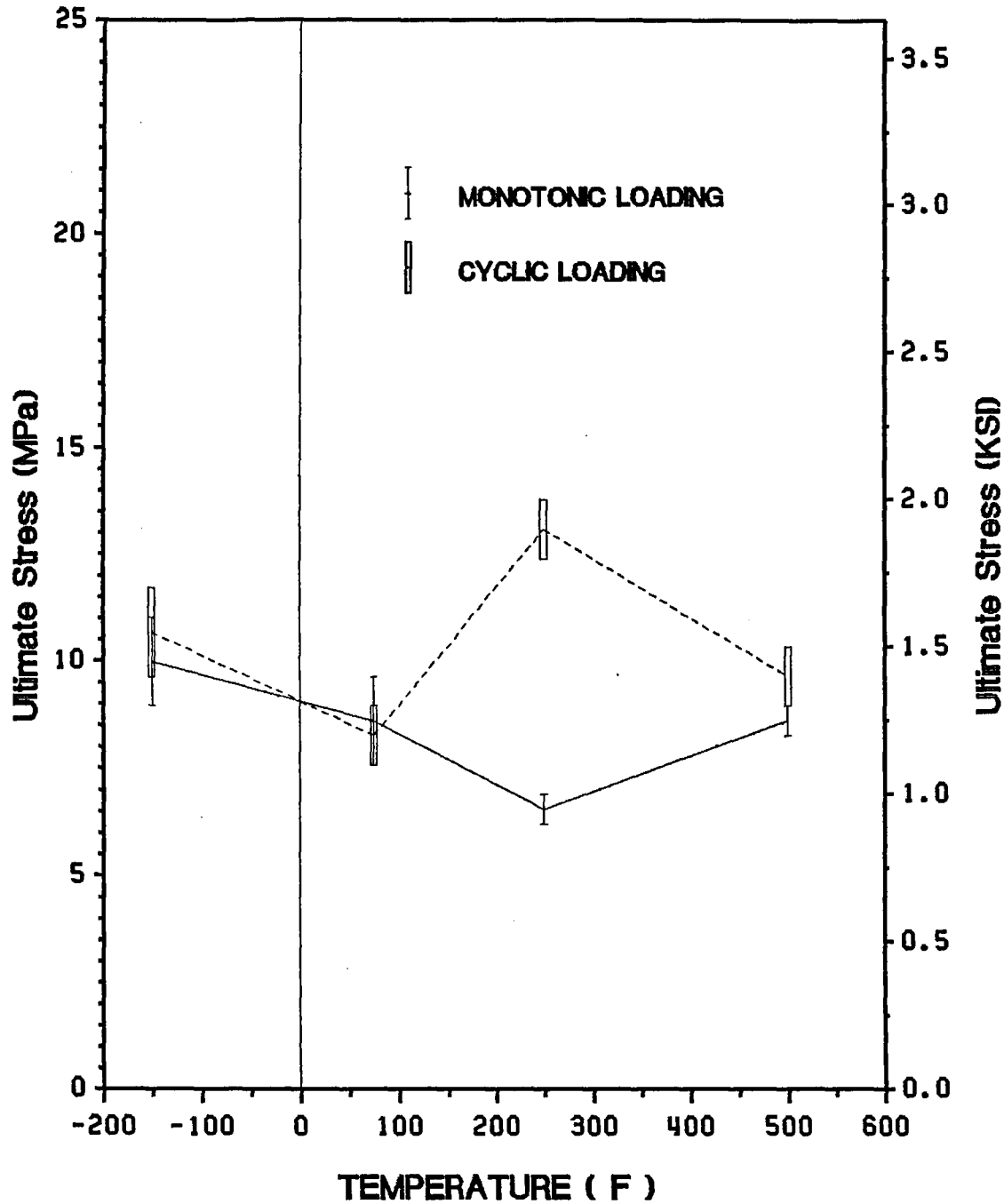

Figure 44. Tensile strength of 90° tension specimens as a function of temperature

However, such a drastic effect is not observed for 90° tests. As mentioned in 3.1.2, transverse strength is so low that it is likely that interfacial bond strength is the more influential factor than temperature for this configuration.

Table 14. Effect of temperature on tensile strength (monotonic loading)

Temperature (°F)	Tensile Strength, σ_{xx}^{u}(ksi)		
	0°	15°	90°
-150	124.0	23.5	1.5
+75	118.1	15.6	1.3
+250	116.5	12.6	1.0
+500	89.8	9.0	1.3

Cyclic Loading: Average values of tensile strength in cyclic loading are listed in Table 15. These values are plotted in Figs. 42 - 44 by bars and compared with monotonic test results. There is little difference between monotonic and cyclic loading for the 0° test results. However, significant increase in strength is observed at elevated temperatures for 15° and 90° tests.

3.2.4.2 Maximum Shear Stress/Strain

As described briefly in 3.1.2, it is not easy to obtain shear strength for the present graphite/aluminum composite. The stress state of the off-axis tension specimen is not pure shear and the specimen fails at a lower stress level. The Iosipescu specimen cannot sustain the applied load until the test section fails; the edges of the

Table 15. Effect of temperature on tensile strength (cyclic loading)

Temperature (°F)	Tensile Strength, σ_{xx}^{u}(ksi)		
	0°	15°	90°
-150	122.5	23.8	1.6
+75	116.1	15.5	1.2
+250	115.5	15.0	1.9
+500	88.2	11.7	1.4

specimen are always crushed beforehand. Therefore, the terms, maximum stress and strain, are used here as a lower bound on the shear strength of the material.

Average values of maximum shear stresses are listed in Table 16. Variations of maximum shear stress of 15° off-axis and 0° Iosipescu specimens as a function of temperature are shown in Fig. 45. It is seen that the Iosipescu test results show higher maximum stresses than the 15° off-axis test results and that the maximum shear stress decreases with increasing temperature for both tests.

However, the maximum shear strain, shown in Table 17 and Fig. 46, exhibits quite different behavior. The 15° off-axis test results give the same trend as maximum stress but for Iosipescu test results, increase in maximum strain with increasing temperature is observed except for the +250°F results. Values of two +250°F Iosipescu tests are rather low because the edges of specimens were crushed during the tests at early stage, as mentioned in 3.1. The apparent conflicting trend between maximum stress and strain reveals another evidence of the quality of the 0° Iosipescu

Table 16. Effect of temperature on maximum shear stress

Temperature (°F)	Maximum Shear Stress, τ_{12}^{M}(msi)	
	15° Off-Axis	0° Iosipescu
-150	5.9	7.4
+75	4.0	5.1
+250	3.2	4.5
+500	2.2	3.9

test. Decrease in maximum stress and increase in maximum strain clearly indicate the development of ductility with increasing temperature, which may not be observed in 15° off-axis test.

Table 17. Effect of temperature on maximum shear strain

Temperature (°F)	Maximum Shear Strain, γ_{12}^{M}(%)	
	15° Off-Axis	0° Iosipescu
-150	0.354	0.431
+75	0.176	0.484
+250	0.123	0.223
+500	0.101	1.574

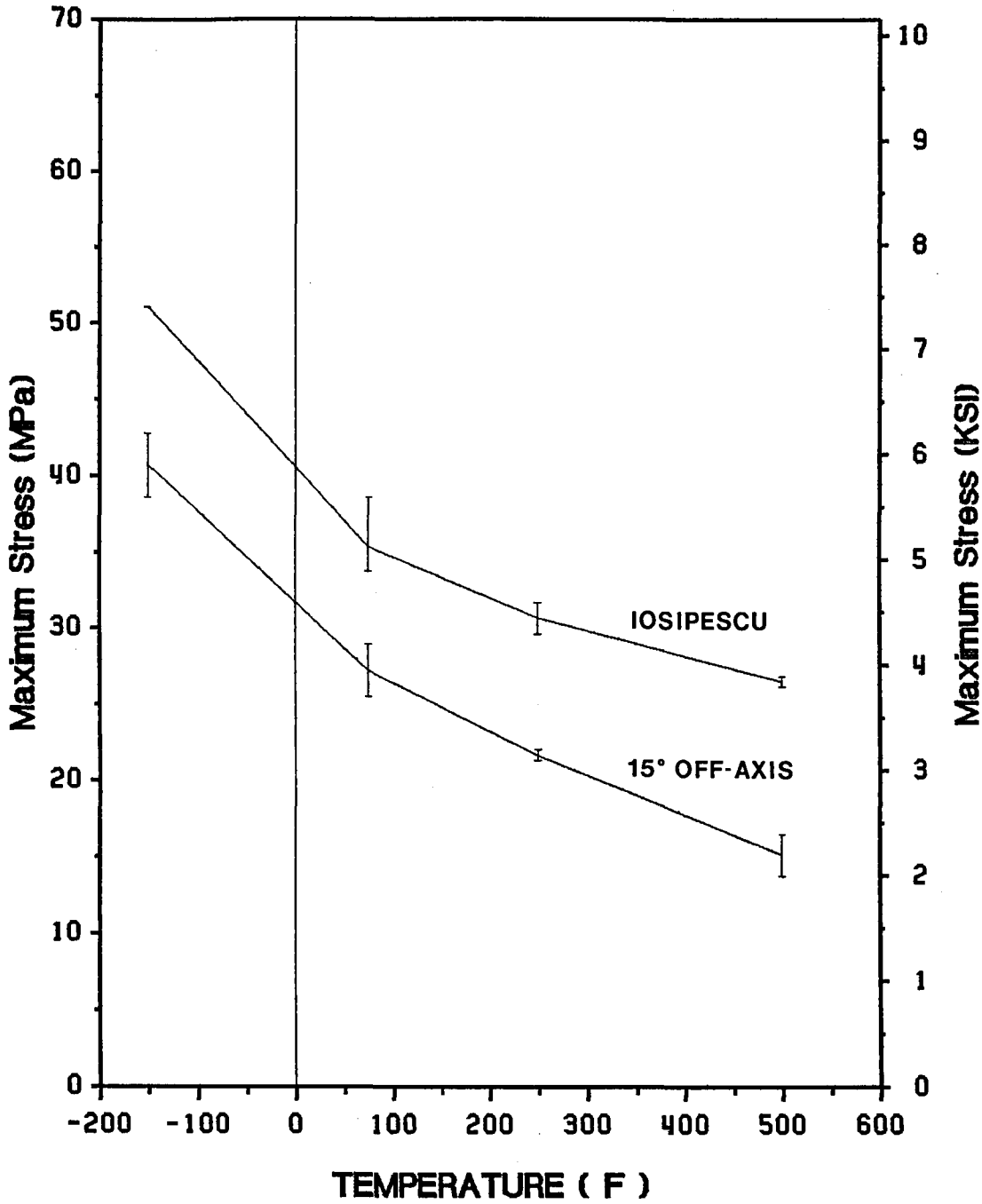

Figure 45. Maximum shear stress of 15° off-axis and 0° Iosipescu specimens as a function of temperature

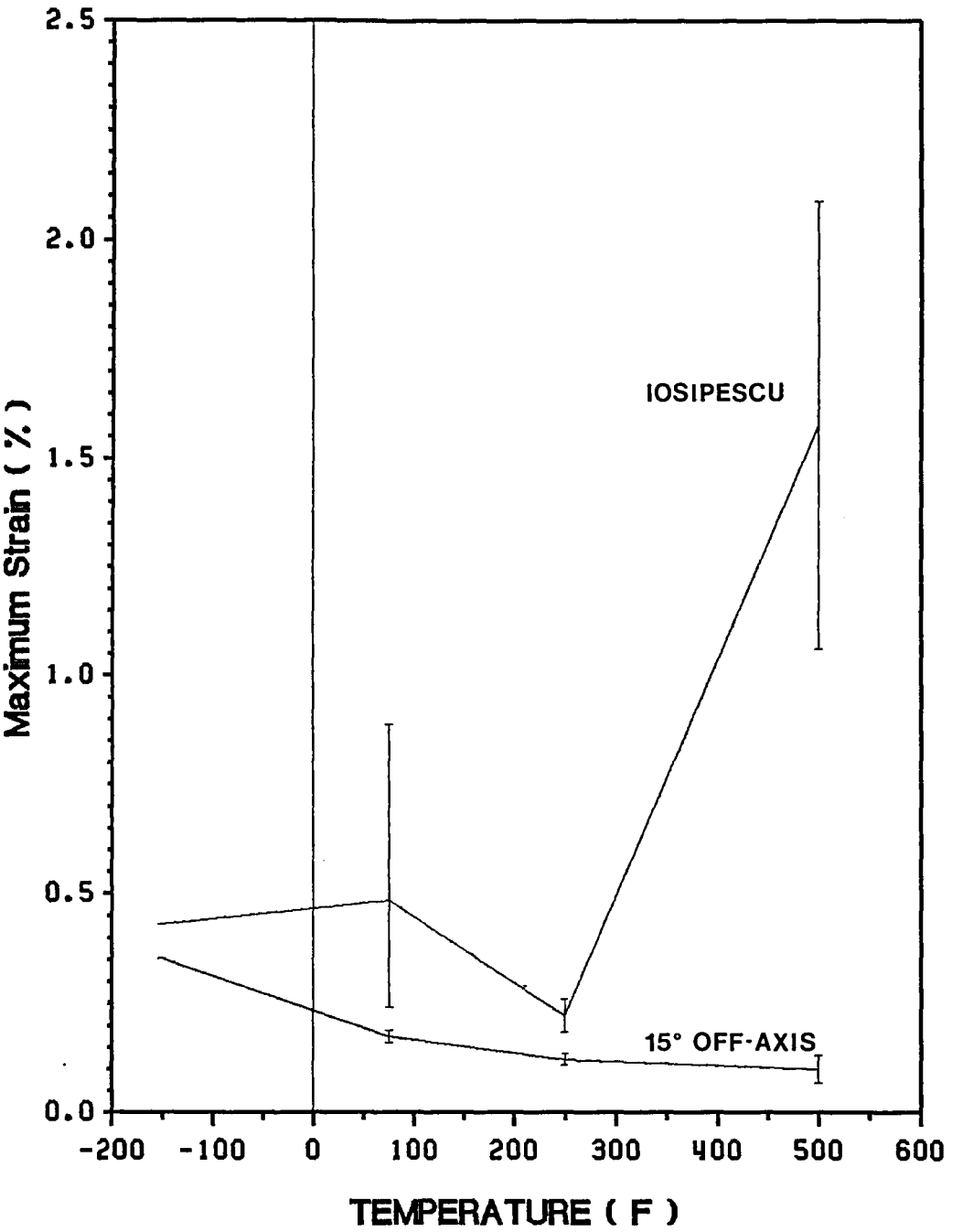

Figure 46. Maximum shear strain of 15° off-axis and 0° Iosipescu specimens as a function of temperature

3.3 *Thermo-Mechanical Properties*

3.3.1 Thermal Expansion

Figure 47 shows the thermal response of graphite/aluminum parallel and perpendicular to the fiber direction. The results of two tests are included in the one figure; in one test the specimen was heated from +75°F to +500°F and in the other test the specimen was cooled from +75°F to -150°F.

Strain along the fiber direction, ε_{11}, decreases slightly as the temperature increases from -150°F to +350°F. The coefficient of thermal expansion in the fiber direction, α_{11}, is estimated as -0.74×10^{-6}/°F in this temperature range. On the other hand, strain perpendicular to the fiber direction ε_{22} increases almost linearly with the increase in temperature. The coefficient of thermal expansion perpendicular to the fiber direction, α_{22}, is 13.2×10^{-6}/°F.

It is obvious that graphite/aluminum has a low coefficient of thermal expansion in the fiber direction, α_{11}, which means that the composite does not expand much in the fiber direction even if being subjected to a large temperature change. As stated in Chapter 1, this is one of the advantages of this material when applied to structures in space where the temperature change is quite large. The coefficient of thermal expansion perpendicular to the fiber, α_{22}, is almost equal to that of aluminum matrix as shown in Table 1.

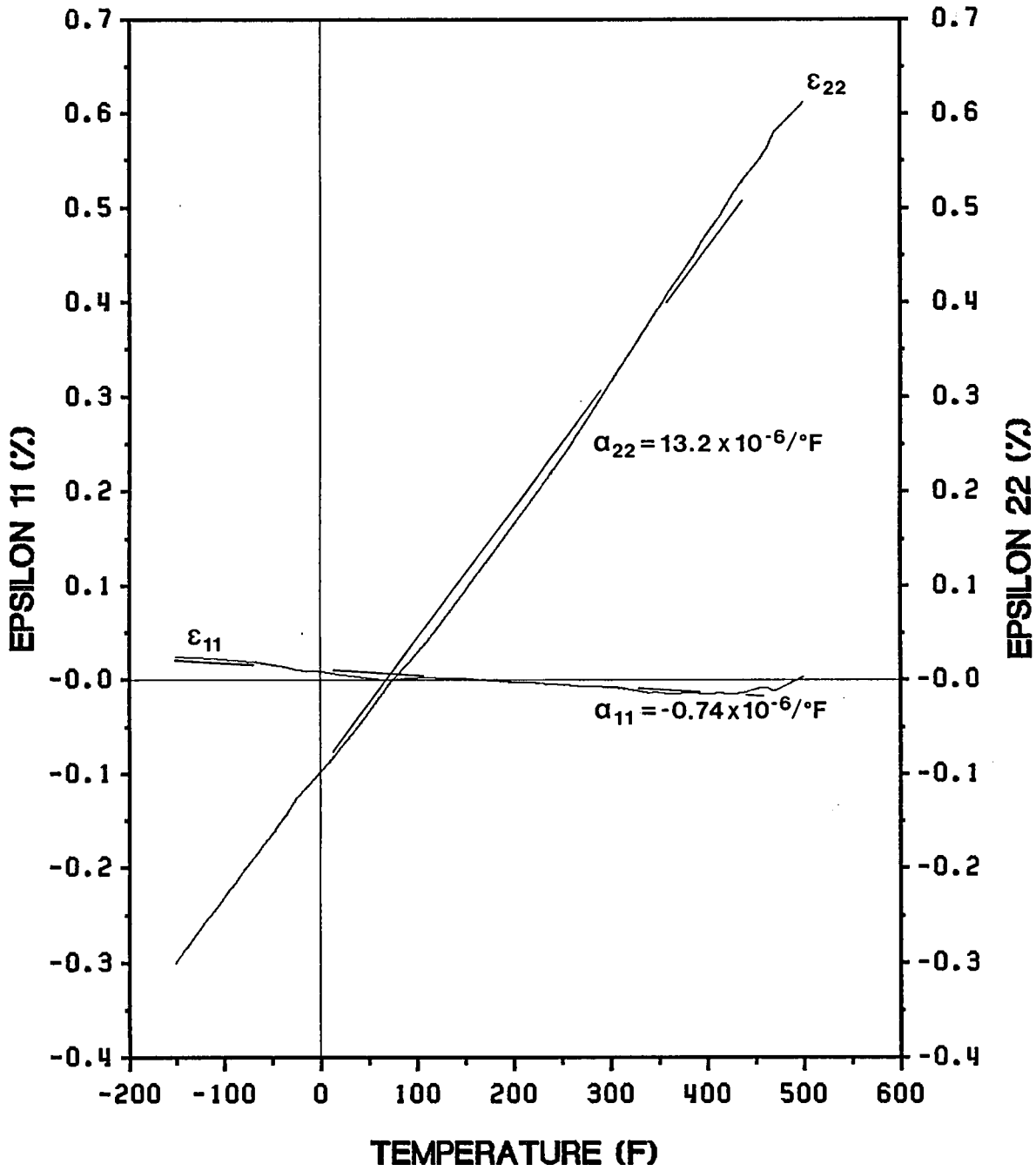

Figure 47. Thermal response of graphite/aluminum

3.3.2 Effect of Thermo-Mechanical History

3.3.2.1 15° Specimen

Figures 48 and 49 show representative thermo-mechanical response of 15° off-axis specimens when subjected to thermal loading from +75°F to +500°F and from +75°F to -150°F, respectively, under constant tensile mechanical loading (mechanical/thermal loading). In these figures, monotonic test results at +500°F and -150°F including thermal strain induced during heating or cooling process prior to loading (thermal/mechanical loading) are also illustrated to examine prior history effect on material response. It is seen that the final points of both loading cases almost overlap. Therefore, it can be said that thermo-mechanical behavior of this test configuration is history independent under the present conditions.

3.3.2.2 90° Specimen

Figures 50 and 51 shows representative response of 90° specimens for mechanical/thermal loading of +75°F to +500°F and +75°F to -150°F, respectively. Thermal/mechanical loading results are also included in the figures. When the specimen was cooled either before or after mechanical loading, as shown in Fig. 51, the final points of both loading cases exactly overlap, which indicates that these loading cases are also history independent.

However, when the specimen was heated from +75°F to +500°F under constant mechanical loading, as shown in Fig. 50, the final strain is a little larger than that of

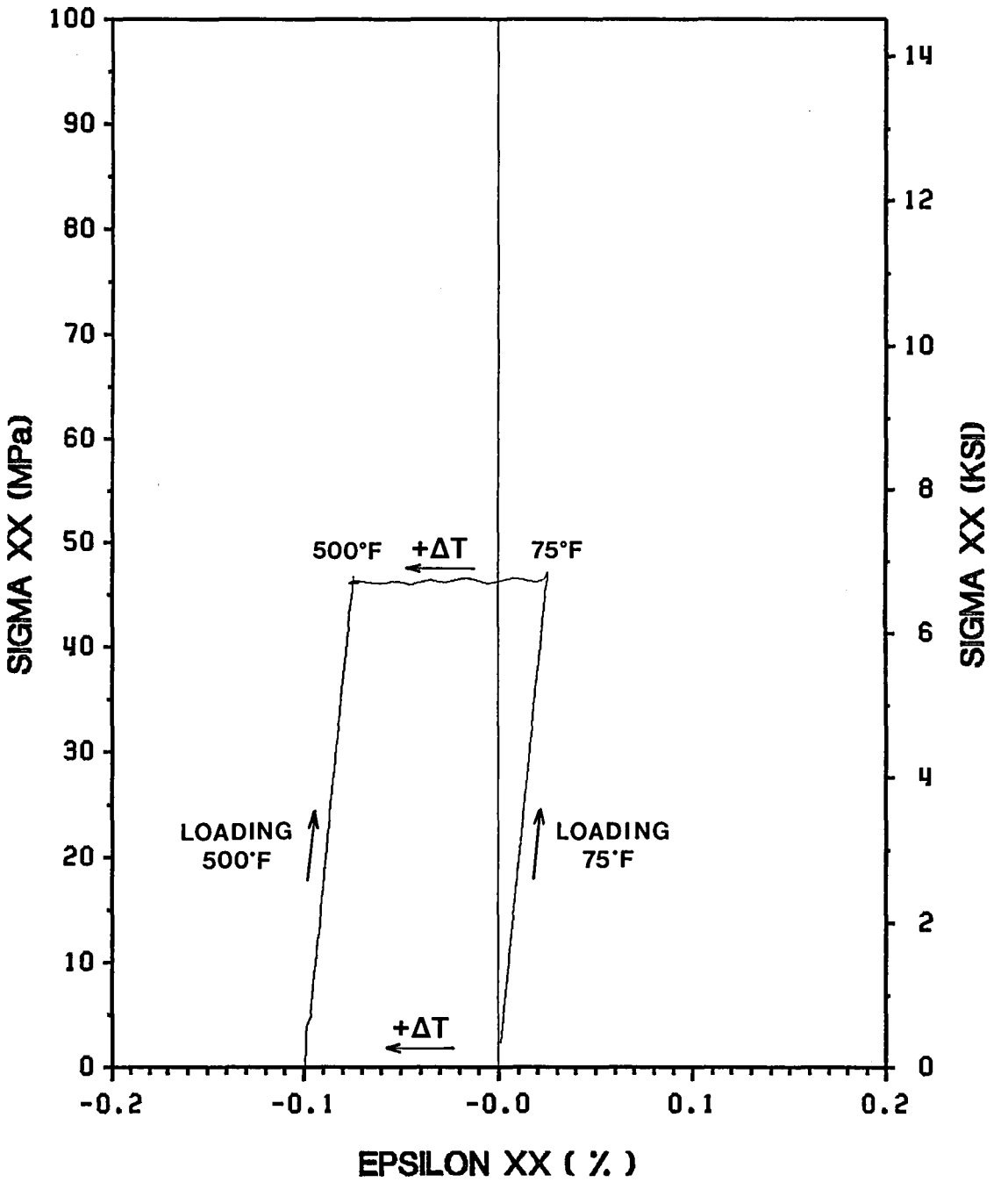

Figure 48. **Thermo-mechanical response of 15° specimen:** temperature change from +75°F to +500°F

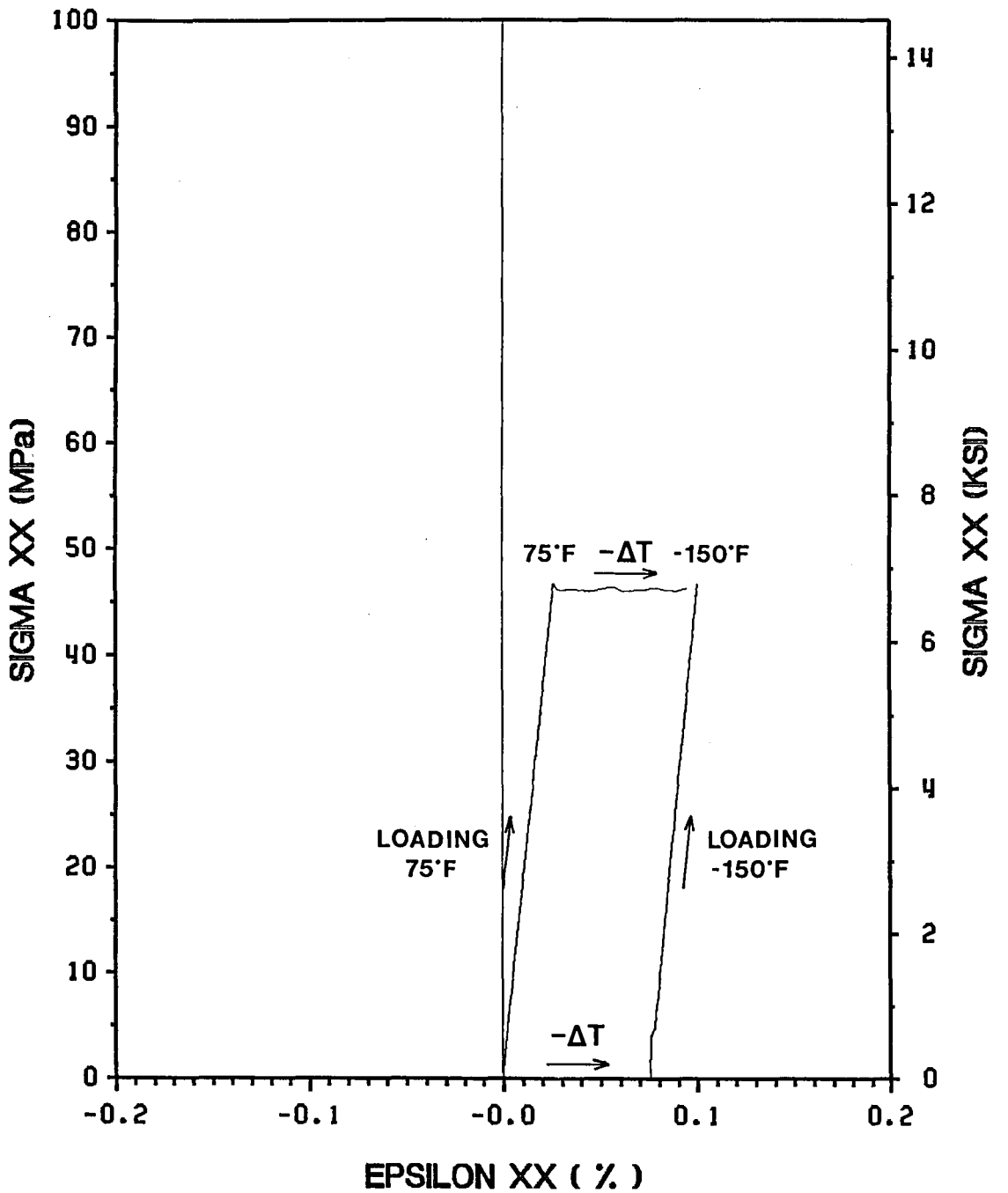

Figure 49. Thermo-mechanical response of 15° specimen: temperature change from +75°F to -150°F

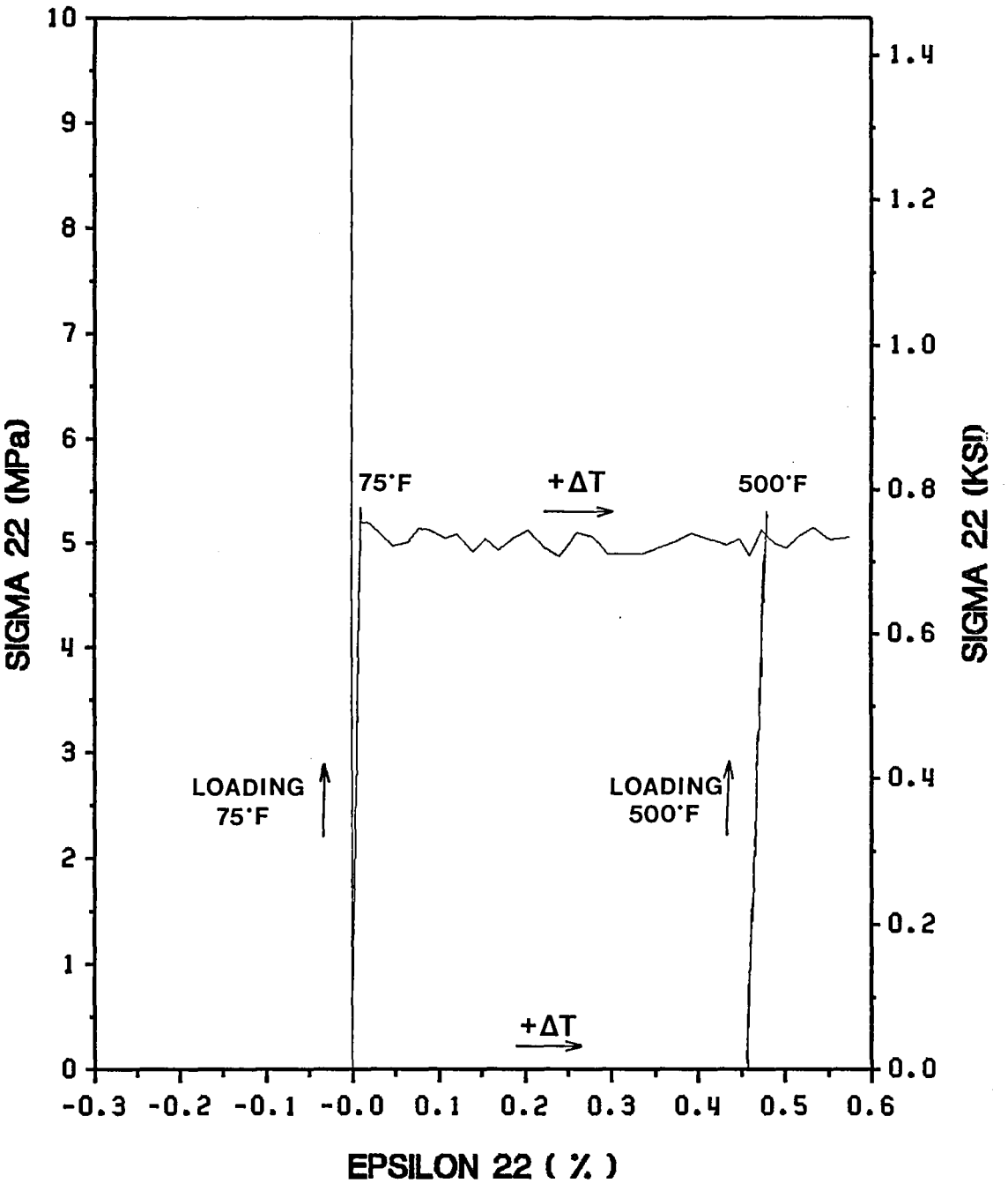

Figure 50. **Thermo-mechanical response of 90° specimen:** temperature change from +75°F to +500°F

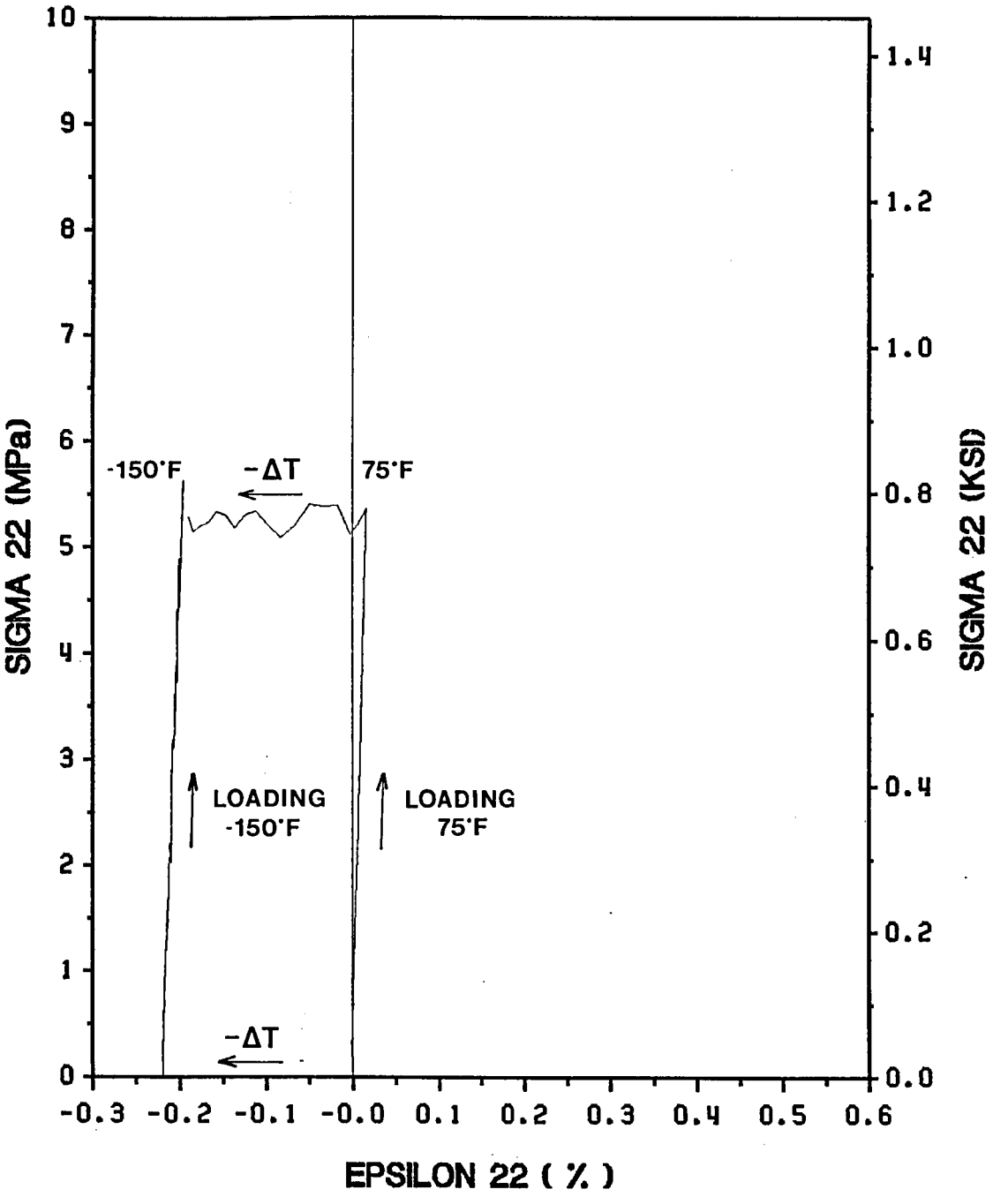

Figure 51. Thermo-mechanical response of 90° specimen: temperature change from +75°F to -150°F

thermal/mechanical loading. Based on their thermo-mechanical tests and analyses on graphite/aluminum composite, Min and Crossman [39] stated that in the plastic range transverse thermal expansion is affected by the applied stress level and the direction of the temperature change. Also, the possibility of transverse creep was suggested by the same authors [50]. Since applied constant stress of 0.75 ksi was beyond the yield stress at +500°F, it is possible that the above stated phenomena occurred during thermal loading. In other words, the material may exhibit history dependent behavior for transverse loading at elevated temperatures. Further experiments and analyses will be needed to confirm this.

4.0 Conclusions

The response of P100/6061 graphite/aluminum composite under mechanical and thermal loading was studied by conducting a series of tensile and shear tests at cold, room and elevated temperatures. The major results obtained from this research are:

1. In-plane elastic properties over the temperature range from -150°F to +500°F are characterized as follows:

    - At room temperature, E_{11} and E_{22} are 58.4 msi and 3.5 msi, respectively. The ratio E_{11}/E_{22} is 16.7.
    - E_{11} is temperature independent (Fig. 27).
    - E_{22}, ν_{12} and G_{12} generally exhibit small decreases with increase in temperature (Figs. 29, 33, 40, 41). A slight increase in these moduli is observed as the temperature increases from +75°F to +250°F.
    - Off-axis moduli are well-predicted by theoretical transformation (Figs. 14 - 16).

2. The strength shows a strong dependency on fiber orientation and temperature.

- At room temperature, X_T and Y_T are 118.1 ksi and 1.3 ksi, respectively. The ratio X_T/Y_T is 90.8.
- X_T and S decrease with increase in temperature (Figs. 43 and 45). This is believed to be due to deterioration of the matrix properties at higher temperatures.
- Y_T is very low; it is suspected that poor interfacial bond strength is the reason for the low transverse strength.
- Off-axis strength is well-predicted by the Tsai-Wu tensor polynomial (Fig. 17).

3. P100/6061 graphite/aluminum composite has very low thermal expansion in the fiber direction (Fig. 47). From thermo-mechanical off-axis and transverse tension tests, only transverse tension at elevated temperature shows history dependent behavior (Fig. 50).

4. The tensile response is strongly influenced by residual stresses which are caused by the mismatch in coefficient of thermal expansion between fiber and matrix (Figs. 20 - 22).

   - The composite exhibits thermal yielding prior to loading or low yield stress at -150°F.
   - The yield stress of the composite increases as the test temperature increases from -150°F to +250°F, but it drops significantly at +500°F because of deterioration of the aluminum matrix properties.

5. Test methods developed at Virginia Tech were successfully applied to the characterization of graphite/aluminum composite.

- The rotating-end grip fixture reduces the end-constraint effect and gives satisfactory tensile properties.
- The 0° Iosipescu test is an excellent method to obtain shear strength. Extensive nonlinear behavior is observed by this test method.

6. Several recommendations for future study are:

   - More complete characterization of the material response using tension, compression and tension-compression test data.
   - Theoretical prediction of residual stresses in the composite and overall response of the composite at various temperatures.
   - Clarification of the cause of poor transverse strength and suggestion for improvement of transverse strength.

5.0 References

1. *Metallic Matrix Composites (Composite Materials, Vol. 4)*, Kreider, K. G., Ed., Academic Press, New York, 1974.

2. Rubin, L., "Applications of Metal-Matrix Composites, the Emerging Structural Materials," *SAMPE Journal*, Vol. 15, No. 4, 1979, pp. 4-10.

3. Delmonte, J., "High Temperature Resistant Matrices for Service above 300°C (Metal Matrices and Carbon/Carbon Composites)," Chapter 13, *Technology of Carbon and Graphite Fiber Composites*, Van Nostrand Reinhold Company, New York, 1981.

4. Baker, A. A., "Carbon Fibre Reinforced Metals-A Review of the Current Technology," *Materials Science and Engineering*, Vol. 17, No. 2, 1975, pp. 177-208.

5. Pfeifer, W. H., "Graphite/Aluminum Technology Development," Chapter 6, *Hybrid and Select Metal-Matrix Composite: A State-of-the-Art Review*, American Institute of Aeronautics and Astronautics, 1977.

6. Meyerer, W., Kizer, D., Paprocki, S. and Paul, H., "Versatility of Graphite-Aluminum Composites," *Proceedings of the Second International Conference on Composite Materials (ICCM-2)*, Toronto, Canada, April 16-20, 1978, pp. 141-152.

7. "Properties of Composite Materials," Chapter 5, *Commercial Opportunities for Advanced Composites, ASTM STP 704*, American Society for Testing and Materials, 1980.

8. Baker, A. A., Shipman, C. and Jackson, P. W., "The Short-Term Compatibility of Carbon Fibres with Aluminium," *Fibre Science and Technology*, Vol. 5, No. 3, 1972, pp. 213-218.

9. Baker, S. J. and Bonfield, W., "Fracture of Aluminium-Coated Carbon Fibres," *Journal of Materials Science*, Vol. 13, No. 6, 1978, pp. 1329-1334.

10. Pepper, R. T., Upp, J. W., Rossi, R.C. and Kendall, E. G., "The Tensile Properties of a Graphite-Fiber-Reinforced Al-Si Alloy," *Metallurgical Transactions*, Vol. 2, 1971, pp. 117-120.

11. Rossi, R. C., Pepper, R. T., Upp, J. W. and Riley, W. C., "Development of Aluminum-Graphite Composites," *American Ceramic Society Bulletin*, Vol. 50, No. 5, 1971, pp. 484-487.

12. Pepper, R. T. and Penty, R. A., "Mechanical Properties of Aluminum-Graphite Composites Prepared by Liquid Phase Hot Pressing," *Journal of Composite Materials*, Vol. 8, 1974, pp. 29-37.

13. Harrigan, Jr., W. C. and Goddard, D. M., "Aluminum Graphite Composites: Effect of Processing on Mechanical Properties," *Journal of Metals*, Vol. 27, No. 5, 1975, pp. 20-25.

14. Amateau, M. F., "Progress in the Development of Graphite-Aluminum Composites Using Liquid Infiltration Technology," *Journal of Composite Materials*, Vol. 10, 1976, pp. 279-296.

15. Pfeifer, W. H. and Kinna, M. A., "Characterization of the Mechanical Property Behavior of Selected Graphite Fiber Reinforced Aluminum Alloys," *Proceedings of the Second International Conference on Composite Materials (ICCM-2)*, Toronto, Canada, April 16-20, 1978, pp. 153-172.

16. Tribendis, J. J., Koczak, M. J. and Gracia, R., "The Effect of Fiber Orientation and Thermal Treatment on the Mechanical Properties of Graphite-Aluminum Composites," *Powder Metallurgy International*, Vol. 13, No. 2, 1981, pp. 88-92.

17. Khan, I. H., "The Effect of Thermal Exposure on the Mechanical Properties of Aluminum-Graphite Composites," *Metallurgical Transactions A*, Vol. 7A, No. 9, 1976, pp. 1281-1289.

18. Hoover, W. R., "Graphite/Aluminum: An Evaluation of State-of-the-Art Material," *Journal of Composite Materials*, Vol. 11, No. 1, 1977, pp. 17-29.

19. Harrigan, Jr., W. C., "The Effects of Temperature and Pressure on the Interface Chemistry in the Graphite-Aluminum Composites," *Metallurgical Transactions A*, Vol. 9A, No. 4, 1978, pp. 503-507.

20. Lamotte, E. D., Phillips, K., Perry, A. J. and Killias, H. R., "Continuously Cast Aluminium-Carbon Fibre Composites and their Tensile Properties," *Journal of Materials Science*, Vol. 7, No. 3, 1972, pp. 346-349.

21. Morita, M. and Baba, H., "Some Mechanical Properties of Carbon Fiber Reinforced Aluminum," *Journal of the Japan Institute of Metals*, Vol. 37, No. 3, 1973, pp. 315-320.

22. Baker, A. A., Martin, A. and Bache, R. J., "Carbon-Fibre/Metal-Matrix Composites: Fabrication by Electrodeposition," *Composites*, Vol. 2, No. 3, 1971, pp. 154-160.

23. Jackson, P. W., Braddick, D. M. and Walker, P. J., "Tensile and Flexural Properties of Carbon Fibre-Aluminium Matrix Composites," *Fibre Science and Technology*, Vol. 5, No. 3, 1972, pp. 219-236.

24. Baker, A. A., Braddick, D. M. and Jackson, P. W., "Fatigue of Boron-Aluminum and Carbon-Aluminum Fibre Composites," *Journal of Materials Science*, Vol. 7, No. 7, 1972, pp. 747-762.

25. Ohsaki, T., Yoshida, M., Fukube, Y. and Nakamura, K., "The Properties of Carbon Fiber Reinforced Aluminum Composites Formed by the Ion-Plating Process and Vacuum Hot Pressing," *Thin Solid Films*, Vol. 45, No. 3, 1977, pp. 563-568.

26. Salibekov, S. E., Zabolotskii, A. A., Turchenkov, V. A., Kantsevich, I. A. and Fadyukov, E. M., "Factors Influencing Structure Formation and Some Properties of Aluminum/Carbon-Fiber Composite Materials," *Soviet Powder Metallurgy and Metal Ceramics*, Vol. 16, No. 2, 1977, pp. 124-129.

27. Zabolotskii, A. A. and Salibekov, S. E., "Development of Al-C Composite Materials," *Metal Science and Heat Treatment*, Vol. 20, Nos. 9-10, 1978, pp. 841-844.

28. Zabolotskii, A. A., Varshavskii, V. Y., Karimbaev, T. D. and Pavlov, V. I., "Composite Materials with an Aluminum Matrix Reinforced with Carbon Fibers," *Metal Science and Heat Treatment*, Vol. 22, No. 4, 1983, pp. 294-297.

29. Mimura, K., Okuno, O. and Miura, I., "Fabrication and Mechanical Properties of Carbon Fiber Reinforced Al Composites," *Journal of the Japan Institute of Metals*, Vol. 38, No. 8, 1974, pp. 757-761.

30. Okura, A., Nakata, E. and Sakai, S., "Studies of Fabrication of Carbon Fiber Reinforced Aluminum Matrix Composites," *Journal of the Japan Institute of Metals*, Vol. 47, No. 3, 1983, pp. 249-257.

31. Asanuma, H. and Okura, A., "Fabrication of Carbon Fiber Reinforced Aluminum Composites by Roll Diffusion Bonding Method," *Proceedings of the Fourth International Conference on Composite Materials (ICCM-4)*, Tokyo, Japan, October 25-28, 1982, pp. 1435-1442.

32. Asanuma, H. and Okura, A., "Studies on the Fabrication of Carbon Fiber Reinforced Aluminum Composites by the Plasma Spray and Roll Diffusion Bonding Method," *Journal of the Japan Institute of Metals*, Vol. 48, No. 11, 1984, pp. 1119-1126.

33. Ratke, L. and Wassermann, G., "Fiber Composites of Aluminium with Graphite," *Powder Metallurgy International*, Vol. 15, No. 2, 1983, pp. 65-68.

34. Ryabinina, O. N., Tuchinskii, L. I., Vishnyakov, L. R. and Drachinskii, A. S., "Electric-Discharge Sintering of an Aluminum-Carbon Fiber Composite Material," *Soviet Powder Metallurgy and Metal Ceramics*, Vol. 19, No. 9, 1980, pp. 615-617.

35. Kyono, T., Hall, I. W., Taya, M. and Kitamura, A., "Thermal Cycling Damage in Carbon Fiber/Aluminum Composites," *Composites '86: Recent Advances in Japan and the United States*, Kawata, K., Umekawa, S. and Kobayashi, A., Eds., 1986, pp. 553-561.

36. THORNEL Graphite Fiber P-100S 2K, Technical Information, Amoco Performance Product, Inc., 1986.

37. Aboudi, J., "The Effective Thermomechanical Behavior of Inelastic Fiber-Reinforced Materials," *International Journal of Engineering Science*, Vol. 23, No. 7, 1985, pp. 773-787.

38. Aboudi, J., "Inelastic Behavior of Metal-Matrix Composites at Elevated Temperature," *International Journal of Plasticity*, Vol. 1, 1985, pp. 359-372.

39. Min, B. K. and Crossman, F. W., "History-Dependent Thermomechanical Properties of Graphite/Aluminum Unidirectional Composites," *Composite Materials:*

Testing and Design (Sixth Conference), ASTM STP 787, American Society for Testing and Materials, 1982, pp. 371-392.

40. Pindera, M. J. and Herakovich, C. T., "Endochronic Theory for Transversely Isotropic Fibrous Composites," VPI-E-81-27, Virginia Polytechnic Institute and State University, October 1981.

41. Pagano, N. J. and Halpin, J. C., "Influence of End Constraint in the Testing of Anisotropic Bodies," *Journal of Composite Materials*, Vol. 2, No. 1, 1968, pp. 18-31.

42. Pindera, M. J. and Herakovich, C. T., "Shear Characterization of Unidirectional Composites with the Off-Axis Tension Test," *Experimental Mechanics*, Vol. 26, No. 1, 1986, pp. 103-112.

43. Herakovich, C. T. and Bergner, Jr., H. W., "Finite Element Stress Analysis of a Notched Coupon Specimen for In-Plane Behavior of Composites," *Composites*, Vol. 11, No. 3, 1980, pp. 149-154.

44. Herakovich, C. T., Bergner, Jr., H. W. and Bowles, D. E., "A Comparative Study of Composite Shear Specimens Using the Finite-Element Method," *Test Methods and Design Allowables for Fibrous Composites, ASTM STP 734*, American Society for Testing and Materials, 1981, pp. 129-151.

45. Walrath, D. E. and Adams, D. F., "The Iosipescu Shear Test as Applied to Composite Materials," *Experimental Mechanics*, Vol. 23, No. 1, PP. 105-110.

46. Walrath, D. E. and Adams, D. F., "Analysis of the Stress State in an Iosipescu Shear Test Specimen," Report UWME-DR-301-102-1, Department of Mechanical Engineering, University of Wyoming, Laramie, WY., June 1983.

47. Pindera, M. J., Choksi, G., Hidde, J. S. and Herakovich, C. T., "A Methodology for Accurate Shear Characterization of Unidirectional Composites," (Accepted for publication in *Journal of Composite Materials*).

48. Hidde, J. S., "A User's Guide for the Materials Testing Package (MATPAC2)," Composite Mechanics Group, Department of Engineering Science and Mechanics, Virginia Polytechnic Institute and State University, May 1987.

49. Dries, G. A. and Tompkins, S. S., "Effects of Thermal Cycling on Graphite-Fiber-Reinforced 6061 Aluminum," NASA Technical Paper 2612, October 1986.

50. Min, B. K. and Crossman, F. W., "Analysis of Creep for Metal Matrix Composites," *Journal of Composite Materials*, Vol. 16, 1982, pp. 188-203.

Appendix A. Summary of Individual Test Results

Table A.1 Off-axis tension test results at -150°F: initial moduli and ultimate strengths

Specimen Group	Specimen Number	Elastic Modulus, E_{xx}(msi)	Poisson's Ratio, ν_{xy}	Shear Modulus, G_{12}(msi)	Ultimate Stress, σ^u_{xx}(ksi)	Ultimate Strain, ε^u_{xx}(%)
0° monotonic						
	1	48.9	0.286	*	110.7	0.221
	2	48.9	0.329	*	137.2	0.278
cyclic						
	1	47.2	0.381	*	115.5	0.239
	2	48.6	0.314	*	129.5	0.262
	mean	48.4	0.328	*	124.0***	0.250***
15° monotonic						
	1	26.4	0.307	2.96	24.6	0.141
	2	27.8	0.270	**	22.4	0.113
cyclic						
	1	27.3	0.262	2.49	24.7	0.137
	2	27.6	0.314	3.78	22.9	0.116
	mean	27.3	0.288	3.08	23.5***	0.127***
90° monotonic						
	1	4.6	0.064	*	1.6	0.047
	2	4.2	0.042	*	1.3	0.039
cyclic						
	1	4.1	0.042	*	1.7	0.053
	2	4.3	0.055	*	1.4	0.035
	mean	4.3	0.051	*	1.5***	0.043***

* Not applicable
** Data not available
*** Only monotonic data included in average

Table A.2 Off-axis tension test results at +75°F: initial moduli and ultimate strengths

Specimen Group	Specimen Number	Elastic Modulus, E_{xx}(msi)	Poisson's Ratio, ν_{xy}	Shear Modulus, G_{12}(msi)	Ultimate Stress, σ^{U}_{xx}(ksi)	Ultimate Strain, ε^{U}_{xx}(%)
0° monotonic						
	1	59.8	0.288	*	113.4	0.197
	2	57.8	0.275	*	106.3	0.190
	3	62.3	0.290	*	134.6	0.228
cyclic						
	1	56.3	0.295	*	118.2	0.216
	2	55.9	0.308	*	114.0	0.211
	mean	58.4	0.291	*	118.1***	0.205***
10° monotonic						
	1	31.2	0.312	2.55	23.7	0.092
	2	42.0	0.222	2.90	23.7	0.080
	mean	36.6	0.267	2.73	23.7	0.086
15° monotonic						
	1	27.5	0.212	2.75	14.6	0.061
	2	28.4	0.321	2.80	16.6	0.069
cyclic						
	1	27.5	0.493**	6.01**	14.6	0.060
	2	27.8	0.287	2.79	16.0	0.074
	3	28.1	0.233	2.84	15.9	0.073
	mean	27.9	0.263	2.80	15.6***	0.065***
45° monotonic						
	1	6.0	0.209	2.39	3.2	0.064
	2	6.3	0.209	2.55	3.5	0.064
	3	5.8	0.107	2.45	3.6	0.070
	mean	6.0	0.175	2.46	3.4	0.066
90° monotonic						
	1	3.6	0.034	*	1.1	0.036
	2	3.4	0.020	*	1.4	0.047
cyclic						
	1	3.4	0.038	*	1.3	0.045
	2	3.7	0.018	*	1.1	0.035
	mean	3.5	0.028	*	1.3***	0.042***

* Not applicable
** Abnormal data (not averaged)
*** Only monotonic data included in average

Table A.3 Off-axis tension test results at +250°F: initial moduli and ultimate strengths

Specimen Group	Specimen Number	Elastic Modulus, E_{xx}(msi)	Poisson's Ratio, ν_{xy}	Shear Modulus, G_{12}(msi)	Ultimate Stress, σ^{u}_{xx}(ksi)	Ultimate Strain, ε^{u}_{xx}(%)
0°						
monotonic						
	1	56.9	0.245	*	122.8	0.212
	2	56.8	0.323	*	110.2	0.192
cyclic						
	1	56.4	0.319	*	110.8	0.194
	2	57.5	0.302	*	120.1	0.206
	mean	56.9	0.297	*	116.5***	0.202***
15°						
monotonic						
	1	25.9	0.142	2.73	12.4	0.051
	2	26.0	0.180	2.67	12.8	0.057
cyclic						
	1	27.5	0.192	2.69	14.9	0.069
	2	26.0	0.204	2.75	15.0	0.069
	mean	26.4	0.180	2.71	12.6***	0.054***
90°						
monotonic						
	1	4.0	0.018	*	1.0	0.026
	2	4.4	0.030	*	0.9	0.022
cyclic						
	1	4.0	0.027	*	1.8	0.052
	2	3.8	0.012	*	2.0	0.064
	mean	4.1	0.022	*	1.0***	0.024***

* Not applicable
*** Only monotonic data included in average

Table A.4 Off-axis tension test results at +500°F: initial moduli and ultimate strengths

Specimen Group	Specimen Number	Elastic Modulus, E_{xx}(msi)	Poisson's Ratio, ν_{xy}	Shear Modulus, G_{12}(msi)	Ultimate Stress, σ^{u}_{xx}(ksi)	Ultimate Strain, ε^{u}_{xx}(%)
0°						
monotonic						
	1	56.3	0.314	*	69.7	0.135
	2	56.9	0.322	*	109.9	0.192
cyclic						
	1	56.6	0.210	*	85.6	0.165
	2	58.0	0.331	*	90.8	0.152
	mean	57.0	0.294	*	89.8***	0.164***
15°						
monotonic						
	1	26.1	**	**	8.2	0.037
	2	26.1	0.146	2.82	9.7	0.047
cyclic						
	1	26.1	0.170	2.86	12.3	0.086
	2	25.9	0.076	2.84	11.1	0.066
	mean	26.1	0.130	2.84	9.0***	0.042***
90°						
monotonic						
	1	3.4	0.035	*	1.3	0.048
	2	3.3	0.058	*	1.2	0.039
cyclic						
	1	3.9	0.000	*	1.3	0.042
	2	3.5	0.037	*	1.5	0.055
	mean	3.5	0.033	*	1.3***	0.044***

* Not applicable
** Data not available
*** Only monotonic data included in average

Table A.5 Iosipescu shear test results at -150°F: initial moduli and ultimate strengths

Specimen Group	Specimen Number	Shear Modulus, G_{12}(msi)	Ultimate Stress, τ_{12}^{u}(ksi)	Ultimate Strain, γ_{12}^{u}(%)
0°				
	1	3.45	7.4	0.431
	2	5.60*	17.3*	0.888*
	mean	3.45	7.4	0.431

* Abnormal data (not averaged)

Table A.6 Iosipescu shear test results at +75°F: initial moduli and ultimate strengths

Specimen Group	Specimen Number	Shear Modulus, G_{12}(msi)	Ultimate Stress, τ_{12}^{u}(ksi)	Ultimate Strain, γ_{12}^{u}(%)
0°				
	1	3.15	4.9	0.243
	2	2.74	5.6	0.888
	3	2.40	4.9	0.322
	mean	2.76	5.1	0.484
90°				
	1	2.16	3.5	0.175
	2	1.70	2.6	0.165
	3	1.66	2.6	0.170
	4	1.59	2.8	0.225
	mean	1.78	2.9	0.184

Table A.7 Iosipescu shear test results at +250°F: initial moduli and ultimate strengths

Specimen Group	Specimen Number	Shear Modulus, G_{12}(msi)	Ultimate Stress, τ_{12}^{u}(ksi)	Ultimate Strain, γ_{12}^{u}(%)
0°				
	1	2.77	4.3	0.260
	2	3.29	4.6	0.185
	mean	3.03	4.5	0.223

Table A.8 Iosipescu shear test results at +500°F: initial moduli and ultimate strengths

Specimen Group	Specimen Number	Shear Modulus, G_{12}(msi)	Ultimate Stress, τ_{12}^{u}(ksi)	Ultimate Strain, γ_{12}^{u}(%)
0°				
	1	2.72	3.8	1.060
	2	2.40	3.9	2.087
	mean	2.56	3.9	1.574

Table A.9 Cyclic test results at -150°F

Initial Loading						
Specimen Group	Specimen Number	Elastic Modulus, E_{xx}(msi)	Poisson's Ratio, ν_{xy}	Shear Modulus, G_{12}(msi)	Yield Stress, σ^{Y}_{xx}(ksi)	Reversal Stress, (ksi)
0°						
	1	47.2	0.381	*	**	102.4
	2	48.6	0.314	*	**	102.8
	mean	47.9	0.348	*	**	102.6
15°						
	1	27.3	0.262	2.49	1.9	19.2
	2	27.6	0.314	3.78	2.6	19.1
	mean	27.5	0.288	3.14	2.3	19.2
90°						
	1	4.1	0.042	*	0.2	1.3
	2	4.3	0.055	*	0.4	1.2
	mean	4.2	0.049	*	0.3	1.3

Second Loading							
Group	Number	Permanent Strain, (%)	Elastic Modulus, E_{xx}(msi)	Poisson's Ratio, ν_{xy}	Shear Modulus, G_{12}(msi)	Ultimate Stress, σ^{U}_{xx}(ksi)	Ultimate Strain, ε^{U}_{xx}(%)
0°							
	1	0.023	54.6	0.371	*	115.5	0.239
	2	0.022	55.6	0.320	*	129.5	0.262
	mean	0.023	55.1	0.346	*	122.5	0.251
15°							
	1	0.022	27.2	0.318	2.96	24.7	0.137
	2	0.022	28.2	0.344	3.17	22.9	0.116
	mean	0.022	27.7	0.331	3.07	23.8	0.127
90°							
	1	0.006	4.0	0.039	*	1.7	0.053
	2	0.003	4.4	0.035	*	1.4	0.035
	mean	0.005	4.2	0.037	*	1.6	0.044

* Not applicable
** Data not available

Table A.10 Cyclic test results at +75°F

Initial Loading						
Specimen Group	Specimen Number	Elastic Modulus, E_{xx}(msi)	Poisson's Ratio, ν_{xy}	Shear Modulus, G_{12}(msi)	Yield Stress, σ^{Y}_{xx}(ksi)	Reversal Stress, (ksi)
0°						
	1	56.3	0.295	*	57.0	95.1
	2	55.9	0.308	*	56.9	95.2
	mean	56.1	0.302	*	57.0	95.2
15°						
	1	27.5	0.493**	6.01**	5.1	12.2
	2	27.8	0.287	2.79	4.9	12.4
	3	28.1	0.233	2.84	5.4	12.2
	mean	27.8	0.260	2.82	5.1	12.3
90°						
	1	3.4	0.038	*	0.4	0.8
	2	3.7	0.018	*	0.4	0.8
	mean	3.6	0.028	*	0.4	0.8

Second Loading							
Group	Number	Permanent Strain, (%)	Elastic Modulus, E_{xx}(msi)	Poisson's Ratio, ν_{xy}	Shear Modulus, G_{12}(msi)	Ultimate Stress, σ^{U}_{xx}(ksi)	Ultimate Strain, ε^{U}_{xx}(%)
0°							
	1	0.009	58.7	0.294	*	118.2	0.216
	2	0.008	55.4	0.314	*	114.0	0.211
	mean	0.009	57.1	0.304	*	116.1	0.214
15°							
	1	0.004	28.6	0.493**	5.00**	14.6	0.060
	2	0.004	26.7	0.269	2.83	16.0	0.074
	3	0.003	27.7	0.241	2.91	15.9	0.073
	mean	0.004	27.7	0.255	2.87	15.5	0.069
90°							
	1	0.003	3.8	0.038	*	1.3	0.045
	2	0.003	3.9	0.017	*	1.1	0.035
	mean	0.003	3.9	0.028	*	1.2	0.040

* Not applicable
** Abnormal data (not averaged)

Table A.11 Cyclic test results at +250°F

Initial Loading						
Specimen Group	Specimen Number	Elastic Modulus, E_{xx}(msi)	Poisson's Ratio, ν_{xy}	Shear Modulus, G_{12}(msi)	Yield Stress, σ^{Y}_{xx}(ksi)	Reversal Stress, (ksi)
0°						
	1	56.4	0.319	*	**	96.3
	2	57.5	0.302	*	**	96.1
	mean	57.0	0.311	*	**	96.2
15°						
	1	27.5	0.192	2.69	3.7	9.4
	2	26.0	0.204	2.75	3.4	10.3
	mean	26.8	0.198	2.72	3.6	9.9
90°						
	1	4.0	0.027	*	0.2	0.8
	2	3.8	0.012	*	0.3	0.8
	mean	3.9	0.020	*	0.3	0.8

Second Loading							
Group	Number	Permanent Strain, (%)	Elastic Modulus, E_{xx}(msi)	Poisson's Ratio, ν_{xy}	Shear Modulus, G_{12}(msi)	Ultimate Stress, σ^{U}_{xx}(ksi)	Ultimate Strain, ε^{U}_{xx}(%)
0°							
	1	0.001	56.4	0.317	*	110.8	0.194
	2	0.000	57.5	0.302	*	120.1	0.206
	mean	0.001	57.0	0.310	*	115.5	0.200
15°							
	1	0.001	26.5	0.195	2.74	14.9	0.069
	2	0.001	25.2	0.216	2.76	15.0	0.069
	mean	0.001	25.9	0.206	2.75	15.0	0.069
90°							
	1	0.001	3.8	0.032	*	1.8	0.052
	2	0.001	3.7	0.017	*	2.0	0.064
	mean	0.001	3.8	0.025	*	1.9	0.058

* Not applicable
** Data not available

Table A.12 Cyclic test results at +500°F

Initial Loading						
Specimen Group	Specimen Number	Elastic Modulus, E_{xx}(msi)	Poisson's Ratio, ν_{xy}	Shear Modulus, G_{12}(msi)	Yield Stress, σ^{Y}_{xx}(ksi)	Reversal Stress, (ksi)
0°						
	1	56.6	0.210	*	**	73.1
	2	58.0	0.331	*	**	72.8
	mean	57.3	0.271	*	**	73.0
15°						
	1	26.1	0.170	2.86	2.4	7.7
	2	25.9	0.076	2.84	2.6	7.7
	mean	26.0	0.123	2.85	2.5	7.7
90°						
	1	3.9	0.000	*	0.4	1.0
	2	3.5	0.037	*	0.4	1.0
	mean	3.7	0.019	*	0.4	1.0

Second Loading							
Group	Number	Permanent Strain, (%)	Elastic Modulus, E_{xx}(msi)	Poisson's Ratio, ν_{xy}	Shear Modulus, G_{12}(msi)	Ultimate Stress, σ^{U}_{xx}(ksi)	Ultimate Strain, ε^{U}_{xx}(%)
0°							
	1	0.002	56.9	0.208	*	85.6	0.165
	2	-0.001	57.7	0.321	*	90.8	0.152
	mean	0.001	57.3	0.265	*	88.2	0.159
15°							
	1	0.003	25.3	0.202	2.57	12.3	0.086
	2	0.004	25.3	0.094	2.46	11.1	0.066
	mean	0.004	25.3	0.148	2.52	11.7	0.076
90°							
	1	0.002	3.7	0.015	*	1.3	0.042
	2	0.004	3.3	0.038	*	1.5	0.055
	mean	0.003	3.5	0.027	*	1.4	0.049

* Not applicable

Table A.13 Thermo-mechanical test results

+75°F to -150°F						
Specimen Group	Specimen Number	Elastic Modulus, E_{xx}(msi)	Poisson's Ratio, ν_{xy}	Shear Modulus, G_{12}(msi)	Constant Stress, (ksi)	Final Strain, (%)
15°						
	1	26.7	0.315	2.83	6.7	0.124
	2	26.1	0.241	2.87	6.7	0.095
	mean	26.4	0.278	2.85	6.7	0.110
90°						
	1	5.0	0.030	*	0.75	-0.174
	2	4.9	0.018	*	0.75	-0.189
	mean	5.0	0.024	*	0.75	-0.182
+75°F to +500°F						
Specimen Group	Specimen Number	Elastic Modulus, E_{xx}(msi)	Poisson's Ratio, ν_{xy}	Shear Modulus, G_{12}(msi)	Constant Stress, (ksi)	Final Strain, (%)
15°						
	1	28.7	0.316	2.95	6.7	-0.048
	2	27.8	0.230	2.98	6.7	-0.075
	mean	28.3	0.273	2.97	6.7	-0.062
90°						
	1	4.7	0.063	*	0.75	0.575
	2	4.8	0.066	*	0.75	0.508
	mean	4.8	0.065	*	0.75	0.542

* Not applicable

BIBLIOGRAPHIC DATA SHEET	1. Report No. CCMS-87-08, VPI-E-87-8	2.	3. Recipient's Accession No.
4. Title and Subtitle Temperature-Dependent Tensile and Shear Response of Graphite/Aluminum			5. Report Date May 1987 6.
7. Author(s) T. Fujita, M. Pindera and C. Herakovich			8. Performing Organization Rept. No. VPI-E-87-8
9. Performing Organization Name and Address Virginia Polytechnic Institute & State University Engineering Science and Mechanics Dept Blacksburg, VA 24061			10. Project/Task/Work Unit No. 11. Contract/Grant No.
12. Sponsoring Organization Name and Address 1. Materials Sciences Corp., Spring House, PA 2. NASA Goddard Space Flight Center, Greenbelt, MD 3. CIT/IMSE, Virginia Tech, Blacksburg, VA			13. Type of Report & Period Covered 14.
15. Supplementary Notes			

16. Abstracts: The thermo-mechanical response of unidirectional P100 graphite fiber/6061 aluminum matrix composites (v_f=0.47) was investigated at four temperatures: -150°F, +75°F, +250°F and +500°F, using test methods developed at VPI&SU. Two types of tests, off-axis tension and Iosipescu shear, were used to obtain the desired properties. Good experimental-theoretical correlation was obtained for E_{xx}, v_{xy} and G_{12}. It is shown that E_{11} is temperature independent, but E_{22}, v_{12} and G_{12} generally decrease with increasing temperature. Compared with rather high longitudinal strength, very low transverse strength was obtained for the graphite/aluminum. The poor transverse strength is believed to be due to the low interfacial bond strength in this material. The strength decreases significantly with increasing temperature. The tensile response at various temperatures is greatly affected by the residual stresses caused by the mismatch in the coefficients of thermal expansion of fibers and matrix. The degradation of the aluminum matrix properties at higher temperatures has a deleterious effect on composite properties. The composite has a very low coefficient of thermal expansion in the fiber direction.

17. Key Words and Document Analysis. 17a. Descriptors

Graphite-aluminum, tension, shear, temperature dependence, elastic properties, nonlinear response, strength, CTE.

17b. Identifiers/Open-Ended Terms

17c. COSATI Field/Group

18. Availability Statement	19. Security Class (This Report)	21. No. of Pages
unlimited	UNCLASSIFIED	137
	20. Security Class (This Page) UNCLASSIFIED	22. Price

End of Document